Modulation of Macrophage Antifungal Activity by the Transcriptional Coregulator, CITED1

by

Aarthi Subramani

A Dissertation Submitted in Partial Fulfillment of the Requirements for the Degree of Doctorate of Science in Molecular Bioscience

Middle Tennessee State University

December 2022

Dissertation Committee:

Dr. David. E. Nelson

Dr. Mary B. Farone, Chair

Dr. Anthony L. Farone

Dr. Rebecca L. Seipelt Thiemann

Dr. Erin. E. McClelland

To my brother for all his love and support, and my little nephew, the cutest boy in the world.

ACKNOWLEDGEMENTS

I would like to express my warmest thanks to Dr. David E. Nelson for being more than a guiding light to me. His excellent support, commitment, and leadership cannot be understated. He has been an inspiration to me and has encouraged me to be the best that I can be at all times. My ability to think critically and handle research efficiently has improved by leaps and bounds. I am proud to have done extensive research in this field and successfully completed my Ph.D. I owe Dr. Nelson a debt of gratitude.

I would like to heartily thank Dr. Erin E. McClelland. She has been a well-wisher and mentor to me. I cannot forget her encouragement and support in the earliest days of my Ph.D. She nurtured me when I was overwhelmed by the gravity of the responsibilities and culture shift that I experienced. Dr. McClelland has significantly assisted me through this project, and I appreciate the numerous pointers and advice she offered me, including the non-academic ones.

I am equally grateful to Drs. Rebecca L. Seipelt-Thiemann, Mary B. Farone, and Anthony L. Farone for their time, support, and willingness to help me through the research. It would not have been possible to reach this far without their constant guidance. Special mention to my fellow Ph.D. candidates for their constant backing.

My lab partners – Prianca Griggs, Grace E. Millican, and Maria E. L. Hite, were extremely cooperative, responsible, and accommodating. I would like to extend my deepest thanks to them as they have been vital cogs in this research.

I thank the MOBI program, the biology department, and especially the program director Dr. Jason Jessen, for constantly working toward the students' welfare. I'm immensely grateful for all the financial and administrative assistance provided by them.

Last but not least, I would like to thank my everlasting friends and family- my parents, Subramani and Mallika, my brother, Nathan Subramani, and my sister-in-law, Sunita Sharma, who have stood by me through thick and thin. They have been my pillar of strength when confronted with challenges, and I am at a loss for words to express my gratitude to them.

ABSTRACT

The fungal pathogen *Cryptococcus neoformans* (*Cn*) causes 220,000 cryptococcosis cases and 181,000 deaths annually, mostly in immunocompromised people. Alveolar macrophages serve as the first line of defense against *Cn*, which typically enters the body as inhaled propagules and is critical to the outcome of the infection. The ability of macrophages to eliminate *Cn* is influenced by their polarization state, a set of transitory phenotypes characterized by the altered expression of >1000 genes, with macrophages polarized to the proinflammatory M1 state by IFNγ-stimulation exhibiting the highest fungicidal activity. RNA sequencing-based transcriptome profiling was employed to assess if *Cn* impacts the expression of M1-associated genes in RAW264.7 macrophages. Intracellular infection partially reverted the gene expression profile to a naïve (M0)-like state. To ascertain the mechanism underlying this gene expression, transcriptional regulators were identified among the differentially expressed genes (DEGs) in mock vs. *Cn*-infected cells. Amongst these, CITED1 exhibited the largest fold increase in expression. CITED1 encodes a member of the CBP/p300-interacting transactivator with glutamic acid (E) and aspartic acid (D)-rich tail (CITED) family of transcriptional co-regulators. Since CITED2 inhibits M1 polarization by preventing STAT1 from recruiting the histone acetyltransferase, CBP/p300, to gene cis-regulatory sites, we hypothesized that CITED1 would have similar effects. This was tested using a loss- and gain-of-function approach coupled with RNAseq. Surprisingly, ectopic CITED1 expression increased the expression of multiple interferon-stimulated genes (ISGs), including *Ccl2*, *ifit1*, *Isg15*, and *Oas2,* and this was reversed In *Cited1* null cells. These findings imply an antagonistic relationship between CITED proteins in controlling macrophage inflammatory activity. Additionally, it was found that *Cited1* activity is regulated at multiple levels post-IFNγ stimulation. *Cited1* transcription was found to be STAT1-dependent, and IFNγ increased CITED1 phosphorylation and nuclear accumulation. Collectively, these data demonstrate that CITED1 enhances the transcriptional response to IFNγ stimulation and acts as a positive regulator of macrophage proinflammatory function.

TABLE OF CONTENTS

LIST OF FIGURES

LIST OF TABLES

LIST OF ABBREVIATIONS

Arg-1	Arginase-1
ANOVA	Analysis of Variance
BCA	Bicinchoninic Acid Protein Assay
BMDMs	Bone Marrow-Derived Macrophages
BP	Biological Process
BSA	Bovine Serum Albumin
Bst2	Bone Marrow Stromal Cell Antigen 2
C3	Complement Component 3
CBP	CREB Binding Protein
CH	Cysteine-Histidine-Rich Domains
CH1	First Cysteine-Histidine-Rich Region
CITED	CBP/P300-Interacting Transactivators with Glutamic Acid (E) and Aspartic Acid (D)-Rich Tail
CITED1	CBP/P300-Interacting Transactivators with Glutamic Acid [E]/Aspartic Acid [D]-Rich C-Terminal Domain 1
CITED2	CBP/P300-Interacting Transactivator with Glutamic Acid (E) And Aspartic Acid (D)-Rich Tail 2
CNS	Central Nervous System
CR2	C-Terminal Conserved Region 2
CREB	cAMP Response Element Binding Protein
CRs	Complement Receptors
C-TAD	C-Terminal TA
DAVID	Database For Annotation Visualization And Integrated Discovery
DEGs	Differentially Expressed Genes
DI-CITED1	Dox-Inducible CITED1
DMEM	Dulbecco's Modified Eagle Medium
DMSO	Dimethylsulfoxide
Dox	Doxycycline

DTT	Dithiothreitol
ECL	Enhanced Chemiluminescence Reagents
ER	Estrogen Receptors
EYFP	Enhanced Yellow Fluorescent Protein
FBS	Fetal Bovine Serum
FcγR	Fcγ Receptor
FDR	False Discovery Rate
GAFs	Gamma-Interferon Activated Factors
GAS	Gamma Interferon Activated Sites
GO	Gene Ontology
GS	Goat Serum
GSEA	Gene Set Enrichment Analysis
GTEx	Genotype-Tissue Expression
gRNA	guideRNA
GXM	Glucuronoxylomannan
HEK	Human Embryonic Kidney Cells
HIF1α	Hypoxia-Inducible Factor 1 Alpha Protein
HK-*Cn*	Heat-Killed *Cn*
Ifit1	Interferon-Induced Protein With Tetratricopeptide Repeat 1
Ifitm1	Interferon-Induced Transmembrane Protein 1
IFNγ	Interferon-Gamma
IKK	IκB kinase
IL-4	Interleukin - 4
INDELs	Insertions and Deletions
iNOS	Inducible Nitric Oxide Synthase
IRF3	Interferon Regulatory Factor 3

IRFs	Interferon Regulatory Factors
ISG	IFN Stimulated Genes
Isg15	Interferon-Stimulated Gene 15
ISRE	Interferon-Stimulated Response Elements
JAK1	Janus Kinase 1
JAK-STAT	Janus Kinase Signal Transducer and Activator of Transcription
KEGG	Kyoto Encyclopedia Of Genes And Genomes
LPS	Lipopolysaccharides
M0	Naïve Macrophages
M1	Classically Activated Macrophages
M1mk	M1 Mock
M2	Alternatively Activated Macrophages
M2mk	M2 Mock
Mab	Monoclonal Antibody
MH-S	Murine Alveolar Macrophage Cell Line
MOI	Multiplicity of Infection
Msg1	Melanocyte-specific gene 1
Mx1	MX Dynamin-Like GTPase 1
NEAA	Non-Essential Amino Acids
NES	Nuclear Export Signal
NF-κB	Nuclear Factor Kappa-Light-Chain-Enhancer Of Activated B Cells
NK	Natural Killer
NO	Nitric Oxide
Nos2	Nitric Oxide Synthase 2
Oas1	2'-5'-Oligoadenylate Synthase 1
PAMPs	Pathogen-Associated Molecular Patterns

PBMCs	Human Peripheral Blood Mononuclear Cells
PBS	Phosphate-Buffered Saline
PCR	Polymerase Chain Reaction
PKC	Protein Kinase C
PMNs	Human Polymorphonuclear Neutrophils
PMSF	Phenylmethylsulfonyl Fluoride
PRRs	Pattern Recognition Receptors
PTH	Parathyroid
qRT-PCR	Quantitative RT-PCR
RIPA	Radioimmunoprecipitation Assay
RNS	Reactive Nitrogen Species
ROS	Reactive Oxygen Species
RT-PCR	Reverse Transcriptase Chain Reaction
sgRNA	Short Guide RNA
SH2	Phospho-Tyrosine-Binding Src-Homology-2
SID	Smad-Interacting Domain
Socs	Suppressor of Cytokine Signaling 1
SRTF	Signal-Regulated Transcription Factor
STAT1	Signal Transducer and Activator of Transcription 1
TAD	Transactivation Domain
TAE	Tris-Acetate-EDTA Buffer
TBS-T	Tris-Buffered Saline with 0.05% Tween
TF	Transcription Factor
TLRs	Toll-Like Receptors
TNF	Tumor Necrosis Factor
TXNIP	Thioredoxin-Interacting Protein

YPD	Yeast Peptone Dextrose
β-ME	β-Mercaptoethanol
λ PP	Lambda Protein Phosphatase

CHAPTER ONE: INTRODUCTION

1.1. *Cryptococcus neoformans* (*Cn*)

1.1.1 Cryptococcosis

Over the course of the last ~ forty years, the AIDS pandemic has contributed to an increase in the relevance of opportunistic infections in the field of medicine. *Cryptococcus neoformans* (*Cn*) is the causative agent of cryptococcosis, a life-threatening fungal meningitis that mostly affects people with HIV/AIDS, organ transplantation, and cancer (1–3) (Fig 1.1). Meningitis caused by *Cn* is responsible for around 15 % of all AIDS-related fatalities annually (4). This basidiomycetous fungus is commonly found in various environmental niches such as pigeon droppings, soil, and decaying wood across the globe and is responsible for causing illness in more than 220,000 individuals each year (3,4). The majority of cryptococcal meningitis instances occur in sub-Saharan Africa and are considered one of the major causes of mortality among HIV/AIDS patients in this region. Since these infections are spread by inhalation of spores, the lungs are usually the initial site of infection for *Cn*. However, it is also capable of colonizing any organ in the human body, including the central nervous system (CNS).

Infections caused by the fungus may be asymptomatic, acute, or chronic. Conversely, in people with healthy immune systems, *Cn* may be eliminated by the body's defense mechanisms or stay dormant inside the host cells, typically macrophages, for extended periods of time without causing overt symptoms (5,6). However, as an opportunistic pathogen, *Cn* infections are more frequently detected in immunocompromised individuals. Typically starting as a pulmonary infection, *Cn* disseminates from the lungs to multiple organs, establishing a systemic infection,

referred to as cryptococcosis. When this involves the CNS, it can result in meningoencephalitis and death (7).

Antifungal therapies are widely available; however, the emergence of drug-resistant and virulent strains makes the treatment of the disease challenging (8). Immunomodulatory medications may need to be included in treatment strategies to successfully control cryptococcosis. For this reason, it is very important to have a solid understanding of the cellular and molecular processes underlying host responses to *Cn* to successfully treat *Cn* infections.

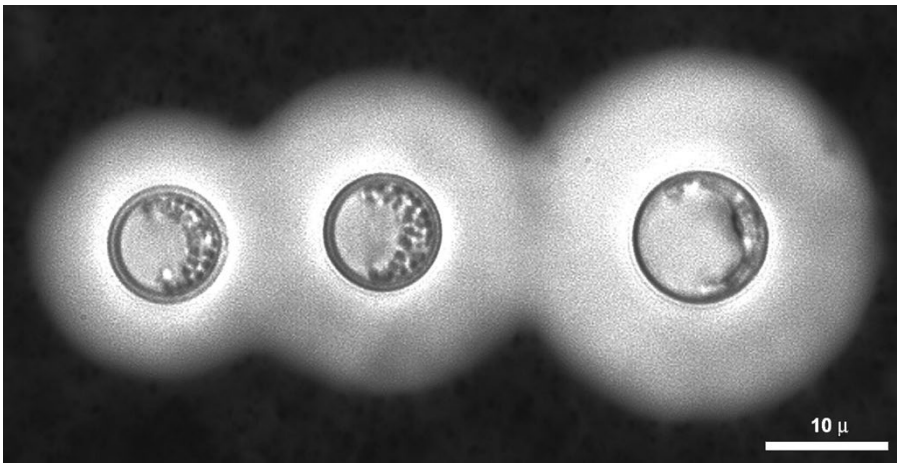

Figure 1.1: India ink-stained picture of *C. neoformans* showing different sizes of the polysaccharide capsule. The image was taken by Dr. Erin E. McClelland.

1.2. Innate Immune Responses to *Cn*

For a host to successfully clear *Cn* and prevent cryptococcosis, both the innate and adaptive arms of the immune system most function in concert (9). The most important

facets of the immune response against *Cn* involve T cells, natural killer (NK) cells, complement, antibodies, and macrophages (10–16). While $CD4^+$ and $CD8^+$ T cells are essential in eliminating the infection (17–19) the non-specific host immune response to *Cn* is primarily regulated by the complement system and phagocytic cells (20,21). Innate phagocytic cells not only play a crucial role in the elimination of the bulk of encountered *Cn* cells but also stimulate adaptive immunity via antigen presentation (3).

1.2.1 Phagocytosis and Host recognition of *Cn*

When fungal spores are inhaled and enter the lungs, they come in contact with a number of different phagocytic cell types, including macrophages, dendritic cells, and neutrophils. The ability of these cells to contain *Cn* is critical for host defense (22–24). Once phagocytosed, *Cn* is captured within a membranous organelle known as a phagosome, which is created by the invagination of the surface membrane of the host cell. These fuse with lysosomes to form phagolysosomes, acidified compartments containing acid hydrolases capable of enzymatically degrading and eliminating internalized microorganisms. The acidic environment, which is crucial for the activity of the hydrolytic enzymes, is maintained through the activity of a large number of transmembrane proton pumps known as V-ATPases.

For phagocytes to internalize a pathogen, they need to be first recognized. This is achieved by pattern recognition receptors (PRRs) present at the plasma membrane (and within phagosomal compartments). For *Cn*, these include Toll-like receptors (TLRs), mannose receptors, and β-glucan receptors and recognize fungal pathogen-

associated molecular patterns (PAMPs), such as mannoproteins, chitin, and glucuronoxylomannan (GXM).

The anti-phagocytic polysaccharide capsule is the major virulence factor that contributes to the pathogenicity of *Cn* (25). The capsule is mainly composed of GXM, but also contains smaller quantities of galactoxylomannan and mannoproteins and is secured to the cell wall by glucans (26). While capsular GXM can be recognized by TLR2 and TLR4 (27,28), it is currently thought that these receptors play a minimal role in response to *Cn* infection (29). The most compelling evidence for specific TLR participation in the host response is reported for TLR9, which is recruited to *Cn*-containing phagosomes (30,31). In comparison with WT mice, cryptococcal infection in TLR9 KO mice resulted in a reduction of cytokines, including IFNγ and tumor necrosis factor (TNFα), and high levels of interleukin-4 (IL-4) (30). Enhanced IL-4 in *Cn*-infected TLR9 KO mice elevated anti-inflammatory markers, such as arginase and FIZZ1, and decreased the proinflammatory marker inducible nitric oxide synthase (iNOS). This reduction in iNOS increased the fungal burden in the lungs and compromised the clearance of *Cn*. Carbohydrates, like mannan and β-glucans on the fungal cell surface, are typically sensed by the C-type lectin receptor Dectin-1, which has been shown to be required to mediate antifungal immunity (32,33). However, these are not likely important in the protection of the host (34).

Cn phagocytosis by innate immune cells is considerably enhanced by opsonization with complement or antibodies that bind capsular components. Complement component 3 (also known as C3) binds to the *Cn* capsule (35,36). The

interaction between *Cn* and human macrophages *in vitro* is significantly reduced when complement receptors (CRs) CR1, CR3, and CR4 are blocked (37). Similarly, Fcγ receptors (FcγR) enable macrophages to bind and engulf IgG-opsonized yeast (38,39). In situations when these opsonins are present, the antiphagocytic property of the capsule is often reduced (40). Thus, the opsonization of *Cn* is essential for efficient phagocytosis by immune cells (41,42).

1.2.2 Macrophages

Macrophages are immune cells that are widely distributed and play a fundamental role in maintaining tissue homeostasis and defense. Derived from monocytes, they are tissue-resident phagocytic cells of the innate immune system, which include alveolar macrophages (43). Since the most common route of exposure to *Cn* infection is through inhalation of spores, alveolar macrophages are regarded as the first line of defense against *Cn*. These macrophages are responsible for internalizing *Cn* and help integrate innate immunity with humoral immunity. Fungal cells are present within lung macrophages of cryptococcosis patients (44), suggesting that macrophages ingest *Cn* cells soon after pulmonary infection.

Following uptake, macrophages have dual roles in *Cn* infections. In murine models of cryptococcosis, macrophages are essential for the successful clearance of *Cn* (45,46). Additionally, they are effective in eliminating *Cn in vitro* (47,48). The fungus has evolved strategies to manipulate host macrophages and treat them as a niche for long-term persistence and dissemination (41,49–52). However, macrophages may also

facilitate the dissemination of *Cn* from the lung (53). In this regard, macrophages have been suggested to operate as a "Trojan horse" and may be instrumental in the passage of *Cn* across the blood-brain barrier (41,51,54–56).

1.2.3 Macrophage Polarization

In the most severe cases of cryptococcosis, fungal infections lead to the recruitment of monocytes and macrophages via a Th1 response (57,58). While monocytes and macrophages play a significant part in preventing *Cn* from spreading throughout the body, the activation state of the macrophage determines whether or not the pathogen survives inside macrophages (59).

Macrophage polarization is a dynamic process through which macrophage phenotypes are changed in response to exogenous signals (microbial ligands) and endogenous cytokines (Fig 1.2). Macrophages adopt the classically activated or 'M1' state when they are exposed to interferon-gamma (IFNγ) or bacterial lipopolysaccharide (LPS), individually or in combination. In this state, there is an increase in the expression of the Nitric oxide synthase 2 (*Nos2*) gene, which encodes iNOS, an enzyme that produces nitric oxide (NO) (60,61). NO contributes to the microbicidal action of M1 cells through the formation of toxic reactive nitrogen (RNS) and oxygen species (ROS) (62). In addition, the acidification of the phagosome and the depletion of iron and other nutrients required by the pathogen are additional aspects

of the anti-microbial activity of the M1 state (61,63,64). All of these actions improve the ability of macrophages to eliminate phagocytosed pathogens, including *Cn* (60,65).

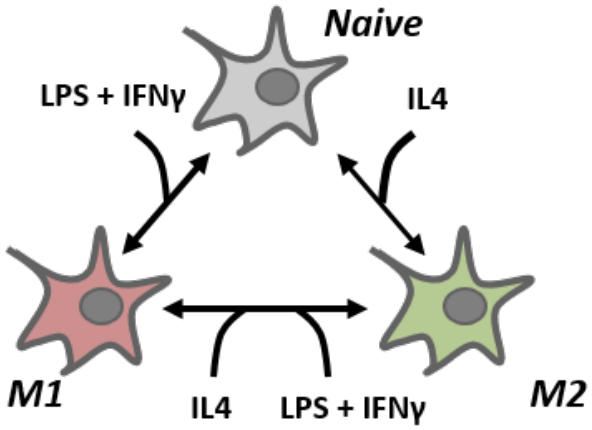

Figure 1.2: Plasticity of Macrophage Polarization. Naïve (M0) macrophages can be polarized to pro-inflammatory M1 or anti-inflammatory M2 state through exposure to IFNγ or IL-4, respectively.

It is widely established that classically activated macrophages are vital components of host defense against intracellular pathogens (53,66–68). Studies using IFNγ-deficient mice have an uncontrolled proliferation of bacterial (*Mycobacteria*, *Salmonella typhimurium*), protozoan (*L. major*, and *Toxoplasma gondii*), and viral infections (HIV, Hepatitis C) with increased morbidity (69–72). Moreover, infection of mice with genetically engineered *Cn* strains expressing murine IFNγ has conclusively shown induction of classically activated macrophages, a protective immune response,

and improved clearance of the pathogen (73). Therefore, a macrophage Th1 immune response and the production of associated cytokines are required in order to successfully control *Cn* infections, demonstrating that the activation state of the macrophage is a crucial factor in determining both the success of phagocytosis and the fate of infection (38,74).

Alternatively activated (M2) macrophages are polarized by Th2 cytokines, such as IL-4 and IL-13, and secrete anti-inflammatory cytokines. The M2 phenotype is a regulatory and wound-healing phenotype, which normally occurs after infections are resolved (75). Microbicidal activity in the M2 state compared to that observed in M1 macrophages is due to the down-regulation of iNOS and the increased expression of arginase-1 (Arg-1) (75,76). Arg-1 is an essential enzyme of the urea cycle and is involved in the detoxification of ammonia; it also competes with iNOS for the same substrate, L-arginine (77). L-ornithine, a product of arginase activity, switches the metabolic pathway of NO to the production of proline and stimulates cell growth, collagen, and tissue formation (77,78). This ratio of iNOS to Arg-1 helps define, at least in part, macrophage phenotype and the induction of each polarization state. Intracellular pathogens, like *Cn,* are sensitive to the NO produced by M1 host cells. For this reason, many of these pathogens have evolved mechanisms to inhibit the signaling pathways that regulate M1 polarization and suppress iNOS expression. This results in M2 polarization of host cells and impairs anti-cryptococcal activity (61,66,76,79,80). An increasing body of research demonstrates that macrophages infected with *Cn* alter their response to an M2 state and increase the production of Th2 cytokines, such as IL-

4, IL-13, and IL-5 (30,76,79). The M2 state is inefficient in killing *Cn* cells and is utilized by the yeast as a protected niche to avoid being recognized by the host immune response, resulting in the progression of cryptococcosis in the brain (80,81).

In an *in vivo* study conducted in a chronic respiratory infection model, macrophages shifted from an M2 phenotype (*Arg1*) to an M1 phenotype (*Nos2*) and then back to a naive state (82). How *Cn* contributes to these changes remains enigmatic. *In vitro* studies using *Cn*-infected macrophages indicated that *Cn* has minimal impact on the polarization state of host macrophages when assayed using the expression of *Nos2* and *Arg-1* transcripts as markers of the M1 and M2 states, respectively. Rather, the effect of IFNγ and IL-4 are dominant and stimulate the repolarization of macrophages, regardless of *Cn*-infection status (50,76,82). These data are indicative of the significance of the cytokine microenvironment in the process of promoting macrophage polarization and that macrophage-*Cn* interaction is not the only factor (76). Although these previous studies looked at how intracellular *Cn* infection alters macrophage gene expression, they only evaluated a very small number of M1 and M2 markers using microarray/qPCR. Given that polarization involves transcriptional reprogramming, the effect of intracellular *Cn* on the host cell cannot be completely understood by examining changes in the expression of a limited number of M1 and M2 markers by themselves. Appraising the broad transcriptome changes will lead to the identification of potential regulators of macrophage-*Cn* interactions. Therefore, targeting these host immune responses in the future by promoting M1 activation and/or attenuating M2

macrophage activation might be a feasible strategy or innovative method that may be adopted as a treatment against cryptococcosis.

1.2.4 Macrophage-*Cn* interactions

Over the course of the last decade, it has become more evident that macrophages play an important and multifaceted role in response to cryptococcal infections. This role is associated with direct interactions of macrophages and *Cn*, particularly those events occurring after phagocytosis. Once internalized, several outcomes are possible (Fig 1.3); (i) *Cn* is killed intracellularly by the macrophages (3,66,83,84), (ii) the yeast utilizes the host cells as an intracellular growth niche, or (iii) the yeast escapes from the host cell by non-lytic exocytosis (Fig 1.3).

Survival within host macrophages is likely possible as *Cn* disrupts phagolysosome maturation, possibly due to the premature removal of Rab5 and Rab11 (85). Furthermore, it promotes phagolysosomal leakage, compromising the microbicidal action of this compartment and preventing its proper acidification (41,49). This partially acidified state may provide an enhanced growth environment for *Cn*, which is known to survive in and even prefer low pH environments (86). Possibly due to the loss of phagolysosome membrane integrity that accompanies intracellular residence of *Cn*, the accumulation of cytoplasmic vesicles that contain fungal capsular polysaccharides and proteins has been detected in host cells (41). The effect of these on macrophage function is currently unclear but is an active area of investigation for labs in the *Cn* field. Additionally, intracellular *Cn* proliferation may result in macrophage

(41,49,87). The mechanical rupture of cell membranes is triggered by the enlargement of the fungal capsule and the active multiplication of the fungus. The presence of *Cn*-derived cytoplasmic vesicles and phagolysosome destruction by *Cn* may compromise macrophage function, contributing to host cell lysis.

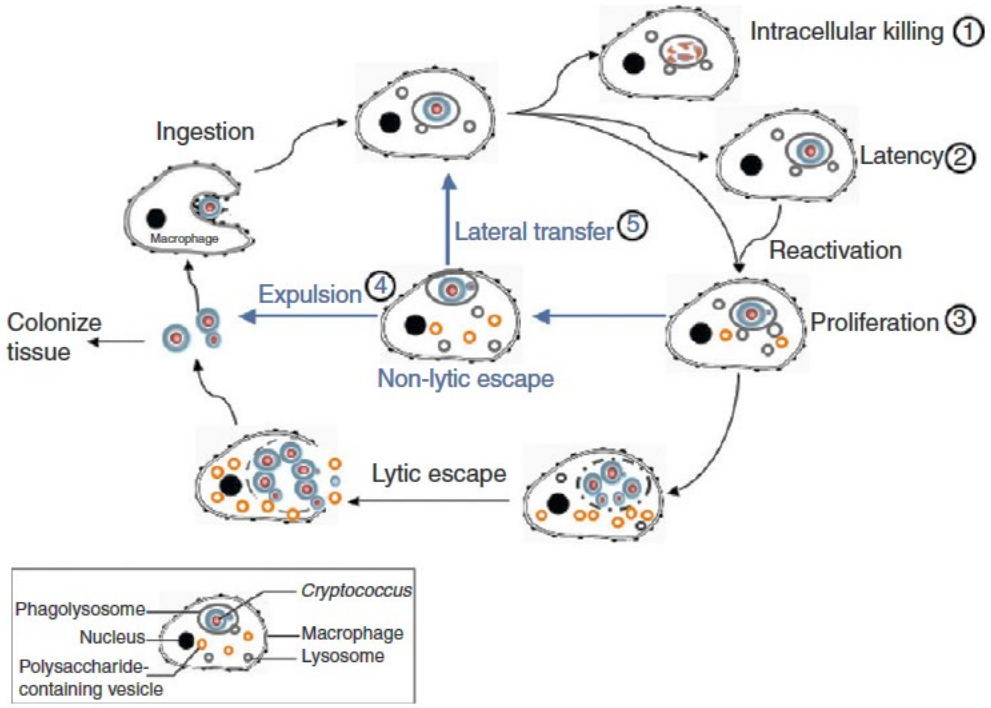

Figure 1.3: Schematic representation of macrophage-*Cn* interaction. Figure showing intracellular parasitism by *Cn* and the different predicted outcomes during the interaction. From Ma and May 2009 (Ma et al., 2009b).

Cn escapes from macrophages by a unique process called vomocytosis, a non-lytic expulsion that releases *Cn* cells without causing the death of both players (51,88). The release of *Cn* cells from macrophages through this process is accompanied by the

development of large vacuoles in the cytoplasm of the host cell (89). In addition to being viable, expelled *Cn* may also be ingested again by adjacent cells (51,56,90). This has been demonstrated in another event where yeast cells move from one macrophage to another without exiting into the extracellular environment (89,91). This process, known as lateral transfer, together with expulsion, is believed to be involved in helping the yeast to migrate from the lungs into the bloodstream and cross the blood-brain barrier by treating macrophages as part of the "Trojan horse" mechanism. Employing macrophages as a trafficking carrier may establish long-term latent infections, which later become active when the immune system is weakened (9,92,93).

Studies using mouse models have reported fluctuations in intra- and extra-cellular residency of *Cn* during the initial stages of infections but a transition to intracellular alone in the later stages of infection. This was accompanied by a higher budding index, indicating that *Cn* proliferates at a faster rate in an intracellular environment (41). Additionally, studies using animal models have shown that different rodent systems respond to cryptococcosis in diverse ways. Respiratory infection of rats leads to increased production of reactive oxygen species (ROS) and lysozyme, resulting in better resistance to *Cn* (6,94). Mouse susceptibility to *Cn* infection is determined by the virulence of the *Cn* strains (95,96). Infection of C57BL/6 mice with the less virulent strain results in Th1 immune responses, whereas mice infected with a high virulent strain develop a Th2 immune response, which results in lower *Cn* clearance and ultimately exhibited increased mortality (97–100).

1.3. Signaling pathways in macrophage polarization

Macrophage polarization involves broad transcriptional reprogramming consisting of 757 genes that are differentially expressed between M0 and M1 macrophages and 436 genes between M0 and M2 macrophages (101,102). These changes in gene expression that define the different polarization states are largely determined by the activation of IFNγ/IL-4 stimulus-specific transcription factors. These transcription factors regulate macrophage polarization by binding to gene promoters to initiate stimulus-specific modification of macrophage phenotype. In this section, we will describe the most important transcription factors responsible for transducing information from the cytokine milieu into an activated macrophage phenotype (Fig 1.4).

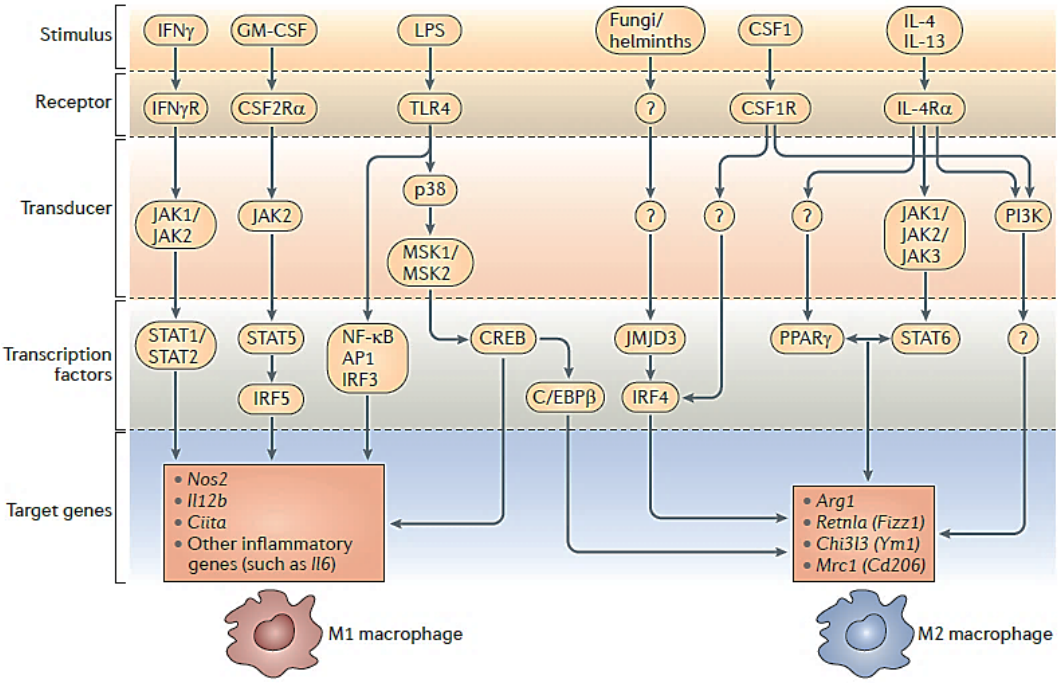

Figure 1.4. Cell signaling pathways in macrophage polarization. Activation of receptor-specific transcription factors initiated by various internal and external cues that mediates the changes in pro- and anti-inflammatory genes. From Lawrence & Natoli, 2011.

1.3.1 The JAK-STAT family

The cytokine-mediated activation or repression of genes is the primary mechanism via which cytokines exert their biological effects. The cytokine, IFNγ, has a significant function in both the innate and adaptive immune systems (71,103). It may also function to increase the production of ROS and RNS in addition to enhancing antigen presentation as part of the response to infectious diseases (104,105). STATs are important signaling molecules in the polarization of macrophages. Specifically, STAT1 (signal transducer and activator of transcription 1), activated via IFNγ, and STAT6, via IL-4, are the critical modulators of M1 and M2 macrophages, respectively. Accordingly, active STAT1 is required for proper M1 macrophage polarization (67,106–108). STAT1 activation begins with IFNγ binding to the specific cell surface receptor, consisting of two subunits called IFNGR1 and IFNGR2, to activate the receptor-associated tyrosine kinases Janus kinase 1 (JAK1) and JAK2 through phosphorylation (109). Activated JAKs phosphorylate the cytoplasmic domains of the IFNGR1 protein creating a docking site for the recruitment of cytosolic transcription factor STAT1 (110). Here, STAT1 proteins are phosphorylated and form transcriptionally active homodimers, known as γ-activated factors (GAFs), that translocate to the nucleus to promote the transcription of IFNγ-stimulated genes (ISGs) by binding to γ-activated sequences (GAS) in the promoter region of target genes.

The interaction between macrophages and lymphocyte derived IFNγ is essential for generating a protective immune response to pathogens (106,111). Signaling via the

IFNγ-JAK1/2-STAT1 pathway is required for resistance to infection with intracellular pathogens, such as *Toxoplasma gondii*, *Mycobacterium tuberculosis*, and *Listeria monocytogenes* (112–114). It is plausible that the JAK/STAT pathway might be altered by *Cn* infection since it is a significant inducer of the M1 polarization of macrophages. In mice with macrophage specific STAT1 ablation, infection with *Cn* strain H99γ induced significant inflammation of the pulmonary region and dysfunctional microbicidal activities, and also increased fungal burden (67,76,107). Previous findings have shown that STAT1 signaling is necessary for NO production, and when NO levels are reduced because of STAT1 or iNOS deletion, an increase in fungal load was seen (115,116). During mycobacterial infections, IFNγ-induced downstream transcriptional responses are inhibited, resulting in disrupted association of STAT1 dimers with its related co-activators, such as cAMP response element binding protein (CREB) and p300 (117). The reduced interactions have been shown to compromise macrophage activity during infections (118). Understanding the function of STAT1 and its downstream effectors in promoting defense against *Cn* and other intracellular organisms may help develop innovative immunological treatments targeting hosts to treat conditions like cryptococcosis.

1.3.2 The IRF family

Interferon regulatory factors (IRFs), first identified from their activity as regulators of the genes encoding type I IFN, bind to the promoter region of the human interferon-

β gene (119). The IRF gene family in mammals is composed of nine different members: IRF-1, IRF-2, IRF-3, IRF-4, IRF-5, IRF-6, IRF-7, IRF-8, and IRF-9. IRF proteins are functionally active as either homo or heterodimers exhibiting considerable N-terminal homologies. This region shares a conserved tryptophan pentad repeat DNA-binding domain that recognizes consensus DNA sequence, referred to as interferon-stimulated response elements (GAAA and AANNNGAA) (120–122). However, the functional specificity and ability to interact with one another through IRF-association domains are all governed by the variable domains at the C-terminus of these proteins (121,123,124).

Activation of the IFNγ receptor triggers the expression, nuclear translocation, and transcriptional activity of other signal-regulated transcription factors (SRTFs), including IRFs. Following the engagement of the IFNγ receptor and homodimerization of phosphorylated STAT1 proteins, GAFs initiate transcription of ISG by binding to GAS promoter elements (125). This includes IRF gene family members, like *irf1* and *irf8,* and their production is required to regulate other secondary genes, including the M1 marker, *Nos2* (126–128). Macrophages having a mutation in either *Irf1* or *Irf8* are more susceptible to infection with intracellular pathogens (129–131). This suggests that *Irf1* expression is required for macrophages to initiate their microbicidal action. A number of important macrophage functions, such as the production of costimulatory molecules, cytokines, and chemokines, are inactivated by the loss of IRF1 function (127).

STAT1, which is phosphorylated by IFN-II, forms homodimers, binds to GAS sites in ISG promoters, and promotes the first wave of IFNγ-regulated gene expression. The second wave of gene expression is regulated by the IRF1 gene and newly generated IRF1 proteins, which bind to interferon-stimulated response elements (ISRE) and IRF-response elements in ISG promoters (Fig. 1.5). IRF1, induced by STAT1 during the IFNγ response, work together and bind to coupled ISRE and GAS-containing regulatory regions resulting in positive feedback control of the STAT1 and IRF1 genes (132–135). These two players are critical regulators of inflammation associated with multiple sclerosis, inflammatory bowel diseases, and rheumatoid arthritis, in addition to their roles in pathogenic diseases (136–139). Therefore, a more profound comprehension of the transcriptional mechanisms that IRF1 and STAT1 activate in response to IFNγ may provide new insights into the molecular mechanisms governing inflammation and infections, eventually identifying potential targets for therapeutic intervention.

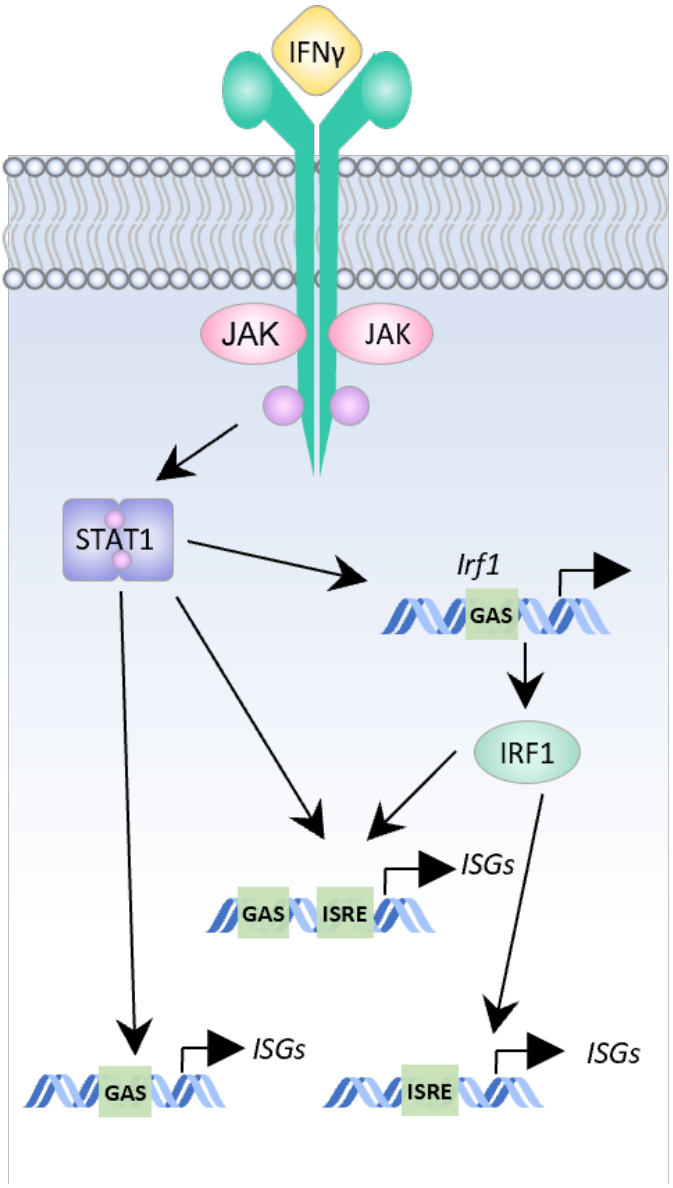

Figure 1.5. Cooperation of STAT1 and IRF1 in regulating Interferon stimulated genes. STAT1 homodimers bind to GAS-containing ISGs, and IRF1 recognizes ISRE-containing ISGs. Both of these transcription factors participate together in the enhanced expression of ISRE and GAS-containing ISGs.

1.3.3 The NF-κB family

The nuclear factor kappa B (NF-κB) pathway is ubiquitous in mammalian systems and is present in almost all cell types, regulating how cells react to infections and cellular stress (140). The NF-κB pathway includes a series of hetero and homo dimeric transcription factors, which can be further classified into two interconnected arms, the canonical RelA (p65)-containing NF-κB dimers and the non-canonical RelB-containing factors (140,141). While NF-κB heterodimers (for example, p65/p50 subunits) are typically sequestered in the cytoplasm in an inactive state by IκB inhibitory proteins, upon stimulation with signals, such as proinflammatory cytokines (TNFα, IL- 1β) or bacterial (LPS) or viral components. Through a series of intermediary stages, this binding results in an association with the IκB kinase (IKK) complex, which leads to the phosphorylation of IκB, followed by ubiquitination and degradation of IκB (142–144). NF-κB dimers then translocate to the nucleus, promoting transcription of NF-κB target genes (145,146). In macrophages, the NF-κB pathway is a major regulator of M1 polarization and the canonical route is of utmost significance for maintaining cell viability.

NF-κB activity is a double-edged sword during intracellular infections, benefiting both the host and the pathogen. For example, during gram-negative bacterial infections, LPS from the bacterial outer membrane activates the canonical NF-κB pathway by binding to TLR2 or TLR4. While this increases microbicidal activities by triggering the production of proinflammatory cytokines and *Nos2*, amongst other genes

(147–149), it also enhances the expression of anti-apoptotic genes, such as *Bcl-2* (150,151). For this reason, persistent NF-κB activation may prolong the survival of infected cells, maintaining an intracellular residence and proliferation niche for the pathogen. A wide variety of pathogens, including *Salmonella* (152–154), *Legionella pneumophilia* (155–157), and *Toxoplasma gondii* (158,159) have been shown to modulate NF-κB throughout the infection process. Additionally, invasive bacteria, such as *Mycobacterium tuberculosis* (160,161) and *Shigella* (162), target NF-κB by inhibiting apoptosis, thus remaining latent in the host.

Several groups, including ours, have studied the impact of *Cn* on NF-κB signaling over the last decade (146,163–167). Ben Abdallah's group demonstrated that *Cn* affects both canonical and noncanonical NF-kB signaling to promote fungal-induced macrophage cell cycle arrest and apoptosis (146). Our team focused on determining whether intracellular *Cn* reduced LPS-induced NF-κB activation and, if so, how that data contrasted to that obtained from other studies that used purified GXM (167). This investigation instead showed that GXM and intracellular *Cn* had opposite effects on the LPS-induced NF-κB signaling, with purified GXM acting as an antagonist of LPS-stimulated p65 nuclear translocation and intracellular *Cn* prolonging stimulus-dependent and independent p65 nuclear residence. Despite the increased nuclear p65 observed in *Cn*-infected cells, particularly those with a high fungal burden, it was not accompanied by the expression of a mCherry reporter of *Tnf* expression. These findings are interesting and may explain why *Cn*-containing granulomas exhibit a lower-than-expected inflammatory profile.

Despite the fact that NF-κB and STAT1 are each activated by different ligands, such as TNF/LPS and IFNγ, respectively, these pathways cooperate to control the activation of several inflammatory genes, including *Nos2* (168–172). The synergy between these transcription factors is regulated by coactivators, like CREB binding protein (CBP) or its paralog p300, by recruiting general transcription machinery to the promoter, therefore increasing gene expression (173). Studies also demonstrated that STAT1 and NF-κB simultaneously interact with the N- and C- terminal regions of CBP and may recruit RNA polymerase II to the promoter of genes such as *Cxcl9* (174). Therefore, detailed knowledge of the mechanisms of how these pathways are controlled individually or overlapped to increase the transcriptional activation of genes is essential to study the changes in the fate and function of *Cn*-infected macrophages.

1.4. The CITED family of transcriptional co-regulators

As previously mentioned, STAT1 and NF-κB play a significant role in controlling M1 polarization, although other transcription factors, including hypoxia-inducible factor 1 alpha (HIF1α) (175–177), STAT2 (178), and p53 (179–181) may either enhance or suppress the proinflammatory and microbicidal activities of macrophages. It is noteworthy that all of these transcription factors control gene expression, in part by recruiting the histone acetyltransferase, CBP/p300, to gene promoters (182–185). However, the interaction between these transcription factors and CBP/p300 may be strengthened or weakened through the action of transcriptional co-regulators,

including members of the CBP/p300-interacting transactivator with glutamic acid (E) and aspartic acid (D)-rich tail (CITED) family of proteins.

Like all transcriptional co-regulators, the CITED proteins cannot bind DNA directly and are reliant on their associations with CBP/p300 and transcription factors for activity. In mammalian systems, the CITED family of transcriptional co-regulators is composed of four members: CITED1, 2, 3, and 4 (186–190). CITED1,2 and 4 are involved in a range of biological processes, such as melanocyte pigmentation (189) and kidney development (191). These proteins operate as a corepressor or coactivator by preventing or promoting the recruitment of CBP/p300 to transcription factor-chromatin complexes, impacting gene expression. These interactions require the presence of a C-terminal conserved region 2 (CR2) domain, which is common to all proteins in the CITED family (192), in addition to an unstructured N-terminal region that differs between CITED proteins. While the CR2 domains are responsible for binding to the cysteine-histidine (CH; also known as TAZ) domains inside CBP/p300 (Fig 1.5), the distinct N-terminus of each CITED family member is responsible for facilitating interactions with various sets of transcription factors. Thus, CITED proteins function as adaptors to stabilize transcription factors:CBP/p300 complexes. However, in circumstances where transcription factors interact with CBP/p300 through the same CH domain as the CITED protein, they may also inhibit the formation of other complexes in a competitive manner. This section discusses how these proteins control gene expression in macrophages.

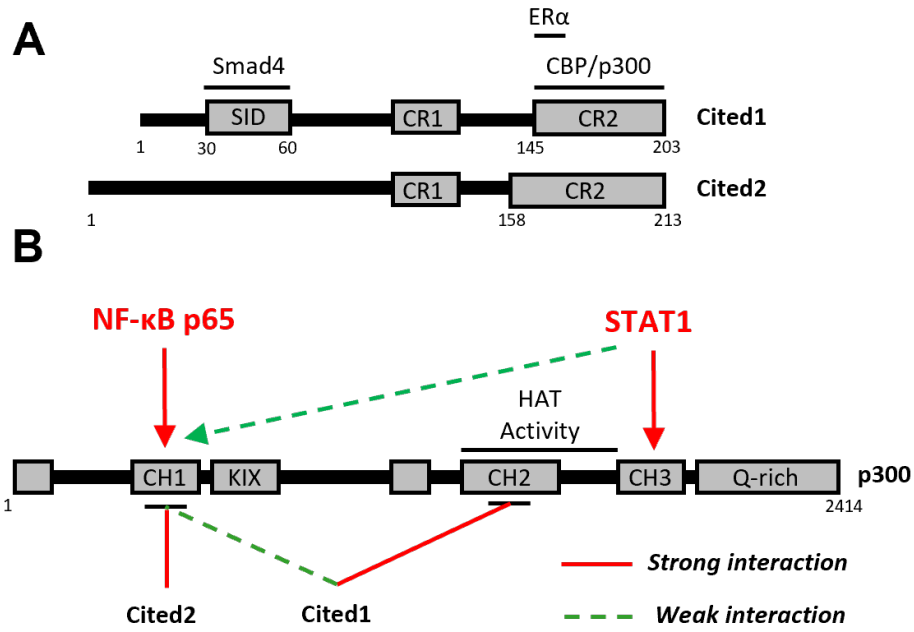

Figure 1.6: CITED1 and 2 as regulators of CBP/p300 complexes. (A) Peptide maps of CITED1+2 protein. (B) Interaction sites of transcription factors with p300. Adapted and modified from Yahata T 2000 JBC, Shi G 2006 JBC.

1.4.1 CITED2

The CBP/p300-interacting transactivator with glutamic acid (E) and aspartic acid (D)-rich tail 2 (CITED2) functions as a fundamental negative regulator of inflammatory gene expression that operates by modulating the activities of numerous transcription factors, including HIF1α, SMAD2/3, LHX2, and HNF4a (193–196). More recently, studies have revealed that CITED2 is abundantly expressed in human and murine macrophages

and has a critical role in inhibiting proinflammatory gene expression in this context (197). Here, CITED2 both cooperates with PPARγ to increase the expression of genes involved in anti-inflammatory processes and decreases the expression of genes involved in proinflammatory processes in macrophages by inhibiting STAT1, IRF1, and NF-κB-regulated gene expression.

Unlike CITED1 and 4, which are either undetectable or present at very low levels in naïve macrophages, CITED2 is constitutively expressed, likely as a mechanism to prevent inappropriate activation of macrophages. Additionally, it has been shown to limit LPS-induced proinflammatory gene expression in these cells by blocking NF-κB and HIF1α transcriptional activity (197,198). CITED2 has been shown to interact with a broad range of transcription factors (193,196,199). Transcriptomic investigations have demonstrated that CITED2 loss greatly increases the expression of proinflammatory genes controlled by NF-κB, STAT5, and STAT3. (198). As IRFs and STATs interact with each other to regulate the expression of inflammatory genes (134), it was expected that IRF family members (IRF1,2 and 9) are also impacted by CITED2 loss (198). Altogether, these data suggest that CITED2 inhibits proinflammatory gene expression by repressing the activities of the above transcription factors in myeloid cells.

CITED2 is a CBP/p300-dependent transcription factor that binds directly and with a high affinity to the first cysteine-histidine-rich (CH1) region of both p300 and CBP (182). The binding of the CITED2 CR2 domain to the CH1 domain disrupts complex formation between HIF1α C-terminal TAD (C-TAD) and CBP/p300, thus suppressing

HIF1 transcriptional activity (182,196,200). Given that the TAD region of the NFκB-p65 subunit directly interacts with the TAZ1 domain of the CBP/p300 complex, several groups have investigated if CITED2 alters the recruitment of NFκB-p65 to target pro-inflammatory gene promoters in macrophages. These studies demonstrated that the CITED2 protein represses NF-κB activities by blocking its recruitment to the CBP/p300 CH1 domain (182,201,202). By functioning as a competitive inhibitor of this interaction, CITED2 also prevented CBP/p300-dependent acetylation of p65-containing NF-κB transcription factors, reducing the ability of these to be associated with enhancer sequences.

In addition to its effects on NF-κB, CITED2 inhibits IFNγ-stimulated STAT1 and IRF1-regulated gene expression in macrophages. This was demonstrated using an RNAseq-based transcriptome approach in primary macrophage cultures from CITED2 deficient mice. Following an inflammatory stimulus, these CITED2-deficient cells showed elevated expression of STAT1- and IRF1-regulated ISGs involved in inflammation in macrophages (203). This was accompanied by an enrichment of STAT1 at the *Irf1* promoter. While the mechanism for this is uncertain, it is also likely to involve CITED2, again operating as a competitive inhibitor of transcription factor:CBP/p300 complex formation. Uncontrolled inflammation caused by macrophages has been linked to a variety of inflammatory and autoimmune diseases. Thus, these studies suggest that CITED2 may act as a molecular 'break' that prevents

excessive and detrimental levels of inflammation by limiting broad proinflammatory gene expression.

1.4.2 CITED1

CBP/p300-interacting transactivators with glutamic acid [E]/aspartic acid [D]-rich C-terminal domain 1 (CITED1; formerly *Msg1*) is a transcriptional regulator that is expressed in a wide range of embryonic tissues, including the heart and developing kidney (204,205). It was first identified in melanocytes and engaged in the process of enhancing TGF-β/Smad4 signaling, as well as estrogen receptor (ER)-regulated gene expression (206–208). CITED1 is expressed at high levels in adult papillary thyroid cancer (209,210), malignant melanoma (211,212), and Wilms tumor (213), which raises the possibility that it may be involved in the etiology of certain malignancies. CITED1 is also responsible for inhibiting Wnt/-catenin-dependent responses, a highly conserved system linked to different forms of cancer (214,215).

As with all CITED proteins, CITED1 does not directly interact with DNA and instead binds to CBP/p300 to promote or repress gene expression. Although CITED1 binds CH1, it has a far stronger affinity for the CH2 domain, which is associated with HAT activity (192) (Fig 1.5). The CITED1 protein has an N-terminal Smad-interacting domain (SID) that it employs to encourage the development of transcriptionally active CBP/p300:Smad complexes (192,216). The CR2 domain, however, also permits CITED proteins to function as co-repressors by blocking transcription factors from building complexes with CBP/p300.

While it is unclear how CITED1 activity is regulated in macrophages, in RAW 264.7 cells, CITED1's phosphorylation status and subcellular location play a role in its transcriptional co-regulatory function. CITED1's interaction with CBP/p300 and function as a coregulator are inhibited by phosphorylation (Serine-16, 63, 67, 71, and 137) (217). This work also indicated that CITED1 phosphorylation on numerous serine residues is dependent upon the cell cycle. Both the phosphorylation status of CITED1 and its subcellular distribution has not yet been investigated in macrophages. Additionally, it is unknown how M1-polarizing stimuli have an effect on these states.

1.4.3 Rationale to investigate CITED1

Although CITED1's involvement in macrophage activity has not been investigated, the actions of another family member CITED2 have been explored in this context and may provide helpful insights into CITED1's function in macrophage polarization. The Mahabaleshwar group at Case Western University has published multiple articles demonstrating the CITED2's ability to repress inflammatory gene expression as a response to M1 polarizing stimuli (LPS and IFNγ), thus restraining molecular, cellular, tissue, and organ damage (197,198,202,203). Considering that CITED1 and CITED2 are structurally quite similar, we postulated that CITED1 might have comparable transcriptional effects to CITED2 expression in macrophages by binding to CBP/p300 and blocking the activity of STAT1 and NF-κB. Given that these transcription factors are involved in the polarization of macrophages to the M1 state, disrupting their activity

may play a role in alterations in the macrophage transcriptome in *Cn*-infected cells (218).

1.5. Aims and dissertation statement

The hypothesis for this investigation was that *Cn* influences the transcriptome of host macrophages, affecting their plasticity and fungicidal activity. This was tested using unbiased RNA-sequencing (RNAseq)-based gene expression profiling. To identify genuine *Cn*-induced transcriptional changes, infection efficiency and culture protocols were optimized prior to transcriptome profiling. Differentially expressed genes (DEGs) were identified between control and infected states, and lists of these genes were used to identify specific pathways and biological processes affected by intracellular *Cn* in IFNγ- and IL-4-stimulated macrophages.

The second objective of this study was to identify the molecular mechanisms by which *Cn* alters gene expression in host cells. To achieve this, DEG lists were used to identify transcriptional regulators that may have contributed to *Cn*-induced changes in gene expression. Amongst these, CITED1 was selected for further characterization. Here, we used a dual gain- and loss-of-function approach to measure the impact of CITED1 expression on the M1 transcriptome. The hypothesis for this part of the investigation was that changes in the levels of this protein would impact the expression of genes regulated by transcription factors that also bind CBP/p300 via CH1. This will be tested using complementary gain- and loss-of-function manipulations paired with RNAseq-based gene expression profiling to identify CITED1-regulated genes and their effects on the M1

transcriptome. CITED1 doxycycline (Dox)-inducible and *CITED1* CRISPR Cas9 KO macrophage cell lines will be produced and validated for this purpose. Changes in the expression of genes identified by RNAseq analysis will be validated by quantitative RT-PCR (qRT-PCR).

Through the completion of these objectives, we will have determined (i) how *Cn* impacts the transcriptional profile of M1 and M2 polarized macrophages and identified genes affected by intracellular *Cn* irrespective of host cell polarization state, and (ii) determined how CITED1 expression impacts the expression of IFNγ-regulated genes. Taken together, our study is innovative and novel and will provide insights into the processes that affect intracellular *Cn* persistence and the functions of the CITED1 protein that will be helpful to the fields of innate immunity and transcriptional regulation.

CHAPTER TWO: MATERIALS AND METHODS

2.1. *Cryptococcus neoformans* (*Cn*)

2.1.1 *Cn* culture and opsonization

The serotype A *Cn* (var. *grubii*) strains of GXM-positive H99S, a GFP-expressing version of H99S (H99S-GFP; received from Dr. Erin McClelland, Marian University), and capsule mutant GXM-negative *CAP59* cultures were grown in 50 mL yeast peptone dextrose (YPD.; Thermo Scientific) with shaking at 150 RPM. H99S and H99S-GFP were cultured at 37 °C for 36 h, whereas the *CAP59* strain was maintained at 30 °C for 72 h. To prevent microevolution, cultures were always prepared fresh from frozen stocks stored at -80 °C. Post-growth of culture, *Cn* cells were centrifuged at 376 x *g* for 5 min and washed 3× with 5 mL phosphate-buffered saline (PBS). Pellets were resuspended in 5 mL PBS and then counted using a hemocytometer. For heat-killed *Cn* (HK-*Cn*), cells were heated at 65°C for 45 min.

Live and HK-*Cn* (1.5×10^6 cells) were opsonized with 20 µg of 18B7, a murine monoclonal antibody (Mab) specific to *Cn* GXM (a kind gift from Dr. Arturo Casadevall), in 1 mL PBS containing 20% goat serum (GS; Sigma-Aldrich, U.S.A.) for 30 min at 37 °C. Unbound 18B7 and complement were removed by washing 3× with 1 mL PBS, with cells recovered by centrifugation at 376 x *g* for 5 min between washes. Finally, opsonized yeast was recounted and resuspended in 200 µL PBS for use in macrophage infections (section 2.2.3).

2.1.2 *Cn* storage conditions

Yeast cells were grown until log phase (Chapter 2.1.1). After culturing, cells were washed with PBS, pelleted by centrifugation, and resuspended in 500 µL YPD and 800 µL glycerol. These cell suspensions were transferred into 1.5 mL cryovials and stored at -80 °C.

2.2. Mammalian Cell culture

2.2.1 Cell lines and conditions

RAW 264.7, a murine macrophage-like cell lines, 293T cells, and human embryonic kidney (HEK) 293 cells were obtained from the American Type Culture Collection (Manassas, VA). RAW 264.7 cells were cultured in Dulbecco's Modified Eagle Medium (DMEM) containing HEPES (Thermo Scientific, Grand Island, NY) supplemented with 10% fetal bovine serum (FBS; VWR/Avantor, Radnor, PA), 200 mM L-glutamine, 1% penicillin and streptomycin, and 50 µg/mL gentamicin (all from Sigma-Aldrich). J774.1 cells were cultured in DMEM (Thermo Scientific) supplemented with 10% FBS, 200 mM L-glutamine, 1% penicillin and streptomycin, 10% NCTC (Thermo Scientific), 1% non-essential amino acids (NEAA; Thermo Scientific). Lenti-X cells, a cell line derived from the HEK 293 cells, were obtained from Takara (San Jose, CA) and maintained in DMEM supplemented with 10% tetracycline-free heat-inactivated FBS (Takara), 1% penicillin and streptomycin. 293T cells, a derivative of HEK cells, were cultured in DMEM supplemented with 10% FBS, 1% penicillin and streptomycin. The Serezani lab (Vanderbilt University Medical Center) generously provided MH-S cells, a murine

alveolar macrophage cell line, which was grown in RPMI 1640 supplemented with 10% heat-inactivated FBS, 1% penicillin and streptomycin, and 0.05 mM β-mercaptoethanol (β-ME). All cell lines were maintained at 37˚C in a humidified 5% CO_2 atmosphere. Typically, cells were grown in 100 mm plates (Thermo Scientific) until they were 90% confluent. Cells were dissociated from the plate using 1X trypsin (Thermo Scientific) and passaged into fresh sterile plates at dilution of 1:4 or 1:5, as appropriate.

2.2.2 Cryostorage of mammalian cell lines

Cells were cultured in 100 mm plates until 90-100% confluent, then washed with 1x PBS (Thermo Scientific) and dissociated from the surface of the plate using 1 mL of 1x EDTA/trypsin. The trypsin was inactivated by adding 9 mL of complete culture medium to the cell suspension. The cells were transferred to 50 mL conical tubes (USA Scientific, Ocala, FL) and pelleted by centrifugation at 300 × g for 3 min. Cell pellets were resuspended in freezing medium (10% dimethylsulfoxide, DMSO, Thermo Scientific and 90% FBS) so that ~1 confluent 100 mm plate of cells was resuspended in 1 mL of medium. The cell suspension was transferred to 1.5 mL cryovials using 1 mL cells per tube. These vials were then either wrapped in ~10 layers of tissue paper or placed in isopropanol-containing freezing chambers and frozen overnight at -80°C. The following day, frozen vials were transferred to a liquid nitrogen dewar and stored in the gas phase.

2.2.3 Macrophage polarization and infection

RAW 264.7 or MH-S cells were plated onto 6-well plates (USA Scientific) at a density of 7.5 x 10^5 cells/well in 2 mL of medium. If required, the cells were incubated for 24 h with 200 U/mL recombinant murine IFNγ (unless otherwise noted: Biolegend, San Diego, CA) to promote M1 polarization. The next day, resuspended, opsonized *Cn* cells (Section 2.1.1) were counted to determine cell concentration. A total of 2.25 x 10^6 *Cn* cells/well were added to achieve a 3:1 multiplicity of infection (MOI). Macrophages were also mock-infected with PBS as a control. Immediately following the addition of *Cn* to the macrophage cultures, the cells were "spinoculated" by centrifuging the plates at 300 x *g* for 1 min, followed by incubation for 2 h 37 ˚C in a humidified 5% CO_2 atmosphere. Extracellular *Cn* was removed by washing 2× with PBS. If required, infected macrophages were incubated with 200 U/mL IFNγ or 100 ng/mL IL-4 (BioLegend and Peprotech, Rocky Hill, NJ) for 24 h to maintain the cells in an M1-polarizing environment or stimulate repolarization to the M2 state, respectively. During this 24 h incubation period, cells were washed, and media was replaced at 6 h intervals to prevent nutrient depletion and remove extracellular *Cn*.

2.3. Phagocytosis assays

RAW264.7 cells were seeded into 35 mm glass-bottom dishes (Cellvis, Mountain View, CA) at a density of 7.5 x 10^5 cells in 2 mL of medium and incubated overnight with 200 U/mL IFNγ or 1 μg/mL LPS from *Salmonella enterica typhimurium* (Sigma-Aldrich). Macrophages were infected with GFP-expressing opsonized *Cn* for 2 h. *Cn*-Infected

macrophages were cultured for another 24 h with appropriate cytokines. The next day, extracellular yeast cells were labeled with 10% calcofluor white (Sigma-Aldrich, St. Louis, MO), and dead macrophages were stained with 10 μg/mL propidium iodide, incubating at 37 °C for 5 min. Samples were then imaged using a Zeiss LSM700 confocal laser scanning microscope equipped with a Plan-Apochromat 20×/0.8 M27 objective (Carl Zeiss, Germany). The proportion of viable macrophages with intracellular *Cn* for each sample was measured.

2.4. Glucose assays

RAW264.7 cells were plated, incubated with cytokines, and infected with *Cn,* as described in section 2.3.3. Plates were cultured for a further 6 and 24 h as needed. For 24 h glucose assays, "*Cn* wash" samples were washed, and the medium was replaced every 6 h to maintain nutrient levels. "No wash" samples did not receive any media replenishment. Supernatants (1 mL) were collected at 6-h intervals as part of the wash/medium replenishment process and centrifuged to remove cellular material and *Cn* cells. According to the manufacturer's instructions, the glucose concentration was determined using the glucose oxidase assay kit (Sigma-Aldrich) by measuring absorbance at 540 nm in a Thermo Spectronic Genesys 5 UV/Visible spectrophotometer.

2.5. Western Blotting

2.5.1 Sample harvest and BCA assay

Cells cultured in 6-well plates were incubated with the desired reagents for the indicated times. At the end of the treatment period, cells were washed with PBS and harvested by scraping into 200 µL radioimmunoprecipitation assay (RIPA) buffer supplemented with 1× protease inhibitor cocktail (Sigma-Aldrich) and 100 mM phenylmethylsulfonyl fluoride (PMSF; Sigma-Aldrich) per well and transferred to 1.5 mL tubes. The cells were lysed by incubating on ice for a total of 20 min with vortexing at high speed every 10 min. The resultant lysates were centrifuged at 13000 x g for 15 min at 4°C to pellet cell debris, and the clarified lysates were transferred to fresh 1.5 mL tubes.

Sample protein concentrations were determined using the Bicinchoninic Acid Protein Assay (BCA; Thermo Scientific) in accordance with the manufacturer's instructions and normalized by dilution with RIPA buffer. Proteins were denatured and prepared for Sodium Dodecyl Sulphate-Polyacrylamide Gel Electrophoresis (SDS-PAGE) by the addition of 6× Laemmli buffer (0.375 M Tris pH 6.8, 12%$_{(w/v)}$ SDS, 60%$_{(v/v)}$ glycerol, 0.6 M dithiothreitol (DTT), 0.06%$_{(w/v)}$ bromophenol blue) to a final 1× concentration and boiling at 95 °C for 10–15 min. The samples were cooled to room temperature and then used immediately or stored at -20 °C.

2.5.2 Co-Immunoprecipitation

293T cells were seeded at a density of 4.6×10^6 cells into 100 mm plates in a 10 mL growth medium. 293T cells were transfected with plasmids encoding proteins of interest as indicated using Lipofectamine 3000, according to the manufacturer's guidelines. At 48 h post-transfection, the plates were treated as indicated and returned to the incubator for the required duration. At the end of the incubation period, cells were carefully rinsed with 5 mL cold PBS and harvested by scraping them into 1 mL cold PBS and transferred into 1.5 mL tubes. The cells were pelleted by centrifugation at 4 °C at 20,000 x *g* in a refrigerated bench-top microcentrifuge for 2 min. The cells were lysed by resuspending in 750 µL 1% Triton buffer (5 M NaCl, 1 M Tris pH 8.0, 0.5 M EDTA pH 8.0, 10%$_{(V/V)}$ Triton X-100) supplemented with 1× protease inhibitors and 100 mM PMSF and sonicating on 25% power for 10–15 sec using a Q125 sonicator (QSONICA, Newtown, CT). The tubes were centrifuged at 15,871 x *g* for 10 min at 4 °C to pellet debris, and the supernatants were transferred to fresh 2 mL tubes. A BCA assay was performed in accordance with the manufacturer's guidelines to determine protein sample concentrations. The protein concentration of the lysates was normalized to 1 mg/mL, and 100 µL of each sample was removed, mixed with 20 µL 6× Laemmli, boiled for 5 min, and used as input. For each sample, 20 µL Flag M2 beads were washed in 1 mL PBS and then twice in 1 mL 1% Triton buffer, pelleting at 587 x *g* for 2 min between washes. Beads were separated equally into fresh, labeled 5 mL tubes for each sample, and the supernatants were added to the corresponding tubes containing the Flag

beads, the screw tops were tightly closed and sealed with Parafilm, and incubated overnight at 4 °C with rotation at 11 RPM. The following day, the samples were centrifuged for 2 min at 4 °C and 587 x *g* to pellet the beads. The supernatant was discarded, and the beads were washed four times in 1 mL 1% Triton buffer for 5 min with rotation. After the final wash, the residual buffer was removed using a loading tip, 60 µL 2× Laemmli was added to each tube, and the beads were boiled for 5 min to release and denature immunoprecipitated proteins. The beads were finally pelleted at max speed for 1 min, and the protein lysates IP and input samples were immediately analyzed by western blotting.

2.5.3 SDS-PAGE

SDS PAGE gels were cast using the Mini-PROTEAN Tetra cell system and glass plates with 1 mm or 1.5 mm spacers (Bio-Rad). Gels with acrylamide concentrations ranging between 6 and 12% were prepared depending on the molecular weight of the protein to be resolved using pre-prepared gel buffer and acrylamide solutions (National Diagnostics, Atlanta, GA), in accordance with the manufacturer's recommendations.

Equal quantities of protein (~20–40 µg) were loaded for each sample to be compared, and the samples were electrophoresed by applying an electric current of 90 V until the samples compacted at the interface between the stacking gel and resolving gel. The voltage was then increased to 150V for approximately 60 min or until the bromophenol blue dye front was <1 cm from the bottom of the gel. The separated

proteins were transferred onto a nitrocellulose membrane (GE Healthcare Amersham, USA) using a Bio-Rad Trans-Blot SD Semi-Dry Transfer Cell with a voltage of 20 V for 60 min. Post-transfer, membranes were blocked with 5% dried non-fat milk powder in Tris-buffered saline with 0.05% Tween (TBS-T) solution for 1 h. Residual milk was removed by washing 3× with TBS-T for 5 min each, with shaking.

2.5.4 Antibody incubation and protein detection

Membranes were incubated with primary antibodies at 4 °C overnight. Antibodies used for the study and their dilutions are as follows: β-actin (1:5,000; Thermo Scientific, PA1-16889), Arg-1 (1:1,000; Cell Signaling, 9819S), iNos (1:1,000; Cell Signaling, 13120S), Cited1/MSG1 (1:500; Santa Cruz, SC- 21795), CBP (1:1,000; Cell Signaling, 7389), Flag (1:1,000; Sigma, F7425), IκBα (1:1000; Cell Signaling, L35A5), and p65 (1:1000; Cell Signaling, D14E12). Primary antibodies were diluted in either 5% bovine serum albumin (BSA) in TBS-T or PBS-T buffer in accordance with the manufacturer's guidelines or our optimized protocols. The following day, unbound antibodies were removed by washing 3× in TBS-T for 5 min each, with shaking. Following these washes, membranes were incubated with appropriate secondary antibodies diluted in 5% dried non-fat milk powder in TBS-T for 30 min at room temperature. Secondary antibodies included anti-rabbit-HRP (Santa Cruz, SC-2357) and anti-mouse-HRP (Santa Cruz, SC-516102) at 1:5,000 dilutions. Blots were then washed with TBS-T 3× for 5 min each with shaking and imaged after a short incubation in a 1:1 mixture of enhanced chemiluminescence (ECL) reagents 1 (250 nM Luminol, 0.1 M Tris

pH 8.5, 90 mM p-Coumaric Acid) and 2 ($30\%_{(V/V)}$ H_2O_2, 0.1 M Tris pH 8.6) using the ChemiDoc MP Imaging System and Image Lab software (Bio-Rad).

2.6. Molecular Biology

2.6.1 Genomic DNA purification from cultured mammalian cells

Cells were cultured in 100 mm dishes until ~80% confluent, harvested, and 2 x 10^6 cells/sample were pelleted in 1.5 mL tubes by centrifugation at 250 x *g* for 5 min. Supernatants were discarded, the pellets were resuspended in 200 µL TE buffer or PBS, and genomic DNA was purified using a GeneJET Genomic DNA Purification Kit (Thermo Scientific), in accordance with the manufacturer's guidelines. In brief, the cells were lysed by adding 200 µL Lysis Solution and contaminating nucleases were degraded by adding 20 µL Proteinase K Solution. Samples were incubated at 56 °C with occasional vortexing or rocking on a platform until the cells were completely lysed. Immediately following this, RNA was removed from the samples by adding 20 µL RNase A Solution, vortexing, and incubating for 10 min at room temperature. Then, 400 µL 50% ethanol was added to the samples, mixed, and transferred to GeneJET Genomic DNA Purification Columns, which were centrifuged at 6,000 x *g* for 1 min to bind genomic DNA to the column. The flow-through was discarded, and the DNA was washed by applying 500 µL wash buffer to the column and centrifuging at 8,000 x *g* for 1 min. This was followed by an additional wash using 500 µL wash buffer II and centrifuging at maximum speed for 3 min. Genomic DNA was finally eluted by applying 200 µL elution buffer to the column matrix, incubating at room temperature for 2 min, and

centrifuging at 8,000 x *g* for 1 min. The eluted DNA was immediately used for downstream applications, such as PCR and Sanger sequencing, or stored at -20 °C.

2.6.2 Primer design and PCR

To characterize insertions and deletions (INDELs) generated by CRISPR/Cas9-based gene editing of *Cited1* in RAW264.7 cells, genomic DNA was prepared from gene-edited clonal cell lines, and then PCR was used to amplify the region surrounding the edit site using primers with 5' overhangs complementary to the sequence flanking the *Bam*HI restriction enzyme site in the pcDNA3 plasmid multiple cloning site. The primers required for the PCR amplification were designed using the In-Fusion Cloning Primer Design Tool (Takara) so that the PCR fragments could be recombined into pcDNA3 using an In-Fusion recombinase reaction. The three In-Fusion PCR primers to amplify *CITED1* had the following sequences:

F1	TACCGAGCTCGGATCCCGGGGTGCCCTTTTTAGACAG
R1	CGTTACTAGTGGATCCAGGGGTAGGATGCAGGTTG
F2	TACCGAGCTCGGATCCGGCCTATAGCCGCACTGCTT
R2	CGTTACTAGTGGATCCATCAAACTCATTCTGCCCCAGC
F3	TACCGAGCTCGGATCCGGCATCAACTGCCACCGAT
R3	CGTTACTAGTGGATCCTTAGAGTGTCTTGGCCACCAG

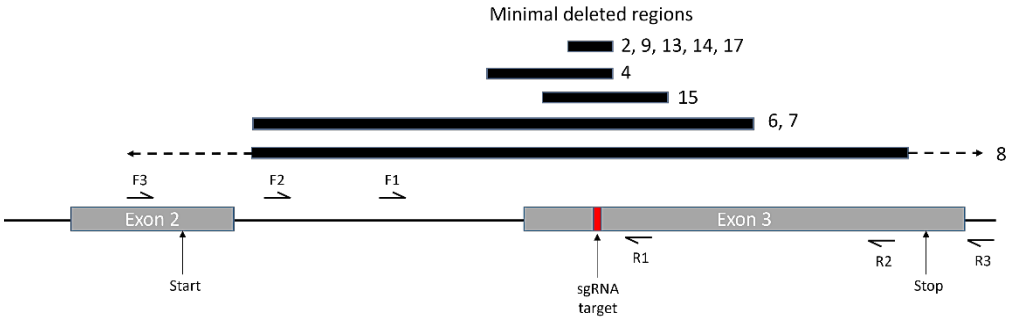

Figure 2.1: In-fusion primer binding sites on *Cited1* gene locus. Figure showing three different sets of primers targeting different regions of the *Cited1* gene. Black bars represent deleted regions in CRISPR Cited1 KO clones. Different primer combinations have been used to characterize clones with larger INDELS.

To perform the PCR, ~100 ng genomic DNA of clones was used as a template (Chapter 2.6.1), along with 12.5 µL Prime Star Max DNA polymerase (Takara) and 0.3 µM of the forward and reverse primers were combined in a PCR tube. The reaction volume was brought up to 25 µL using DEPC-treated water. The tube was briefly centrifuged to ensure all reagents were mixed prior to loading into a Mastercycler® Nexus Thermocycler (Eppendorf), and the following settings were used for the amplification:

32 cycles

98°C – 10 sec

57.5°C – 5 sec

72°C – 10 sec

In preparation for cloning the resulting PCR products into pcDNA3, the plasmid was linearized through digestion with *Bam*HI (New England BioLabs, Ipswich, MA) in 1× ANZA Red Buffer (Thermo Scientific) at 37 °C for 30 min. The products of the pcDNA3 *Bam*HI endonuclease reaction and the PCR products were separated by gel electrophoresis.

2.6.3 DNA gel electrophoresis

To separate DNA fragments, agarose gels containing 0.8–2% agarose$_{(w/v)}$ were prepared depending on the estimated size of the DNA fragments of interest. The gels were produced by dissolving the appropriate mass of agarose in 50 ml Tris-acetate-EDTA (TAE) buffer (40 mM Tris pH 7.9, 5 mM sodium acetate, 0.9 mM EDTA) and heating in a microwave until the agarose completely dissolved (~30–60 sec). The mixture was allowed to cool to below 60 °C before adding ethidium bromide to a final concentration of 0.25 μg/mL and pouring it into the casting tray. When fully set, the gel was transferred to a DNA Plus Complete Mini Gel System (USA Scientific) gel electrophoresis tank and fully submerged in TAE.

After being mixed with 6× TriTrack loading buffer (Thermo Scientific) to 1× final concentration, DNA samples were loaded onto the gel alongside 1 Kb Plus DNA Ladder (Invitrogen) and electrophoresed at 120 V for approximately 1 h. A UVP High-Performance UV Transilluminator was used to view DNA (Thermo Scientific). Using a

scalpel blade, DNA fragments were removed from the gel and transferred to sterilized 1.5 mL tubes.

2.6.4 DNA extraction and gel purification

To extract and purify DNA fragments from agarose gel slices, a NucleoSpin Gel and PCR Clean-up Kit (Takara) were used. Agarose gel fragments were dissolved by heating for 10 min at 50 °C in binding buffer NTI, with 200 µL buffer per 100 mg gel. The solubilized gel fragments were transferred to NucleoSpin Gel and PCR Clean-up Columns and centrifuged at room temperature for 30 sec at 11,000 x *g* using an Eppendorf 5424R tabletop centrifuge. To eliminate impurities, the column-bound DNA fragments were washed with ethanolic Wash Buffer NT3, and the purified DNA was eluted using Elution Buffer NE (5 mM Tris/HCl, pH 8.5). The concentration of DNA samples was determined using a NanoDrop (Thermo Scientific) and stored at -20 °C until needed.

2.6.5 In-Fusion cloning of genomic DNA sequences into pcDNA3

To recombine PCR fragments amplified from *Cited1* into pcDNA3, 100 ng of the purified PCR fragments were combined with 100 ng linearized pcDNA3 vector and 2 µL 5× In-Fusion HD Enzyme Premix (Takara Bio). The volume was adjusted to 10 µL using DI water, and the reactions were incubated at 50 °C for 15 min. The samples were returned to room temperature and immediately transformed into chemically competent DH5α *E. coli*.

2.6.6 Bacterial Transformations

For the transformation of closed plasmid DNA, DH5α *E. coli* subcloning competent cells were used (Life Technologies). In brief, 1 ng plasmid DNA was added to 50 µL DH5α cells in round-bottomed polypropylene tubes and incubated on ice for 30 min. The cells were heat-shocked for 45 sec at 42 °C, then returned to ice immediately for 2 min to recover. Following this, 450 µL LB broth was added to the cells and then incubated in a shaking incubator at 37 °C for 45–60 min. A total of 50 µL from this mixture was plated onto selective LB agar containing 100 µg/mL ampicillin or kanamycin as appropriate. The remaining cells were pelleted at 6,000 x g for 5 min. The pellet was resuspended in 100 µL LB broth and plated onto selective LB agar plates. The plates were incubated overnight (12-18 h) at 37°C. For the transformation of In-Fusion reaction products, the same procedure was followed, except Stellar Competent *E. coli* (Takara) was used instead of DH5α *E. coli* subcloning competent cells.

2.6.7 Small-scale plasmid DNA purification (Mini-prep)

Miniprep purification of plasmid DNA was performed using the EZNA Plasmid DNA Mini Kit II (Omega Bio-Tek, Norcross, GA). Single transformed bacterial colonies were used to inoculate 3 mL ampicillin or kanamycin-containing LB broth and were cultured overnight (14–18 h at 250 RPM/37 °C). The following day, cultures were retrieved and centrifuged at 10,000 x *g* for 5 min at room temperature. Bacterial pellets were resuspended in 500 µL Solution I containing RNase A. An alkaline buffer (Solution II) was used to resuspend and lyse bacteria. The mix was incubated at room

temperature for 2 min with gentle rotation to allow for complete lysis of the bacteria. The lysis reaction was stopped by adding 700 µL neutralizing buffer (Solution III), and the tubes were inverted until a white precipitate formed. These tubes were then centrifuged at full speed (>13,000 x *g*) for 10 min at room temperature to pellet the precipitate. The clarified lysates were transferred to HiBind DNA Mini Columns that had been activated prior to use with 3 M NaOH and centrifuged at full speed in a bench-top centrifuge for 1 min. This process was repeated if the lysate volume exceeded 700 µL with the flow-through discarded between spins. Columns were washed with ethanol-containing HBC buffer and centrifuged at 13,000 x *g*. Excess ethanol was then removed by centrifuging empty tubes for 2 min at 13,000 x *g*. Plasmid DNA was finally eluted by placing the column in a sterile DNase-free 1.5 mL tube, adding 50 µL elution buffer to the center of the column matrix, incubating for 1 min at room temperature, and centrifuging the buffer through the column twice at 13,000 x *g* for 1 min each for optimal yield. Eluted DNA was quantified using a Nanodrop (Thermo Scientific) and stored at -20 °C.

For all new plasmid constructs, DNA insert sequences were determined using the Sanger sequencing service provided by Eurofins Genomics (Louisville, KY). The resulting chromatograph data was visualized using 4Peaks (Nucleobytes, Netherlands), and DNA sequences were analyzed using a combination of SnapGene (GSL Biotech LLC, San Diego, CA) and BLAST (NCBI, Bethesda, MD).

2.6.8 Large-scale plasmid DNA purification (Maxi-preps)

The Invitrogen PureLink Expi Endotoxin-Free Maxi Plasmid Purification Kit was used to perform maxiprep purification of plasmid DNA. Transformed bacterial colonies were cultured overnight (16 h at 250 RPM/37 °C) in 125 mL ampicillin- or kanamycin-containing LB broth. The following day, cultures were retrieved and centrifuged at 4,000 x *g* for 15 min at room temperature in 50 mL conical tubes. The bacterial pellets were resuspended in 6 mL R3 Resuspension buffer containing RNase A. Next, 6 mL Lysis Buffer was used to lyse bacteria, which were incubated at room temperature for 5 min. The lysis reaction was stopped by adding 6 mL N3 Precipitation Buffer, and the conical tubes were inverted until a white precipitate formed. The lysates were centrifuged for 4 min at room temperature at 2,000 x *g* to pellet the precipitate. Cleared lysates were achieved by repeated centrifugation (2,000 x *g* for 4 min) using Lysate Clarification columns. To ensure the removal of contaminating bacterial lipopolysaccharide, 2.5 mL Endotoxin Removal Buffer was added to the clarified lysates. The DNA in the lysates was transferred to DNA binding columns and bound to the column matrix by centrifugation (1,000 x *g* for 1 min). The bound DNA was washed using 20 mL wash buffer and centrifuged at 1,000 x *g* for 1 min. Plasmid DNA was finally eluted in 15 mL elution buffer by centrifugation at 1,000 x *g* for 1 min. The eluates were mixed with 10.5 mL isopropanol and centrifuged for 30 min at 4 °C at > 12,000 x *g* to precipitate and pellet the plasmid DNA. After discarding the supernatant, DNA pellets were washed with 5 mL 70% ethanol and centrifuged at > 12,000 x *g* for 10 min at 4 °C. DNA pellets

were air-dried for 2 min to remove residual ethanol and resuspended in 1 mL TE buffer. The concentration was quantified using a Nanodrop. If necessary, the DNA was diluted to 1 µg/µL in TE, aliquoted, and stored at -20 °C.

2.7. Generation of a stable RAW264.7 pINDUCER20-CITED1 cell line

2.7.1 Lentiviral transductions

Lenti-X cells were seeded into a 100 mm tissue culture dish at a concentration of 4.6×10^6 cells in 10 mL medium containing tetracycline-free FBS and grown to ~80% confluency. The following day 7 µg of purified pLV-lentiviral construct DNA was added to a Lenti-X Packaging Single Shots (Takara) tube containing an optimized formulation of Xfect™ Transfection Reagent premixed with Lenti-X lentiviral packaging plasmids. The volume was adjusted to 600 µL using sterile DI water mixed by vortexing and incubated at room temperature for 10 min to allow transfection complexes to form. The entire transfection mix was added dropwise to Lenti-X cells, and then the cells were incubated for 4 h. Following this, the medium was replaced with 6 mL fresh growth medium, and the plate was incubated for 2 days to allow the cells to shed lentiviral particles. Following the incubation period, 6 mL lentiviral supernatant was harvested and stored at 4 °C and replaced with 6 mL fresh growth medium. On the same day, RAW264.7 cells were seeded into a 6-well plate at a density of 8.5×10^5 cells per well in 2 mL medium. The plate was then incubated for an additional 24 h, which is when another 6 mL of lentiviral supernatant was collected and combined with the previously

collected lentiviral supernatant. Contaminating Lenti-X cells were removed from the supernatant by centrifugation, and then the viral particles were concentrated using Lenti-X Concentrator Solution (Takara) in accordance with the manufacturer's guidelines. In brief, ~18 mL of concentrated supernatants were incubated at 4 °C for 30 min and centrifuged at 1,500 x *g* for 45 min to generate lentiviral pellets, which were then resuspended in 1 mL of RAW 264.7 cell growth medium. The amount of lentivirus in viral supernatants was quantified using Lenti GoStix Plus following the Protocol-At-A-Glance (Takara, USA) methodology.

In the presence of 4 µg/mL polybrene, serial dilutions of the concentrated lentiviral particles were used to infect RAW264.7 cells. Since polybrene was toxic to cells, the cells were washed, and fresh growth medium was added 24 h post-infection. Successfully transduced cells were selected by incubation in growth medium containing 500 µg/mL G418 (Fisher Scientific), with untransduced RAW264.7 cultures treated as controls to help determine when the selection process had gone to completion. This typically took 5–7 days.

2.7.2 Generation of clonal cell lines

Clonal cell lines were produced from stably transduced RAW264.7 cell populations using a dilution-plating strategy. In brief, a cell growth medium containing appropriate antibiotics (e.g., G418) was added to a reagent reservoir. In a 96-well plate, 100 µL medium was added to all but the A1 well using an Eppendorf Research Plus 12-channel multichannel pipette. A total of 200 µL of the cell suspension (2 x 10^4 cells/mL)

was added to well A1, 100 µL was moved to well B1 and gently mixed, and the process was repeated for the remainder of column 1. The cell suspensions in all column 1 wells were diluted by adding 100 µL growth medium, gently mixed by repeat pipetting, and then 100 µL was subsequently transferred to the adjacent wells in column 2. This process was repeated across the plate, discarding 100 µL from each of the wells in the last column. This created a cell concentration gradient across the plate, with the cell concentration reduced by one-half when moving one well to the right or down. After producing this cell gradient, 100 µL of the medium was added to all the wells to bring the total volume to 200 µL. Plates were then maintained at 37 °C in a humidified 5% CO_2 environment. Cells were then closely monitored every day, and the medium was replenished as needed. Wells containing a single colony were carefully expanded to produce clonal lines.

A minimum of eight clones were screened for each stably transduced cell line using appropriate methods. For example, for RAW264.7pINDUCER20-CITED1 cells, CITED1 protein levels were measured by western blotting after incubating the cells with 100 ng/mL doxycycline for 24 h. Clones expressing the highest level of CITED1 were retained for further work.

2.7.3 Optimization of doxycycline-induced CITED1 expression

To determine the optimum doxycycline dose and incubation time required to induce CITED1 expression in RAW264.7pINDUCER20-CITED1 cells, separate dose-response, and timecourse experiments were performed. In brief, cells were treated

with different concentrations of doxycycline (0, 3, 10, 30, 100, 300 ng/mL) for 24 h or incubated with 100 ng/mL for various durations (0, 4, 8, 12, 16, 24 h) and protein lysates were produced. CITED1 levels were measured by western blotting with a doxycycline dose of 100 ng/mL and 24 h treatment selected for subsequent experiments.

2.8. Generation of Murine CRISPR Cas 9 KO Cell Lines

2.8.1 Lentiviral transductions

A total of 4.6×10^6 Lenti-X cells were plated onto a 10 cm plate in 10 mL medium and grown to ~80% confluency. The following day 7 µg of purified lentivirus expressing Cas9 and single guide RNA (sgRNA) targeting CITED1 exon 3, STAT1 exon 9, and CITED2 exon 2 was added to Lenti-X Packaging Single Shots (Takara Bio) tubes containing Xfect™ Transfection Reagent premixed with an optimized formulation of Lenti-X lentiviral packaging plasmids. The remaining procedure was followed from Chapter 2.7.1. The clonal cell lines were generated according to the steps in Chapter 2.7.2. The guide RNA (gRNA) sequences used for the gene editing are as follows:

Cited1 TACCCCGGGGTCACCGCAAA

Stat1 GTTGGGCGGTCCCCCGATGC

Non-targeting “scramble” gRNA GTGTAGTTCGACCATTCGTG.

2.9. Transcriptome analysis

2.9.1 RNA extraction

To prepare macrophage RNA, cells were plated in 6-well plates at a density of 3 x 10^5 cells/well in 2 mL medium. Cells were cultured for the indicated duration with the agents of interest. In those experiments involving the infection of macrophages with *Cn* (live or heat-killed; Chapter 2.2.3), the cells were imaged by light microscopy to determine the infection efficiency (calculated as the percentage of macrophages containing at least 1 *Cn*) immediately prior to cell lysis. Only samples with >50% of infected cells were used for experiments. These samples were washed with 1 mL PBS, and the RNA extraction was performed using an RNeasy Mini Kit (Qiagen), according to the manufacturer's instructions with the following modification. The cells were resuspended in 1 mL RLT buffer containing β-ME and lysed by shearing, passing the cell suspension through a 20-gauge needle 10 times. Lysates were centrifuged at 376 x *g* for 5 min at room temperature to pellet *Cn*. The standard RNeasy Mini Kit protocol was then followed as described in the user manual.

Genomic DNA was removed from purified RNA using the Message Clean kit (GenHunter). To perform the digestion, the supplied 10× buffer was combined with samples to a 1× concentration, 1 µL DNase was added, and the reaction mixes were incubated at 37 °C for 30 min. Following DNA digestion, ~70 µL RNA was further cleaned by adding 80 µL phenol:chloroform: isoamyl alcohol (25:24:1), vortexing for 30 sec, and incubating on ice for 10 min, followed by centrifugation at 20,570 x *g* for 5 min. This

process was performed two times, finally extracting the clear top layer of RNA. The RNA was mixed with 10 µL 3M sodium acetate and 400 µL 100% ethanol and incubated at -80 °C for 60 min. It was then pelleted at 20,570 x *g* for 20 min. Residual ethanol was removed, the RNA was resuspended in DEPC water, and the concentration was determined using a Nanodrop. Additionally, RNA integrity and quality were appraised using a Qubit 4 Fluorometer and agarose RNA electrophoresis. In instances where RNA was sent directly to Novogene for RNA sequencing, the second round of RNA quality control was used prior to cDNA library preparation, with RNA sample integrity assessed using a 2100 Bioanalyzer (Agilent).

2.9.2 cDNA library preparation

Macrophage cDNA libraries were prepared from 1 µg isolated RNA using NEBNext UltraTM Directional RNA Library Prep Kit for Illumina, the NEBNext Multiplex Oligos for Illumina Index Primers, and the NEBNext Poly(A) Magnetic Isolation Module (all from New England BioLabs), according to the manufacturer's instructions. Libraries were sent to Novogene (Sacramento, CA) for an initial quality assessment. Once the samples had passed the QC test, sequencing was performed using the HiSeq 2500 system to produce 150 bp transcriptome paired-end reads.

For reverse transcriptase chain reaction (RT-PCR) and qRT-PCR experiments, cDNAs of isolated RNA samples were prepared using 3 µg as a starting RNA template. For each RT-positive sample, 3 µg purified mRNA in a total of 12.5 µL (diluted with DEPC treated water) was combined with 4 µL 5× First-Strand Buffer (Thermo Scientific), 1 µL

10mM dNTP mix (Thermo Scientific), 1 µL 20 µM Oligo (dT) 18 Primer (Thermo Scientific), 0.5 µL RiboLock Rnase inhibitor (Thermo Scientific), and 1 µL Maxima H-Reverse Transcriptase (Thermo Scientific) in PCR tubes. For RT-negative samples, 1 µL Maxima H-Reverse Transcriptase was replaced by 1 µL DEPC water. These tubes were incubated in the thermal cycler (Eppendorf Mastercycler® nexus) with the following settings:

50 °C – 30 min (cDNA synthesis)
85 °C – 5 min (termination of reaction)

cDNA samples were stored at -20 °C or immediately used for qRT-PCR.

2.9.3 Bioinformatics analysis of RNA Sequencing data

Analysis of transcriptome data was performed using Cyverse Discovery Environment online platform (219). The quality of fastq files was checked using FastQC (version 0.11.5)(220). The STAR aligner (version 2.5.3a-index-align) was used to align paired-end reads to their respective genome (221). Bam files generated from the STAR alignment and the appropriate genome annotation files were utilized within the Galaxy platform to quantify each gene's number of reads in the genome annotation file (222). The resulting FeatureCounts files were then joined using Multi-Join into one tabular form (223,224). These read counts were further analyzed using edgeR (225). Multi-dimensional scale plots and cluster dendrograms were created based on the read counts to determine the overall relatedness among replicates and treatment groups. Species-relevant genome and genome annotation files were used to assemble the transcripts of the STAR output files using StringTie (version 1.3.3)(226). These

transcripts were later combined using StringTie-merge (version 1.3.3) within the CyVerse Discovery Environment. CuffDiff2 (version 2.2.1;(227)) was finally used to identify differentially expressed genes (DEGs) between the treatments. Biologically relevant and statistically significant DEGs were selected if the fold-change was 2.0 or greater and the q-values were 0.05 or smaller. For macrophage-specific DEGs, functional analysis was performed using the Database for Annotation Visualization and Integrated Discovery (DAVID) bioinformatics resource tool (228) to identify specific pathways and biological processes affected and enriched due to treatment. Additionally, protein-protein interactions of DEGs were identified via the Search Tool for the Retrieval of Interacting Genes/Proteins (STRING, version:11.0) (229).

2.10. qRT-PCR

In this dissertation, qRT-PCR was used primarily to validate DEGs identified in RNAseq-based transcriptome profiling experiments. For this, cDNA was prepared as described in section 2.9.2 and used together with Perfecta-SYBR Fastmix (VWR) and primers designed using Primer-BLAST (NCBI). All qRT-PCR was performed using the AriaMx Real-Time PCR System (Agilent) or CFX Opus 96 Real-time PCR Detection System (Bio-Rad). Primer sequences used for the detection of murine transcripts were as follows:

Reference genes (used in all qRT-PCR experiments)

Actb (F-CACTGTCGAGTCGCGTCC, R- TCATCCATGGCGAACTGGTG)

Cyc1 (F-CTAACCCTGAGGCTGCAAGA, R- GCCAGTGAGCAGGGAAAATA)

Targets

Cited1: (F- CTGCCACCGATTTATCGGACTT, R- CTCCTGGTTGGCATCCTCCTT)

Cited2: (F- GCAAAGACGGAAGGACTGGA, R- CGTAGTGTATGTGCTCGCCC)

*Ccl2: (*F-CAGATGCAGTTAACGCCCCA, R-TGAGCTTGGTGACAAAAACTACAG)

Ccl3: (F-CCAAGTCTTCTCAGCGCCATA, R-TCTCTTAGTCAGGAAAATGACACC)

Ccl4: (F-CTGTGCAAACCTAACCCCGA, R-AGGGTCAGAGCCCATTGGT)

Cd40: (F-TTGTTGACAGCGGTCCATCT, R-TTCCTGGCTGGCACAAATCA)

Cd52 (F-CAAAGCTGCTACAGAGCCCA, R-CCAAGGATCCTGTTTGTATCTGAAT)

Ifit1: (F-TCTGCTCTGCTGAAAACCCA, R-CACCATCAGCATTCTCTCCCAT)

Ifit3b: (F-CCTTCCTGCCAAGGATTGCT, R-TGTGATCAAAAGGTGGTCTGTGA)

Isg15: (F-TCTGACTGTGAGAGCAAGCAG, R-CCTTTAGGTCCCAGGCCATT)

Isg20: (F-TGAAGCCAGGCTAGAGATCC, R-AGGGCATTGAAGTCGTGCTT)

Oas2: (F-GCCTTGGAAAGTGCCAGTACC, R-CCTTGGTCCTGCCACAAGAT)

2.11. RT-PCR

As an alternative to qRT-PCR, multiplex RT-PCR was employed to evaluate the change in the expression of select mRNAs. For these experiments, cDNA libraries were prepared as described in section 2.9.2, and cDNAs of interest were amplified by PCR. To perform the PCR, 1 µg of each cDNA library sample was combined with 5 µL 2× Clone Amp DNA polymerase (Takara), 100 ng/µL of primers targeting the cDNA of interest, and CPSF6 primers (F-TTACACTGGGAAGAGAATCGC, R-CTGGAAAAGGTGGAGGTGG) as control were combined in PCR tubes. The reaction was brought up to a total volume of

9 µL using DEPC-treated water. Reactions were briefly centrifuged in a bench-top microfuge and then the tubes were loaded into the thermal cycler (Eppendorf Mastercycler® nexus) with the following settings:

32 cycles

98 °C – 1 min

98 °C – 10 sec

62.3 °C – 5 sec

72 °C – 5 sec

The PCR products were resolved by DNA gel electrophoresis using 2% agarose gels (Chapter 2.6.3) and visualized using UV illumination.

2.12. Luminometry

293T cells were plated at a density of 2 x 10^5 cells/well in 1 mL medium in 24-well plates (USA Scientific) and grown to 80% confluency. Wells were transfected in triplicate using lipofectamine 3000 with the indicated combinations of plasmid DNA, transfecting 0.5 µg total plasmid DNA per well. At 48 h post-transfection, wells were treated as indicated in triplicate, and the plates were returned to the incubator for an additional 6 h. At the end of the incubation period, plates were placed on ice, and the growth medium was removed. To each well 250 µL lysis buffer (25 mM Tris-HCl pH 7.8, $1\%_{(w/v)}$ BSA, $0.025\%_{(w/v)}$ DTT, 1% Triton X-100, $15\%_{(v/v)}$ glycerol, 0.1 mM EDTA, 8 mM $MgCl_2$) supplemented with 1× protease inhibitor cocktail and 1 mM PMSF was added,

and the cells were lysed by shaking the plate at room temperature for 15 min at 200 RPM. Following this, 10 µL 25 mM ATP (Fisher, ICN19461401) was added to each well, and 100 µL was transferred in duplicate to an opaque-white 96-well plate. To stabilize the luciferase reaction, 20 µL 10 mM sodium pyrophosphate (Thermo Scientific) was added to each well. Finally, 100 µL 2 mM D-Luciferin (Gold Biotechnology, Olivette, MO) was added to each well immediately before reading the plate. Luciferase activity was measured using the CLARIOstar plate reader, and the data were exported to Microsoft Excel for analysis. Counts were measured, and the average of the triplicates was calculated. These values were then normalized to untreated controls, and the error was calculated as SEM for each condition.

CHAPTER THREE: TOOL DEVELOPMENT

3.1. Introduction

The primary purpose of this study was to elucidate the effects of intracellular *Cn* infection on macrophage polarization and function. To achieve this objective, it was first essential to develop an *in vitro* system using a cultured macrophage cell line that could (i) adopt distinct M1 and M2 phenotypes and (ii) exhibit high rates of phagocytosis when exposed to opsonized *Cn*. As an additional consideration, consistent growth conditions would also need to be maintained throughout the experiments, so any changes in gene expression and phenotype detected in our assays were driven by interactions between the host and pathogen rather than the depletion of key nutrients in the growth medium. While similar systems have been used in prior investigations of the macrophage:*Cn* interaction (82,167,230–233), we decided it was vital to develop and test our own system to ensure the validity and reproducibility of our experiments.

A variety of macrophage cell lines have been used to study the outcome of intracellular *Cn* infections. These include J774.16, a murine macrophage-like cell line derived from reticulum sarcoma that has been employed to investigate the intracellular survival strategy of *Cn* (49), the influence of Th1, Th2, and Th17 cytokines on yeast proliferation (50), and how *Cn* infection impairs host cellular functions (233). Another murine cell line, RAW 264.7, is a widely used model to understand how intracellular pathogens alter gene expression of the host (231,234,235) and how intracellular infection antagonizes macrophage polarization (73,214). Of these two, RAW 264.7 is perhaps the most commonly used and has been successfully employed by our lab for

prior studies investigating the effects of *Cn* on the regulation of proinflammatory gene expression (150).

The primary mechanism by which macrophages kill *Cn* requires the internalization of the yeast by phagocytosis. However, *Cn* may avoid ingestion in the absence of opsonins, such as complement proteins or antibodies (237), due to the presence of a highly antiphagocytic polysaccharide capsule. The capsule is a major virulence factor of *Cn* that is enhanced *in vivo* and provides protection against the host immune response (216,217). Several groups have shown that the use of antibodies that bind capsule epitopes successfully opsonized the yeast, enhancing the clearance *of Cn* in animal models and *in vitro* studies (240,241). Specifically, capsule-binding antibodies have been reported to enhance phagocytosis (242,243). The MAb 18B7 is a well-characterized antibody that binds to GXM of four serotypes of *Cn* and has been employed as a therapy to treat fungal disease in humans (42,244). Furthermore, it caused a significant increase in the ingestion of yeast cells by J774.16 cells, human peripheral blood mononuclear cells (PBMCs), and human polymorphonuclear neutrophils (PMNs). The above evidence suggests that MAb 18B7 enhances phagocytosis of cultured macrophages and would serve as a suitable opsonin for this study.

Following ingestion, the pathogen may replicate and exit phagocytic cells through non-lytic exocytosis (51,245,246), which is a *Cn*-driven process (51). As yeast cells are continuously extruded into the culture medium during experiments, it was anticipated that their accumulation may result in the depletion of essential nutrients,

such as glucose, from the culture medium. This potentially impacts signaling in both the macrophages and *Cn,* leading to artifactual changes in gene expression that are not caused by intracellular *Cn* growth. For example, it is known that decreased glucose levels result in decreased thioredoxin-interacting protein (TXNIP). This may impact gene expression as TXNIP is a regulator of the transcription factor, p53 (247). For this reason, it was vital to employ culture conditions that both remove extracellular *Cn* and maintain a near-constant growth environment during experiments.

In this chapter, we present data to show that it is possible to successfully obtain *Cn*-infected M1 and M2 polarized macrophages through controlled nutrient and cytokine replenishment and optimized phagocytosis conditions. In this way, we define a basic infection methodology that will be used in the following chapters to answer the central question of this dissertation.

3.2. Verification of M1 and M2-polarized macrophages

As a first step to efficiently characterize the changes in gene expression stimulated by intracellular *Cn* infection, it was imperative to verify if the RAW 264.7 cell line responds to appropriate M1 and M2 polarizing stimuli and expresses the markers of these phenotypes. To determine this, naïve macrophages were stimulated overnight with either IFNγ or IL-4 to promote M1 and M2 polarization, respectively. At 24 h post-treatment, IFNγ-stimulated cells exhibited a 300-fold increase in the M1 marker, iNos, but direct IL-4 did not alter the expression of the M2 marker, Arg-1 (Fig 3.1A and B). This was consistent with prior studies showing that IL-4 alone cannot stimulate

measurable levels of Arg-1 protein expression in murine macrophages, possibly due to cAMP deficiency (248). To further confirm this, we co-stimulated RAW 264.7 with IL-4 and the cAMP analog, 8-bromocAMP, and observed a robust increase in Arg-1 protein expression (Fig 3.1C).

The polarization of macrophages is highly plastic, and an M2 state is typically achieved once infections are resolved directly from M1 rather than from M0. For this reason, we hypothesized that this could be utilized as a strategy to generate M2-polarized RAW 264.7 macrophages. To examine if this approach worked, RAW 264.7 cells were primed with IFNγ for 24 h to induce M1 polarization and then repolarized to the M2 state with IL-4, which resulted in a >100-fold increase in Arg-1 protein levels (Fig 3.1A and D). Furthermore, protein expression in samples treated with IL-4 alone was nearly identical to untreated controls. Altogether, these data showed that RAW 264.7 macrophages could be used as an *in vitro* model to characterize the responses of M1 and M2 polarized macrophages to *Cn* infection (Fig 3.1E).

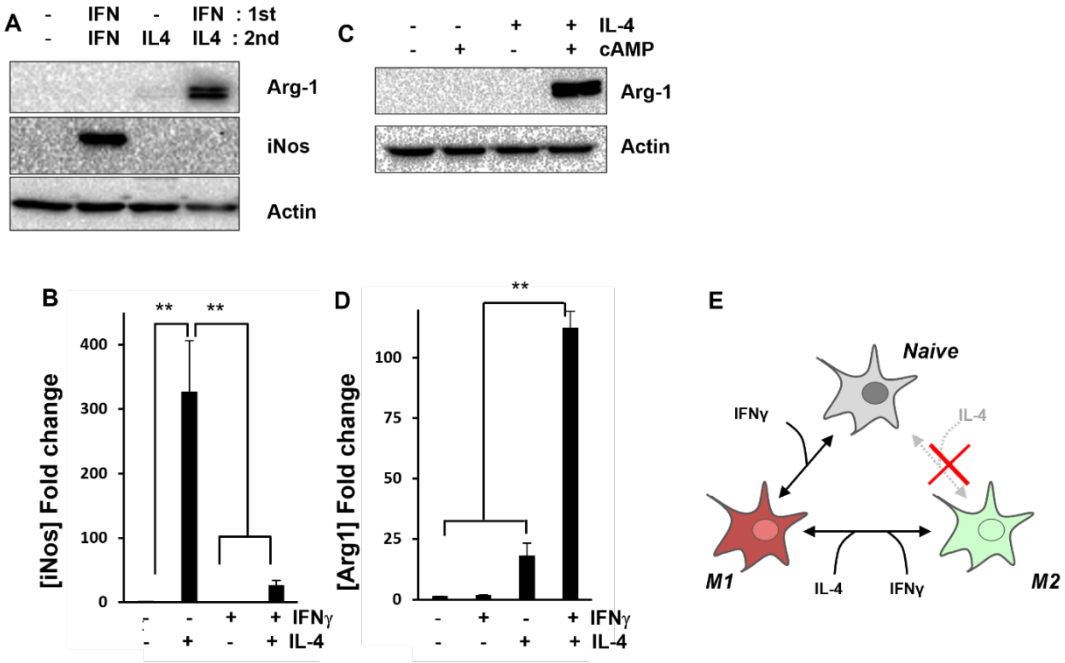

Figure 3.1: Verification of M1 and M2 phenotypes in a murine macrophage cell line. Immunoblot analysis of RAW 264.7 macrophages for iNos and Arg-1, M1, and M2 markers, respectively, after 24 h incubation with (A) IFNγ and IL-4 (C) IL-4 and cAMP. (B+D) Quantification of iNos and Arg-1 protein levels in (B) by densitometry. (E) Schematic representation to show that the M2 state in RAW 264.7 cells is attained via M1 and not through M0. Error is represented as SE. Statistical differences were determined using a one-way analysis of variance (ANOVA) followed by Tukey's multiple comparison test. Statistical significance is indicated as follows: *, $p < 0.05$; **, $p < 0.01$. (A, B, and D) Data is from six biological repeats.

3.3. Optimization of *C. neoformans* phagocytosis conditions

As the transcriptome profiling techniques used in this dissertation are a form of bulk-cell analysis (i.e., they use large populations of cells rather than individual cells), when preparing samples, the infected macrophages must outnumber uninfected cells to adequately assess the transcriptional changes induced by intracellular *Cn*. To maximize the ratio of infected to uninfected cells, we optimized our cell infection procedure. This was performed using GFP-labeled yeast cells opsonized with different concentrations of 18B7, a monoclonal antibody raised against GXM of *Cn* (244) and goat serum (GS) as a source of complement and measured their uptake by RAW 264.7 cells. Here, 50% of the macrophages contained *Cn* when the yeast was opsonized with 20% GS and a 3X concentration of 18B7 (30 µg per 1.5×10^6 *Cn*) (Fig 3.2A). Decreasing the MOI, GS, or 18B7 concentration reduced infection efficiency. Additionally, 18B7 was necessary for phagocytosis as we observed no macrophages with phagosomal *Cn* in the absence of antibody. When this experiment was repeated using constant GS concentrations but varied 18B7 and MOI, the data suggested that a higher MOI may not necessarily result in increased intracellular infection as a 10:1 MOI yielded fewer infected cells than 3:1. This is possibly due to insufficient antibodies to opsonize the increased amount of *Cn* (Fig 3.2B). As a caveat, 18B7 concentration also differed between the MOI 3:1 and 10:1 conditions, making it difficult to draw a definitive conclusion.

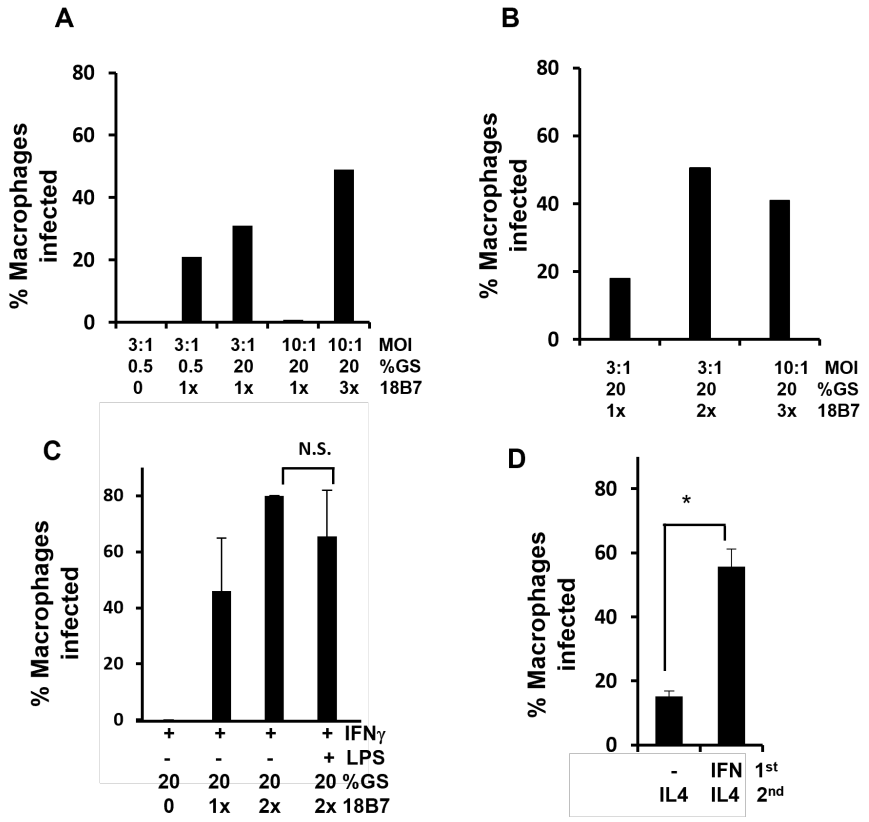

Figure 3.2: Infection efficiency is driven by opsonins. Quantification of GFP labeled H99S-infected macrophages by confocal microscopy 24 h post-infection (A) with different concentrations of 18B7, GS, MOI (B) optimized goat serum but with different concentrations of 18B7 and MOI (C) M1 activated macrophages (D) IFNγ primed and unprimed M2 repolarized macrophages. Calcofluor white, a blue fluorescent dye, was used to identify extracellular *Cn* and propidium iodide to stain dead cells. 1× 18B7 is 10 µg per 1.5 × 10^6 *Cn*; GS is goat serum; MOI is the multiplicity of infection. Error is represented as SE. Statistical differences between samples were determined using one-way ANOVA followed by Tukey's multiple comparison test. (C & D) Statistical significance is indicated as follows: *, $p < 0.05$. Data is from three biological repeats.

Overall, these optimization studies suggested that 20% GS, 2X 18B7 (20 μg per 1.5×10^6 *Cn*), and a 3:1 MOI were sufficient to achieve >50% infection macrophage. These conditions were used for all subsequent infections.

Having successfully optimized 18B7 and GS concentrations, we conducted experiments to test these conditions in M1 and M2 polarized macrophages. As expected, infection efficiency improved to 80% in IFNγ-stimulated M1 macrophages infected with *Cn* opsonized with the new optimized conditions (Fig 3.2C). In agreement with our prior experiment (Fig. 3.2A), no internalization of *Cn* was seen in polarized macrophages without 18B7, confirming that antibody opsonization plays a significant role in *Cn* phagocytosis. These data also showed that although LPS is a potent enhancer of M1 polarization (218), it did not increase the infection percentage over the use of IFNγ-stimulation alone. For this reason, LPS was excluded from the infection protocols. As co-infections with Gram-negative bacteria are seldom reported in cases of cryptococcosis, it was also deemed that it was not a biologically relevant stimulus for this study.

While M1 cells efficiently ingest *Cn*, cells exposed to M2-polarizing conditions (i.e., IL-4 only) prior to infection exhibited low levels of infection (<20% cells containing internalized *Cn*). However, priming macrophages with IFNγ 24 h prior to infection and repolarizing them to M2 with IL-4 post-phagocytosis increased the number of cells with intracellular *Cn* to 55.3% (Fig 3.2D). In this way, populations of *Cn*-infected M2-polarized macrophages could be produced that would be suitable for downstream transcriptome profiling experiments.

3.4. Modification of culture protocols to maintain nutrient levels

The preliminary RNAseq experiments indicated that intracellular *Cn* infection affected the expression of *TXNIP* transcripts (decreased 8.34-fold; q=0.0016) in RAW 264.7 macrophages. Studies have reported that *TXNIP* gene expression is upregulated in hyperglycemic circumstances, while reduced glucose availability may cause *TXNIP* suppression (249). Macrophages and *Cn* are typically co-cultured in all of these investigations in high glucose (4.5 g/dL) DMEM medium. Intracellular pathogens, especially *Cn,* replicate within host cell phagolysosomes and are extruded by macrophages into the surrounding culture, which may lead to glucose depletion during the 24 h course experiment. We reasoned that this could result in confounding transcriptional changes not directly driven by intracellular *Cn* growth.

To test whether TXNIP could be used as an indicator of glucose depletion in our culture system, RAW 264.7 cells were grown in DMEM containing 4.5 g/dL, 1.0 g/dL, or 0 g/dL for 24 h, and then TXNIP protein levels were measured by western blot analysis. Here, TXNIP was detected in cells grown in high glucose but was absent under decreased glucose conditions (Fig 3.3A).

As TXNIP was considered a suitable marker of altered gene expression due to glucose depletion, we performed immunoblotting studies to determine the effects of *Cn* infection and the accumulation of extracellular *Cn* macrophages on TXNIP protein expression. Our data demonstrated that intracellular *Cn* infection resulted in the complete loss of TXNIP protein levels in RAW 264.7 macrophages, indicating that *Cn*

growth in closed *in vitro* culture systems influenced transcriptional profiling (Fig 3.3B). To avoid this issue in future experiments, we altered our culture methods to incorporate medium changes every 6 h to eliminate extracellular *Cn*. The glucose levels were assessed post-*Cn* infection to determine whether our alteration had produced the desired response. Media replacement maintained the glucose concentration in *Cn*-infected samples at a steady level, indistinguishable from the mock-infected macrophages (Fig 3.3C).

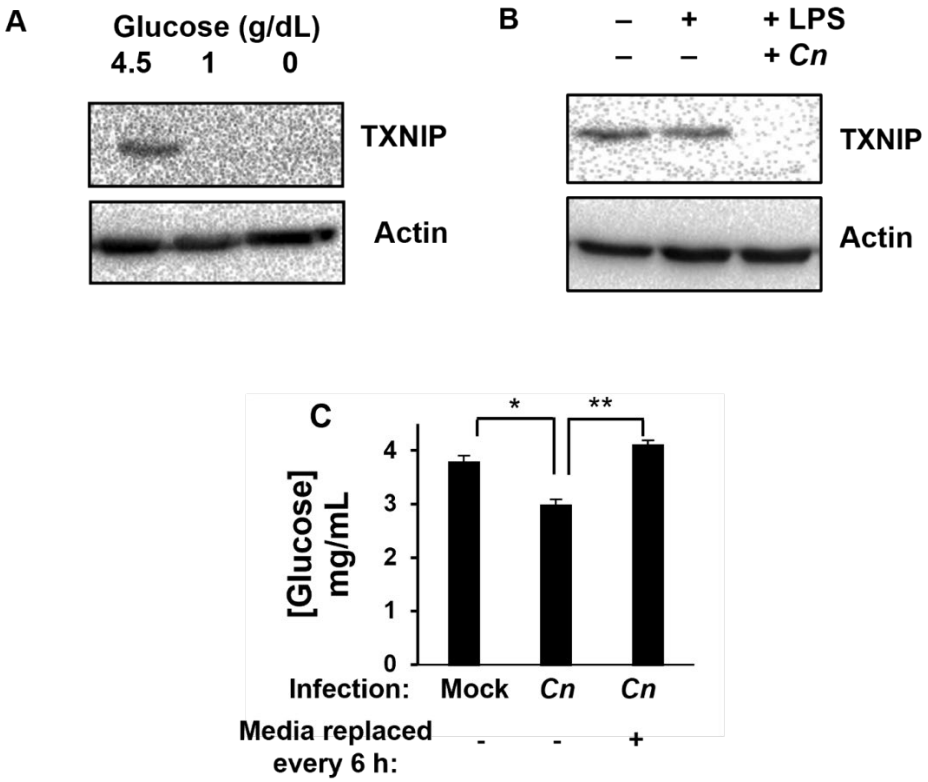

Figure 3.3: Media replenishment stabilizes glucose levels in *Cn*-infected macrophages. TXNIP, a glucose level marker, was assessed by western blotting in RAW264.7 macrophages following a 24h incubation in growth media containing (A) the respective glucose concentrations or (B) opsonized *Cn* or LPS for 2 h during infection, (C) Estimated glucose levels after media replacement 24 h post-infection using a glucose oxidase assay kit. Error is represented as SE. Statistical differences between samples were determined using one-way ANOVA followed by Tukey's multiple comparison test. Statistical significance is indicated as follows: *, $p < 0.05$; **, $p < 0.01$.

3.5 Discussion

The focus of this initial results chapter is the evaluation of tools for producing M1 and M2 polarized RAW 264.7 cells with optimum infection efficiency while maintaining a stable growth environment during the post-infection period. The establishment of this methodology prior to performing the transcriptome profiling experiments was critical to mitigate any spurious gene expression changes that may result from the increased rate of nutrient depletion caused by the rapid growth of intra- and extracellular *Cn* in our *in vitro* model.

The overarching goal of this study was to better understand how *Cn* affects macrophage polarization and function. While RAW 264. 7 macrophages are commonly used to investigate the mechanisms employed by the pathogen to alter host cell signaling, it was previously unclear whether they could be used to measure the impact of *Cn* infection on macrophage polarization due to the difficulty in polarizing these cells to the M2 state (167). Previous studies have shown that expression of the canonical M2 marker, Arg-1, is minimal in these cells when stimulated with IL-4 alone, indicating that this method cannot be used to induce an M2-like state. The expression of Arg-1 under these conditions can be improved by using agents that increase cAMP levels (250), such as 8-Br-cAMP (248). In our hands, cotreatment with IL-4 and 8-Br-cAMP elicited robust Arg-1, confirming that cAMP deficiency is likely responsible for the absence of Arg-1 expression in the presence of IL-4 alone (Fig 3.1C). While this approach is suitable for the study of Arg-1 expression, the addition of 8-Br-cAMP to macrophage cultures will

likely have broader transcriptional effects and may compromise our ability to study the impact of *Cn* infection on the M2 transcriptome. For this reason, a different approach to generating the M2 state is required.

As macrophages repolarize from one state to another in response to cytokines, we reasoned that it may be possible to achieve M2-like RAW264.7 by repolarizing them from the M1 state rather than directly polarizing naïve macrophages. This assumption proved correct. In these experiments, cells were treated with IFNγ for 24 h prior to IL-4 treatment, and care was taken not to reintroduce M1 cytokines after this point to avoid the residual expression of M1 markers. By following this procedure, we were able to achieve robust Arg-1 expression in RAW264.7 and, fortuitously, were able to increase the infection percentage of M2 cells by infecting macrophages immediately prior to repolarization with IL-4.

Using carefully optimized concentrations of capsule-specific antibodies and goat serum as potent opsonins in this research enabled us to attain >50% phagocytosis in M1 and M2-activated macrophages. The addition of MAb 18B7 activates the complement pathway, resulting in the early deposition of C3 on the cryptococcal capsule (244). In our study, we observed a similar response to the introduction of 18B7, which significantly enhanced the activity of goat serum, resulting in increased yeast cell ingestion by macrophages (Fig 3.2A and C). Overall, these data suggest that while goat serum helps promote phagocytosis, 18B7 is essential for the ingestion of *Cn*.

Although the growth of macrophages alone is unlikely to impact the glucose level in the medium over a 24 h period, provided that they are not over-confluent, *Cn*

doubles every 3 h and exits macrophages via phagosome extrusion, contributing to glucose depletion in the culture (51,245). The collection of live, extracellular *Cn* resulted in a substantial decrease in the expression of the glucose-responsive gene TXNIP at the transcript and protein levels in initial experiments (Fig 3.3B). TXNIP is a transcriptional regulator of central pathways involved in macrophage polarization (228,229). Reduced TXNIP levels owing to glucose deprivation may generate misleading gene expression alterations that may not represent the possible impacts of intracellular *Cn* growth on the transcriptome of host macrophages. Regular washing and replenishment of culture medium maintained nutrients and prevented loss of TXNIP expression, suggesting that under these conditions, we would be able to accurately assay the impact of intracellular *Cn* growth on host cell gene expression. Finally, we assert that data in Chapter 3 demonstrate the importance of developing a standard *in vitro* macrophage infection protocol under carefully regulated culture conditions, which will be utilized to investigate macrophage:*Cn* interaction in this thesis.

CHAPTER FOUR: TRANSCRIPTOME PROFILING OF M1 AND M2-*Cn* INFECTED MACROPHAGES

4.1. Introduction

The data in this chapter seek to determine the effects of intracellular *Cn* growth on host macrophages. Previous experimentation from Chapter 3 demonstrated that we developed an efficient macrophage infection protocol to address these questions using the RAW 264.7 murine macrophage-like cell line as an *in vitro* model system. To obtain insight into changes in gene expression in *Cn*-infected macrophages, we employed an unbiased RNAseq-based approach to identify the cellular processes affected due to the intracellular residence of *Cn*. This would enable us to ascertain how macrophage polarization is impacted on a broad transcriptional level.

Macrophage polarization is a dynamic process, not a terminal differentiation, shifting between functionally distinct states. This requires reprogramming of > 1000 genes that are primarily controlled by Janus kinase signal transducer and activator of transcription (JAK:STAT) and NF-κB pathways (101,102), which are often circumvented by a variety of pathogens as part of their intracellular survival (68,161,253,254). The infection of mice with the pathogenic H99S strain of *Cn* initially promotes a Th2 response, and the alterations in cytokine production linked with this infection drive M2 macrophage polarization (100,255–257). The phagosomes of these cells present a less hostile environment to the pathogen, resulting in an increased intracellular proliferation of fungal cells (81). *Cn* has relatively minor impacts on the expression of the primary markers of the M1 and M2 states, *Nos2,* and *Arg1* (82). However, the influence on the larger transcriptome associated with these states remains unknown.

Over the past decade, several reports have documented the transcriptional response of macrophages to *Cn* infection (233,258,259). The first suggestion that intracellular *Cn* might influence macrophage stress response pathways, along with altering protein translation rate in host cells, was published by the Casadevall group (233). Our lab also demonstrated that intracellular *Cn* alters the activity of the NF-κB pathway, a key regulator of M1 polarization that controls the response to cell stress. Specifically, *Cn* infection promotes NF-κB accumulation of p65-containing transcription factors without a corresponding increase in the expression of *Tnf*, a bona fide NF-κB target. While the mechanism by which this is achieved is not clear, computation modeling indicated that it may involve translational interference (167), a known effect of intracellular *Cn* infection (233).

As protection against cryptococcosis is associated with the M1 phenotype, the JAK-STAT pathway may also be modulated by *Cn* to enhance their persistence (67,107). In multiple investigations, TLR signaling has been found to play a crucial role in macrophage:*Cn* interactions (260,261). In addition to NF-κB, p53, another apoptotic pathway, gained more recognition in the past few years for its role in macrophage polarization and diseases (262–264). Many pathogens attenuate p53 levels and use it as a strategy to extend their survival in a hostile environment, such as host cells (265).

In vivo studies conducted in rodents indicated downregulation of M1 markers in *Cn*-containing granulomas and that intratracheal *Cn* infection altered pulmonary macrophage polarization from a resting state to an M2 phenotype, followed by an M1 phenotype and then back to a resting state (6,82). It is presently unknown how *Cn*

contributes to these alterations; thus, more research is needed. The latter study also demonstrated that the cytokine environment is the primary governing factor of macrophage polarization, and the plasticity property of macrophages extended to the microbicidal activity of host cells (82). While attempts were made in the above investigation to opsonize *Cn* to increase macrophage infection, it is unclear how effective these efforts were or what percentage of macrophages were really infected. This study used RAW 264.7 cells and relied only on qPCR to examine the transcript levels of M1 and M2 markers. However, in the above study, macrophage polarization was examined only by evaluating the expression of a limited number of M1 and M2 markers. Considering macrophage polarization is regulated by >1000 genes (95), assessing broader transcriptional changes is crucial for understanding macrophage-*Cn* interactions comprehensively.

In this chapter, we present data demonstrating alteration in the transcriptome of host macrophages by intracellular *Cn*, causing gene expression profiles of M1 and M2 cells to revert to a more M0-like state. While there was a disruption of the broad transcriptome of M1 and M2 macrophages during the course of an infection, the expression of core polarization markers, Nos2 and Arg1, were found to be only minimally affected. Furthermore, a critical finding of this study was the identification of the transcriptome signature of *Cn* infection. This included the upregulation of a transcriptional co-regulator, *Cited1*, in both polarization states.

4.2. Intracellular *Cn* increased iNos protein levels in M1-activated murine macrophages

The data presented in Chapter 3 led us to devise a strategy to produce *Cn*-infected M1 and M2 polarized RAW 264.7 macrophages (Fig 4.1A). This methodology was used for all subsequent transcriptome profiling and immunoblotting experiments. To start, M1 polarization was achieved by incubating naïve macrophages with IFNγ for 24 h, followed by mock or *Cn* infection using goat serum and 18B7-opsonized H99S for 2 h at 3:1 MOI. After 2 h, cells were washed to remove extracellular *Cn* and repolarized to M2 or maintained in an M1 polarization state by exposure to the appropriate cytokines. Macrophages were then washed, and the medium was replaced every 6 h to prevent nutrient depletion and eliminate extracellular *Cn*.

Before proceeding to a comprehensive analysis of differentially expressed genes (DEGs) of each state, as an initial control step, it was essential to evaluate changes in gene expression of core polarization markers in M1 mock- (M1mk) and M2 mock- (M2mk) infected samples (101,102). Through pairwise comparisons of M0 with M1mk and M2mk cells, we found upregulation of *Nos2*, *Stat1*, surface markers such as *Fcgr1*, *Cd86,* and a number of M1-associated chemokines and cytokines (*Il1b*, *Cxcl9*, *Cxcl10*, and *Ccl5*; Table 1) in M1mk cells. Likewise, we observed key M2 markers (*Arg1* and *IL10*) to be upregulated in M2mk cells (Table 2). A similar analysis was carried out in *Cn*-infected M1(M1*Cn*), and M2(M2*Cn*) samples, where we discovered the expression of *Nos2* was unaltered in M1mk vs. M1*Cn* or M2mk vs. M2*Cn*. Furthermore, *Ccl5* was

increased in M1mk and M1*Cn* comparison (FC = 3.71, *q* = 0.046) among the other M1 markers. These data were in agreement with prior reports showing that *Cn* infection has minimal influence on the expression of M1 and M2 hallmarks (82). However, *Arg1* was decreased in M2*Cn* compared to M2mk (FC = 3.97, *q* = 0.006). The levels of Arg-1 and iNos were assessed by western blotting to determine if these changes were also visible at the protein level. *Cn* infection enhanced iNos levels by ~40% in M1 polarized macrophages (Fig 4.1B and D). While there was a reduction in Arg1 mRNA levels in the M2 state, we did not notice a significant difference in Arg-1 protein expression in both polarization states (Fig 4.1B and C).

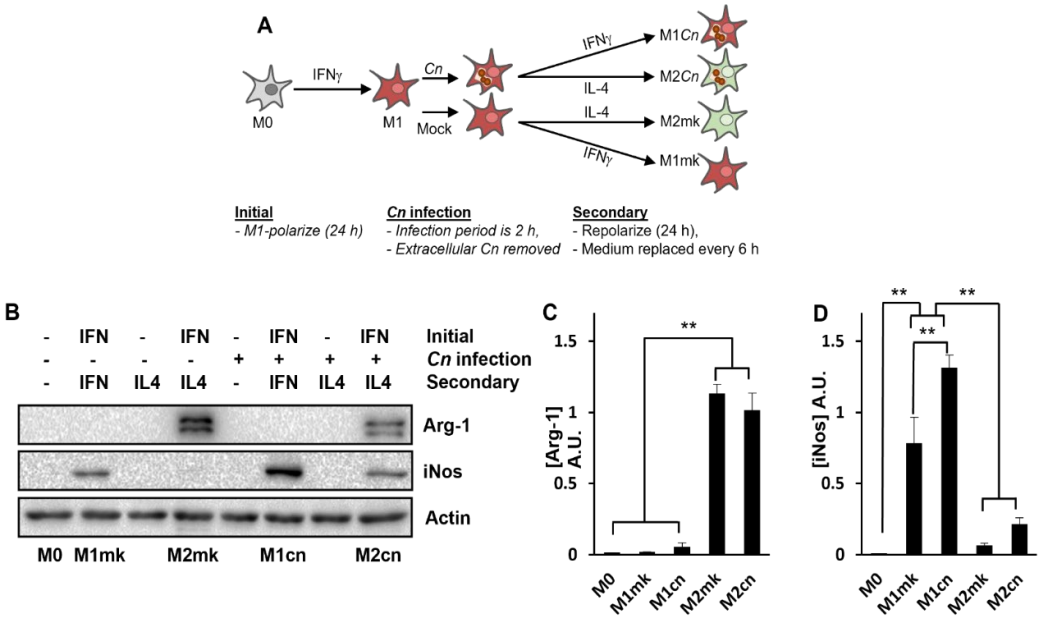

Figure 4.1: iNos protein expression is increased by 40% in M1-polarized macrophages during *Cn* infection. (A) Illustration to show macrophage infection protocol used in sample preparation for transcriptome profiling and immunoblot studies. (B) iNos and Arg-1, M1, and M2 markers, respectively, were assessed by western blotting in RAW264.7 macrophages after the indicated treatments. Quantification of (C) Arg-1 and (D) iNos protein levels in (B) by densitometry. Error is represented as S.E. Statistical differences were determined using a one-way ANOVA followed by a Tukey's multiple comparison test. Statistical significance is indicated as follows: *, $p < 0.05$; **, $p < 0.01$. (C and D) Data is from six biological repeats.

Table 1: M0 vs. M1mk: Changes in the expression of M1 macrophage markers observed in pairwise comparison in M0 with M1mk. FC = Fold-change.

M0 vs. M1mk			
Gene	**FC**	**Direction**	***q* -value**
Cxcl9	682.63	UP	0.00626191
Gbp2	369.19	UP	0.00626191
Cd86	356.53	UP	0.0383977
Nos2	150.18	UP	0.00626191
Cxcl10	139.62	UP	0.00626191
Stat1	46.87	UP	0.0334391
IL1b	46.41	UP	0.0161112
Fcgr1	17.61	UP	0.00626191
Ccl5	6.66	UP	0.0370904

Table 2: M1mk vs. M2mk: Changes in the expression of M1 and M2 macrophage markers observed in pairwise comparison in M1mk with M2mk. FC = Fold-change.

M1mk vs. M2mk			
Gene	**FC**	**Direction**	***q* -value**
Arg1	623.88	UP	0.00626191
Atp6v0d2	14.06	UP	0.0350194
IL10	10.08	UP	0.0413593
Cxcl10	18.9	DOWN	0.00626191
Cxcl11	15.77	DOWN	0.0200165
Nos2	12.24	DOWN	0.00626191
Cxcl9	8.84	DOWN	0.00626191
GBP2	5.21	DOWN	0.00626191

4.3. Distortion of the M1 transcriptome in *Cn*-infected macrophages

Examining changes in the expression of a small number of M1 and M2 markers alone is insufficient to thoroughly understand the influence of intracellular *Cn* on the host cell phenotype. To investigate critical processes altered in each state, we performed pairwise comparisons for DEGs between M0 and M1mk, and M2mk RNA using a fold change of 2. Equivalent analysis was performed on *Cn*-infected samples to generate lists of M0:M1*Cn* and M0:M2*Cn* DEGs. Of the 931 DEGs associated with M0 to M1 polarization, 332 (~36%) were common to the 460 DEGs from the M0:M1*Cn* comparison. The 128 DEGs (~28%) unique to the M0:M1*Cn* comparison were believed to be *Cn*-induced changes in gene expression not associated with the normal M1 transcriptional profile, whereas the remaining 599 DEGs (~ 64%) associated with M1 polarized state shifted towards a more M0-like state. (Fig. 4.2).

The Kyoto Encyclopedia of Genes and Genomes (KEGG) database was utilized to conduct a Gene Ontology (GO) analysis of the transcriptome data where DEGs from M0:M1mk and M0:M1*Cn* were compared (Fig 4.2). In the pool of M0:M1mk-exclusive DEGs, there was enrichment of genes associated with 'Endocytosis,' 'Phagosome,' 'Chemokines,' 'Antigen processing and presentation,' and 'Toll-like receptor signaling,' indicating that these processes were affected by *Cn* infection. Additionally, a shared pool of DEGs present in both pair-wise comparisons was also enriched with genes associated with fundamental M1 processes, including 'JAK-STAT signaling,' 'Toll-like receptor,' 'Cell-adhesion molecules,' and 'p53-signaling'. Genes related to GO terms

such as 'JAK-STAT' and 'NF-κB signaling' were found to be significant in the M0:M1*Cn* only pool, suggesting changes to these M1-associated processes during *Cn* infection, promoted a more M0-like host cell state. This is consistent with the notion that pathways linked to the establishment of the M1 transcriptional profile were impacted by *Cn* infection (67,115,146,167). One gene associated with the 'NF-κB signaling' GO term in this analysis was B cell leukemia/lymphoma 2-related protein A1a (*Bcl2a1a)*, the murine orthologue of *Bcl2a1*, encoding an anti-apoptotic Bcl2 family protein. The expression of *Bcl2a1a* was significantly upregulated in *Cn*-infected M1 and M2 polarized cells (FC = 4.95, q=0.006; FC=4.93, q=0.006). This is a bona fide NF-κB-responsive gene (266). Collectively, these data were consistent with the notion that *Cn*-infection impacts core pathways important for M1 polarization reported by prior studies (146,167).

M0:M1mk and M0:M1*Cn* DEGs were examined using STRING to produce a visual representation of protein-protein interaction networks in *Cn*-infected M1 polarized host cells (Fig 4.3A and B). As expected, this analysis revealed an antigen processing and presentation cluster, while the innate immune function gene cluster was smaller in the M0:M1*Cn* DEGs than that in the M0:M1mk DEGs, indicating potential disruption of M1 polarization.

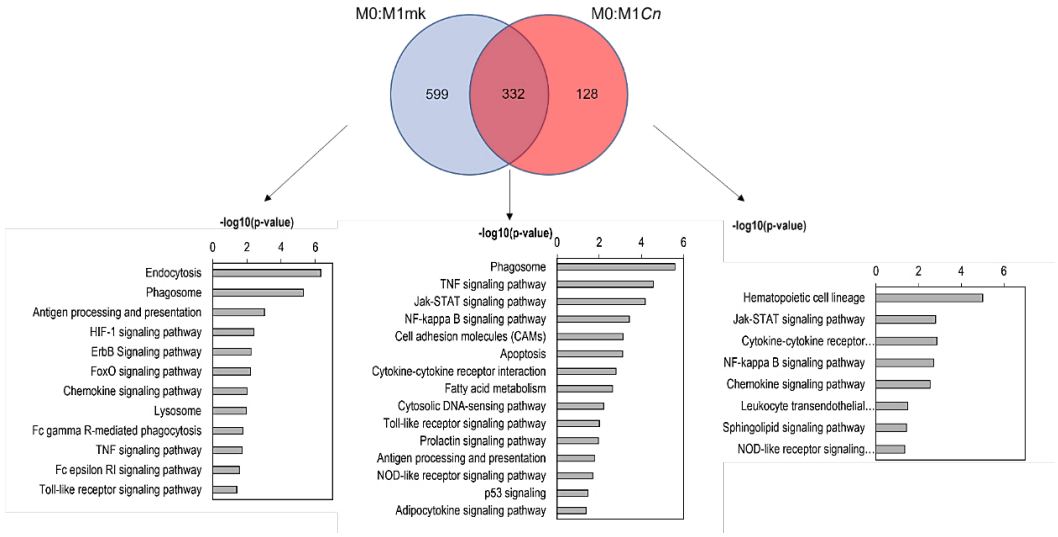

Figure 4.2: Gene ontology (GO) analysis of *Cn*-infected M1 macrophages: Pairwise comparisons for common and differentially expressed genes (DEGs) between M0:M1mk and M0:M1*Cn* are represented as Venn diagrams. Relevant pathways are ranked by–log(p-value).

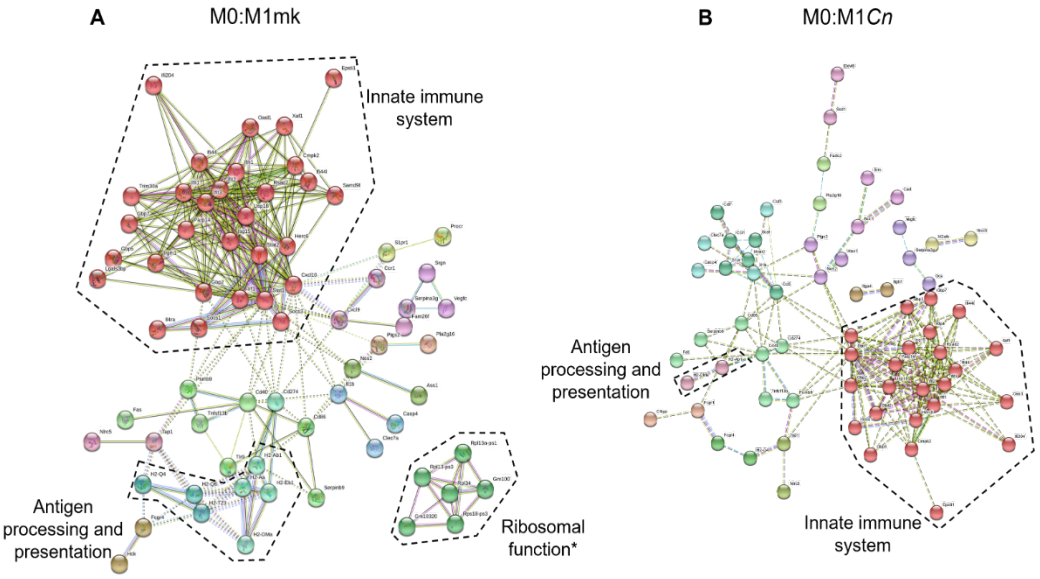

Figure 4.3: Disruption of M1 polarization during *Cn*-infection. Differentially expressed genes (DEGs) from M0:M1mk and M0:M1*Cn* were analyzed using the Search Tool for the Retrieval of Interacting Genes/Proteins (STRING). Gene ontology (GO) term data and information from the literature were used to create boundaries encompassing gene clusters with similar functions. *Genes within the 'Ribosome function' boundary are pseudogenes.

4.4. Distortion of the M2 transcriptome in *Cn*-infected macrophages

The analyses described in section 4.3 were repeated using DEG sets obtained from pairwise comparisons involving M2-polarized samples. Here, 234 genes (~40%) of the 583 DEGs associated with M0 to M2 polarization were shared between mock and *Cn*-infected cells. While only 106 DEGs appeared to be unique to the *Cn*-infected state, 349 DEGs (~60%) were unique to the mock-infected cells. This implied that the gene expression changes associated with this later group were reversed by *Cn* infection. Overall, this analysis indicated that *Cn* infection promotes macrophages to adopt a more M0-like state, even under M2-polarizing conditions.

The GO analysis was performed on these three separate DEG groups (Fig. 4.4), and the GO term 'p53 signaling' was identified. This pathway, centering around the activity of the tumor suppressor protein, p53, is more commonly associated with cell cycle arrest and apoptosis. However, it has more recently also been shown to function as a suppressor of M2-associated gene expression in bone marrow-derived macrophages (BMDMs) (267). In our analysis, genes associated with this GO term that were significantly upregulated in M2mk cells included *CCng1*, *Cdkn1a* (p21), and *Mdm2*. Additionally, we found a few KEGG pathway terms, such as 'Phagosome' and 'Antigen processing and presentation,' enriched amongst common and M0:M2mk unique pools of DEGs. We also observed that 'NF-κB signaling' was the only GO term associated with the M0:M2*Cn* pool. The pool was relatively small and included *Plau*, *Cd40*, and *Traf1*. This pool also included *Bcl2a1*, which was upregulated in *Cn*-infected M2 polarized cells

(FC=4.93, *q*=0.006). This is notable as this anti-apoptotic gene was also upregulated in M1-polarized *Cn*-infected cells.

M0:M2mk and M0:M2*Cn* DEGs were used to perform equivalent STRING analysis (Fig. 4.5A and B). The antigen processing and presentation clusters in M0:M2mk and M0:M2*Cn* macrophages were similar in size, indicating that *Cn* infection had a more negligible impact on this process. Although the innate immune function gene cluster differed in M2 macrophages, the cluster was larger for M0:M2*Cn* than M0:M2mk DEGs (23 vs. 17 genes).

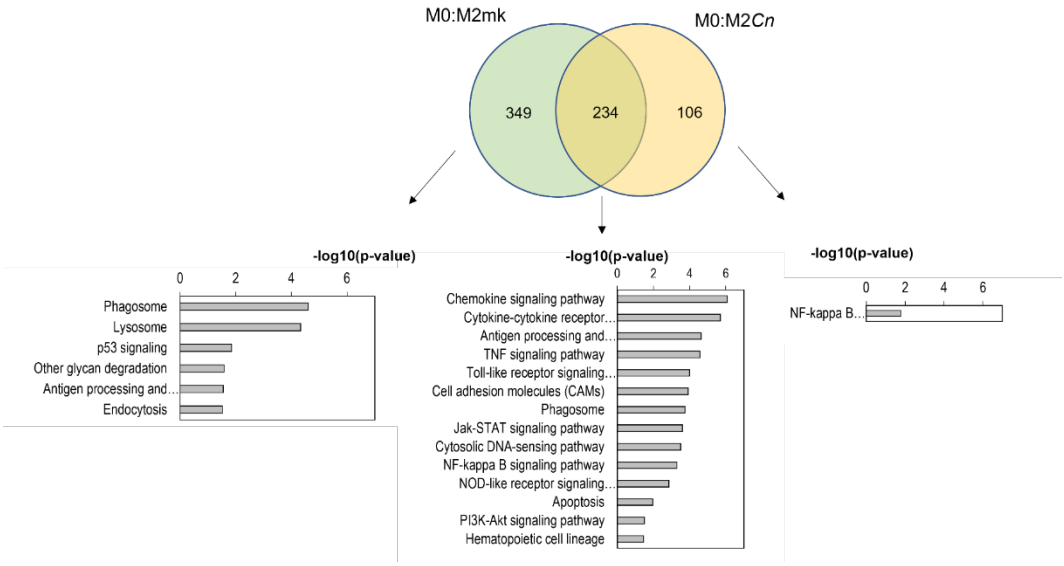

Figure 4.4: Gene ontology (GO) analysis of *Cn*-infected M2 macrophages: Pairwise comparisons for common and differentially expressed genes (DEGs) between M0:M2mk and M0:M2*Cn* are represented as Venn diagrams. Relevant pathways are ranked by–log(p-value).

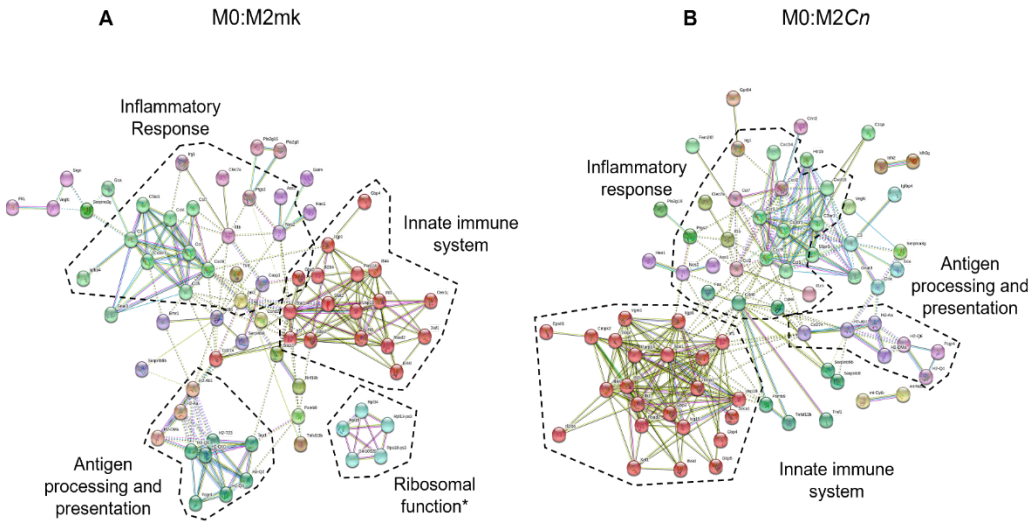

Figure 4.5: Disruption of M2 polarization during *Cn*-infection. Differentially expressed genes (DEGs) from M0:M2mk and M0:M2Cn were analyzed using the Search Tool for the Retrieval of Interacting Genes/Proteins (STRING). Gene ontology (GO) term data and information from the literature were used to create boundaries encompassing gene clusters with similar functions. *Genes within the 'Ribosome function' boundary are pseudogenes.

4.5. A transcriptome signature of *Cn* infection

We hypothesized that intracellular *Cn* infection would result in a subset of gene expression changes that would be common amongst host macrophages regardless of the polarization state. We describe these as a 'transcriptome signature of *Cn* infection.' This hypothesis was tested in two steps. First, we examined DEGs from the M1mk:M1*Cn* and M2mk:M2*Cn* DEGs pairwise comparisons separately using STRING and GO analysis to identify broad patterns in gene expression changes in M1 and M2 cells post-*Cn* infection. Next, the two DEG sets were directly compared to identify common concordant genes. The outcome of this analysis is detailed below.

For the first phase of the analysis, 204 DEGs were identified in the M1mk:M1*Cn* pairwise comparison (101 upregulated and 103 downregulated) and 254 for M2mk:M2*Cn* (144 upregulated and 110 downregulated). These data were then utilized to determine changes in M1- and M2-associated gene interaction networks. STRING analysis showed gene clusters associated with the innate immune system and ribosome function in both states (Fig 4.6). However, the number of genes in these clusters was different, suggesting distinct roles of these processes in M1 and M2 states. Cell cycle regulation was the smallest cluster identified in M1mk:M1*Cn,* comprising three downregulated genes (*Klf4*, *Cdkn1a,* and *CCng1*). In contrast, despite the expression of *Ccng1*, this cluster was missing in M2mk:M2*Cn* because of the absence of *Klf4* and *Cdkn1a.* A GO analysis using the same DEG lists for GO keywords associated with biological processes (BP) revealed an enrichment of genes related to 'Chemotaxis,'

'Endocytosis,' and 'Inflammatory response'(Fig 4.7A and B). In addition to the similarities, there were also differences between the M1 and M2 states. Genes associated with 'Positive regulation of phagocytosis' and 'Phagocytosis' were only observed in the M2mk:M2*Cn* comparison. In contrast, the terms 'leukocyte cell-cell adhesion', 'Toll-like receptor 9 signaling pathway', 'Positive regulation of inflammatory response,' and 'Negative regulation of NF-κB' were only enriched in M1mk:M1*Cn* DEGs.

For the second phase of the analysis, where the DEGs from the M1mk:M1*Cn* and M2mk:M2*Cn* pairwise comparisons were directly compared, we identified 38 common and concordant genes (15%–19%), with 8 being upregulated and 30 being downregulated (Tables 3 and 4, respectively). A substantial proportion of these genes constituted reversals or partial reversals of gene expression changes that occurred after repolarizing from M0 to M1, M0 to M2, or both. Seven genes from this collection appeared to be exclusive to *Cn*-infected cells and did not initially appear to be associated with M1 or M2 polarization. These included the upregulation of three genes, *Cited1*, *Ccl22*, and *Bcl2a1a*, and the downregulation of four, *Itgax*, *Ank*, *Lrp1,* and *Atp2a2*. However, it was later determined that *Cited1* upregulation could be induced by IFNγ alone, although infection with *Cn* stimulated a larger increase in the expression of this gene (see Chapter 5).

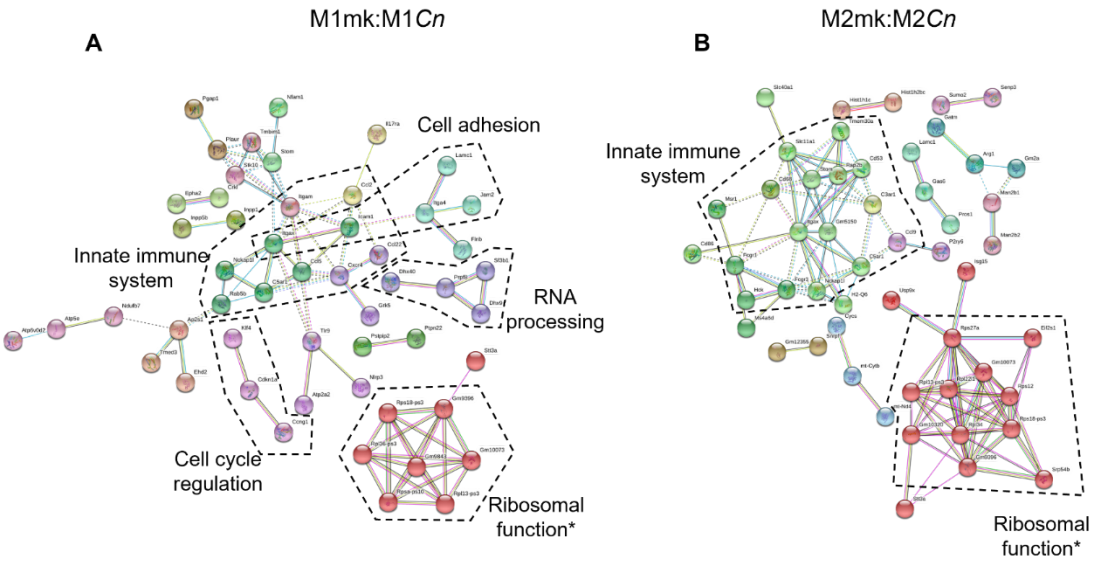

Figure 4.6: Search Tool for the Retrieval of Interacting Genes/Proteins (STRING) analysis of differentially expressed genes (DEGs) from (A) M1mk:M1*Cn* (B) M2mk:M2*Cn*. Gene ontology (GO) term data and information from the literature were used to create boundaries encompassing gene clusters with similar functions. *Genes within the 'Ribosome function' boundary are pseudogenes.

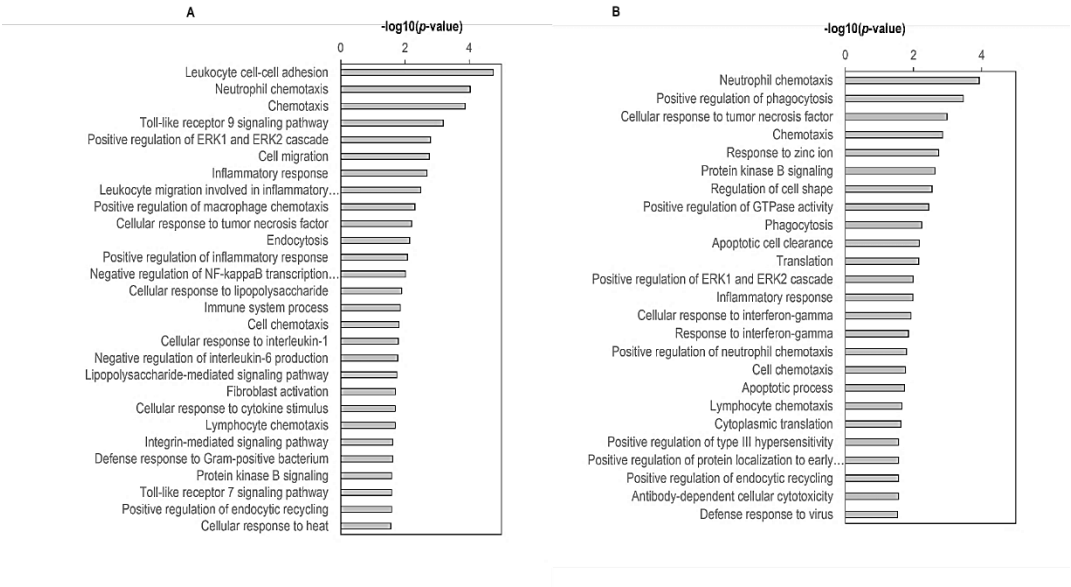

Figure 4.7: Gene ontology (GO) analysis of *Cn*-infected M1 and M2 macrophages: Pathway analysis performed in the Database for Annotation Visualization and Integrated Discovery (DAVID) on differentially expressed genes (DEGs) from (A) M1mk:M1*Cn* (B) M2mk:M2*Cn*.

Table 3: M1mk vs. M1*Cn* and M2mk vs. M2*Cn*. Common concordant upregulated genes in *Cn*-infected cells. FC = Fold-change.

	M1mk vs. M1*Cn*		M2mk vs. M2*Cn*	
Gene	**FC**	**q-value**	**FC**	**q-value**
Cited1	14.81	6.26E-03	20.49	1.61E-02
Hsf3	7.93	2.86E-02	8.04	0.0200165
Jarid2	5.45	2.52E-02	2.88	0.0389813
Tmtc2	5.14	9.61E-03	3.94	0.00626191
Ccl22	5.09	3.50E-02	4.1	0.00626191
Sspn	3.66	4.28E-02	3.21	0.0251778
Wdr89	3.09	3.34E-02	2.43	0.0389813
Bcl2a1a	2.68	4.68E-02	2.95	0.0171929

Table 4: M1mk vs. M1*Cn* and M2mk vs. M2*Cn*. Common concordant downregulated genes in *Cn*-infected cells, FC = Fold-change.

Concordant down-regulated genes in *Cn* -infected cells				
	M1mk vs. M1*Cn*		M2mk vs. M2*Cn*	
Gene	FC	q-value	FC	q-value
Sorl1	37.12	3.90E-02	3.86	0.046023
Dusp6	14.54	1.29E-02	6.72	0.0375289
C5ar1	12.07	6.26E-03	5.45	0.00626191
Ehd2	11.63	6.26E-03	5.08	0.00626191
Grk5	8.83	6.26E-03	4.48	0.0128586
Cd300ld	7.24	6.26E-03	2.7	0.0389813
Zfp146	6.31	1.61E-02	3.97	0.0304857
Endod1	6.21	6.26E-03	2.57	0.027269
Usp9x	6.11	2.00E-02	3.88	0.0383977
Xdh	6.02	6.26E-03	3.21	0.0171929
Stom	4.86	6.26E-03	2.84	0.00626191
Pik3ap1	4.48	6.26E-03	3.52	0.0389813
Car5b	4.36	2.52E-02	3.91	0.034954
Itgax	4.2	2.25E-02	3.73	0.0171929
Gatm	4.06	6.26E-03	7.79	0.00626191
Ms4a6b	3.46	3.50E-02	4.81	0.0128586
Fgd3	3.42	1.29E-02	2.64	0.0383977
Man2b1	3.27	1.29E-02	3.37	0.00961334
Lamc1	3.23	3.63E-02	3.69	0.0200165
Tep1	3.1	4.60E-02	2.74	0.0375289
Dhx40	3.07	4.77E-02	3.22	0.0322409
Ank	3.07	2.00E-02	2.97	0.00626191
Ccng1	2.9	2.00E-02	2.89	0.00626191
Stt3a	2.9	2.73E-02	2.81	0.0249383
Plekho2	2.88	3.84E-02	3.36	0.0251778
Cdc42se2	2.82	2.86E-02	2.39	0.0383977
Lrp1	2.75	4.77E-02	2.55	0.0357649
Myo1e	2.7	3.63E-02	3.75	0.00626191
Nckap1l	2.63	3.75E-02	2.52	0.0251778
Atp2a2	2.5	4.28E-02	2.23	0.0420558

4.6 Discussion

It has long been known that *Cn* infection promotes transient M2 polarization during the infection of macrophages in murine cryptococcosis models (82). The reasons for this have been enigmatic, and it is unclear whether this is driven by the broader immune response to *Cn* and the production of M2-polarizing cytokines or a cell-autonomous effect operating at the level of individual host macrophages. Early attempts to make this distinction using *in vitro* cell culture models have suggested that the former model was the most plausible as the polarization state of macrophages was dictated by the cytokine environment of the cells and not the presence or absence of opsonized *Cn* (82). While that study is instructive and shaped the design of the current work, it measured the effect of *Cn* on macrophage polarization by looking at a handful of canonical M1 and M2 markers. Given that the gene expression changes accompanying polarization exceed 1000 genes, this approach may not have provided a complete picture of the effects of *Cn* infection. Indeed, more recent transcriptome profiling studies have shown extensive gene expression changes after infection of macrophages with live or heat-killed *Cn*, although this work did not consider the polarization state (233). For these reasons, it remained unclear what the impact of *Cn* infection was on the transcriptional regulatory processes controlling polarization at the level of individual macrophages.

The data presented in this chapter support the notion that intracellular *Cn* infection disrupts polarization, as we show that the gene expression changes

accompanying both M1 and M2 polarization are partially reversed with *Cn* infection, causing gene expression to shift towards an M0-like state. In this sense, our study at least partially agrees with the findings of earlier *in vivo* studies and indicates that these changes in gene expression are not entirely driven by the cytokine environment of the cells and may have a cell-autonomous component. However, it is important to recognize that these shifts toward a naïve macrophage transcriptome state post-infection are uniform. To our surprise, *Cn* infection affected the core polarization markers. Infection of M1-polarized macrophages increased iNos protein levels by 40% (Fig 4.1B and D). Given the vital importance of this protein in macrophage anticryptococcal activity (67), this has the potential to enhance macrophage fungicidal activity despite the reversal of other M1-associated gene expression changes. Furthermore, our study detected increased expression of some proinflammatory cytokines, including *Ccl2,* in *Cn*-infected macrophages, which is not consistent with a fully attenuated M1 state. Conversely, *Arg-1* transcript levels were slightly reduced in *Cn*-infected M2 macrophages, although this change did not extend to the protein level (Fig 4.1B and C). Additional regulatory factors, such as translational or posttranslational processes governing the iNOS and Arg1 proteins' translation and/or stability, may explain the discrepancies observed in M1 and M2 markers. As these markers make a large and tangible contribution to the outcome of macrophage:*Cn* interactions, these results merit further investigation.

Aside from the influence of *Cn* on the primary polarization markers, our data demonstrated broader impacts on the host cell transcriptome and essential processes

associated with each polarization state. We believe these alterations are genuine and not impacted by the growth environment of the macrophages, as we implemented measures in our experiment design to control nutrient levels (see Chapter 3.4). Using GO and STRING analyses of the transcriptome data sets, we identified common and distinct cellular processes affected in M1 and M2 *Cn*-infected cells. The appearance of GO terms 'Phagosome', 'Lysosome,' 'Endocytosis,' and 'Chemokine signaling pathway' in the M0:M1-exclusive pool from the M0:M1 vs. M0:M1*Cn* comparison indicated that *Cn* infection reversed the transcriptome changes in these pathways to a more M0-like state (Fig 4.2). A similar effect was observed in the M0:M2 vs. M0:M2*Cn* analysis but not for the 'Chemokine signaling pathway,' which was associated with the DEG list common to the M0:M2 and M0:M2*Cn* pairwise comparisons, implying that *Cn* infection in the M2 state did not revert the expression of these genes to an M0-like state. However, these analyses do not explicitly consider fold change, so it is possible that *Cn* infection may still perturb the expression of these genes, and this nuance has been missed.

When examining individual genes in this analysis, *Atp6v0d2* was upregulated in *Cn*-infected M1-polarized cells (M1mk:M1*Cn* FC = 12.98, q = 0.036). This is potentially meaningful as the gene encodes a subunit of the V-type proton pump. These pumps are essential for the acidification of the phagolysosome, and this macrophage-specific component of the pump promotes autophagosome-lysosome fusion during *Salmonella* Typhimurium infection (268).

Given the role of NF-κB signaling in the establishment of the M1 phenotype and its role in macrophage antimicrobial and proinflammatory function, changes in the expression of NF-κB-regulated genes were of great interest. According to the GO analysis, the altered expression of NF-κB signaling-regulated genes was another similarity between M1 and M2 cells in response to *Cn* infection (Figs 4.2 and 4.4). Perhaps, this is the most notable GO term and the only one found in M2 cells (Fig 4.4). When examining the NF-κB-regulated genes identified, *Bcl2a1a,* the murine ortholog of *Bcl2a1*, was notable. This encodes the anti-apoptotic Bcl2 family protein A1, which is one of the few common concordant genes detected, exhibiting a similar fold change between mock and *Cn*-infected cells in both polarization states and which has not previously been associated with *Cn* infection of macrophages. This result was of interest as the intracellular residence of *Cn* causes both cellular and molecular damage to host cells while causing minimal cell death and apoptosis (269). Considerable evidence has indicated that *Bcl2a1a* is an NF-κB regulated gene and suppresses TNF-α-induced apoptosis (270). Another Bcl-2 family gene, *Bfl1a1*, has been established as a negative regulator of autophagy in mycobacterial infection (271). The significance of *Bcl2a1a* in *Cn*-harboring host cells remains unclear and should be investigated further to better understand its role in infection.

The striking difference between the two polarization states was the enrichment of the ‘p53 signaling‘ term in M2mk-exclusive genes (Fig 4.4). Although the alterations in p53 signaling have never been linked to intracellular infection by *Cn* before, a recent investigation of extracellular vesicles from infected human and murine host cells found

that immune-related pathways, including p53, were impacted (272). Another notable difference was the presence of 'Phagocytosis' and 'Positive regulation of phagocytosis.' in the M2mk:M2*Cn* pool, where all genes associated with these terms (counts of 4 and 5, respectively) were downregulated. This included *Pros1*, which encodes Protein S, a vital regulator of phagocytosis in macrophages (273). However, KEGG pathway analysis in M2 polarized cells revealed enrichment of 'Lysosome' (p = 0.034) and 'Chemokine signaling pathway' (p = 0.034). It is worth noting that except for *Ccl22* and *Grk5*, the list of genes associated with the 'Chemokine signaling pathway' term for M1 and M2 cells (7 and 6 genes, respectively) differed.

The establishment of a transcriptome signature of *Cn* infection was one of the most noteworthy findings of this study. We identified a set of genes commonly and concordantly affected by *Cn* infection, regardless of host polarization states. The concordant list comprised a total of 38 genes, with 8 upregulated and 30 downregulated (Tables 3 and 4). The transcriptional regulators *Cited1*, *Hsf3*, and *Jarid2*, the cytokine *Ccl2*, and the anti-apoptotic factor *Bcl2a1a* were all part of the small upregulated pool. Amongst these, *Cited1* (formerly Melanocyte-specific gene 1; *Msg1*) exhibited the highest fold change in *Cn*-infected M1- and M2-polarized macrophages (Table 3). CITED1 has been demonstrated to control estrogen receptor alpha (208), TGF-4/Smad4 (192), and Wnt/-catenin-responsive genes (192,208,274). CITED1, being a transcriptional co-regulator, regulates the interaction of other transcription factors with CBP/p300 to promote or repress gene expression (207). This is the first time CITED1 has been shown to be expressed in macrophages, and its role in this context is

unclear. However, another CITED family member, CITED2, has been demonstrated to suppress proinflammatory transcription factors in macrophages, which is attained through the destabilization of the HIF1α protein (197). A more recent study showed that CITED2 suppresses a wide range of proinflammatory gene programs by inhibiting NF-κB and STAT1 transcription factor activity (198,203). Collectively, these data suggest that CITED2 blocks all major transcription factor pathways that regulate macrophage M1 polarization. This suggests the intriguing idea that CITED1 may exhibit a similar role in fungal infection. Induction of CITED1 has not been previously reported in *Cn* infection and should be explored further. Questions and experiments addressed in Chapter 5 seek to validate CITED1 at the protein level and investigate its impact on the function of transcriptional regulators that govern macrophage polarization.

CHAPTER FIVE: REGULATION OF MACROPHAGE IFNγ-STIMULATED GENE EXPRESSION BY THE TRANSCRIPTIONAL COREGULATOR CITED1

5.1 Introduction

The data in this chapter seek to determine the effects of the transcriptional coregulator CITED1 on IFNγ-stimulated gene expression. Previous experimentation from Chapter 4 demonstrated that *Cn*-infection alters gene expression programs important for M1 polarization, promoting a more M0-like host cell state and upregulating several transcriptional coregulators, including CITED1. Further investigation revealed that IFNγ stimulation alone was sufficient to induce CITED1 expression in macrophages. To examine the more general effects of CITED1 expression on the transcriptome in response to polarizing and proinflammatory stimuli and to identify CITED1-regulated genes, we decided to employ complementary gain- and loss-of-function manipulations paired with RNAseq-based gene expression profiling.

Innate immune cells like macrophages are crucial for preserving tissue homeostasis (43). Under healthy conditions, macrophages participate in tissue regeneration and repair by removing dead cells and other cellular debris, as well as limiting inflammatory responses (275). However, the inflammatory cascade brought on by an infection or immunological response mostly involves activated macrophages. These macrophages primarily use PRRs, including TLRs, to recognize pathogen-derived ligands and coordinate a suitable inflammatory response (276). These receptor-ligand interactions stimulate signaling cascades that culminate in the activation of various transcriptional regulators, including NF-κB, AP1, STAT1, HIF1a, interferon regulatory factor 1,3 or 5 (IRF1, IRF3, or IRF5), which in turn promotes the production of a variety

of proinflammatory cytokines and chemokines, as well as other genes associated with phagocytosis and antimicrobial activity (277–280).

Microbial ligands are not the only signals that affect macrophage activation. This process can be triggered or enhanced by endogenous cytokine signals. One of the most important of which is IFNγ, the only type II IFN. This cytokine regulates innate and adaptive immunity and triggers cellular defense mechanisms that interfere with viral replication (104). Critically, it also stimulates classical or M1 activation of macrophages. This is achieved through the activation of STAT1 and IRF1 transcription factors, which coordinate the expression of ISGs (281).

IFNγ homodimers promote STAT1 activity by binding to and assembling tetrameric IFNGR complexes from IFNGR1 and IFNGR2 dimers. Through phospho-tyrosine-binding Src-homology-2 (SH2) domains, active JAK 1 and 2 allow STAT1 proteins to dock with the receptor complex. This brings these transcription factors close to activated JAK proteins, which then phosphorylate Y701 in the STAT1 C-terminus. The same SH2 domains required for receptor engagement also help phosphorylated STAT1 proteins homodimerize, resulting in the formation of γ-activated factors (GAF). These GAFs translocate to the nucleus and bind enhancers, including palindromic IFNγ ISG expression (125). To regulate the second wave of gene expression, activated STAT1 also stimulates the expression of *Irf1*, which is itself an ISG.

IRF1 proteins bind to ISRE and IRF-response elements in ISG promoters (120,282). A few examples of these include the interferon-stimulated gene 15 (*Isg15*), the 2'-5'-

oligoadenylate synthase 1 (*Oas1*), interferon-induced protein with tetratricopeptide repeat 1 (*Ifit1*), and the MX dynamin-like GTPase 1 (*Mx1*) genes (135). Furthermore, GAS and ISRE cis-regulatory site-containing genes are co-regulated by IRF1 and STAT1 (132,133,283). These include bone marrow stromal cell antigen 2 (*Bst2*), interferon-induced transmembrane protein 1 (*Ifitm1*), and *Irf9*. This set of co-regulated genes also includes *Stat1* itself, constituting a positive feedback loop that may help to further amplify the transcriptional response to IFNγ (284).

Several systems restrict macrophage IFNγ signaling to avoid tissue damage from uncontrolled or persistent inflammation (218,285,286). Anti-inflammatory cytokines, such as IL-4 and IL-13, are endogenous negative regulators of inflammation. IL-4 activates STAT6, which promotes changes in gene expression that drive cells toward the anti-inflammatory M2 polarization state and reduces NO production in cells through the expression of *Arg1*. In addition, cells also express cell-intrinsic factors during an IFNγ-response that suppresses proinflammatory gene expression. This includes the suppressor of cytokine signaling 1 (*Socs1*), an ISG co-regulated by STAT1 and IRF1, which serves as a strong antagonist of IFNγ signaling at the JAK level (287–289). A more recent study has identified a transcriptional co-regulator known as CITED2 that functions as a suppressor of proinflammatory gene programs in macrophages (197).

CITED2 is one of three mammalian CITED family proteins that enhance or inhibit gene expression by enabling or blocking transcription factors from establishing chromatin complexes with histone acetyltransferase, CBP, or p300 (186,187,189,192).

These interactions require the CR2 domain common to all CITED proteins and protein interaction motifs present within the largely unstructured N-terminal region (192). In myeloid cells, including macrophages, CITED2 is constitutively expressed and localizes to the nucleus. Here, most of the cellular pool of the protein is associated with CBP/p300 (196), and limits HIF1α and p65-containing NF-κB transcription factors' access to CBP/p300, thus suppressing proinflammatory gene expression (182,196,198,202,290). In addition, CITED2 has been shown to inhibit both STAT1- and IRF1-dependent ISGs in bone-marrow-derived macrophages and RAW264.7 macrophage-like cells (203).

In this chapter, I present data demonstrating that IFNγ-stimulation induces the expression of CITED1, another CITED family member, in a STAT-1-dependent manner. In contrast to the reported effects of CITED2 (203), the production of ectopic CITED1 significantly increased the expression of STAT1- and IRF1-dependent ISGs in IFNγ-stimulated macrophages; however, in *CITED1* KO cells, this effect was reversed. Collectively, these data indicate that CITED1 plays a significant role in the control of the transcriptional response to IFNγ and acts largely as a positive regulator of STAT1- and IRF1-regulated genes. Based on the kinetics of CITED1 expression, these findings suggest that CITED1 may be a part of a later wave of ISG expression that may enhance the IFNγ response for a subset of STAT1- and IRF1-regulated genes.

5.2. IFNγ stimulates CITED1 Expression in RAW 264.7 Macrophages

CITED2 is abundantly expressed at both the transcript and protein levels in human/murine monocytes and macrophages and has been demonstrated to have a crucial role in innate immune activity (197,198,202,203,291). This protein is essential for cellular development and differentiation (292) and functions as an antagonist of the transcriptional regulators NF-κB, HIF1, STAT1, and IRF1 (197,198,203). *CITED1* and *CITED4* are also members of the mammalian CITED family, but their expression levels are 100-fold lower than *CITED*2, indicating that they may not have a significant biological function in macrophages. However, in our prior experiments (see Chapter 4), *CITED1* showed the highest fold increase in both *Cn*-infected M1 and M2 cells amongst observed concordant DEGs (FC = 14.81 and 20.49 in M1 and M2 cells, respectively) (Table 3), indicating that this gene is expressed in macrophages as part of the transcriptional response to intracellular *Cn* infection.

Further investigation revealed that whereas *CITED1* expression was not detected in M0 macrophages, it was expressed in these cells after IFNγ treatment polarized them to the M1 state, and infection with live *Cn* further increased this expression by ~15-fold (Fig. 5.1A). To corroborate this finding and examine the kinetics of IFNγ-stimulated *CITED1* expression, RNA was extracted from RAW264.7 macrophages. qRT-PCR was used to assess *CITED1* transcript levels in these cells at 3, 6, 12, 24, and 48 h post-IFNγ treatment. *CITED1* levels, in this case, were evident at 24 h and increased further by 48 h post-stimulation (>300-fold increase in t = 0 vs. 48 h; Fig. 5.1B). This result was also

reflected at the protein level (Fig. 5.1C). In contrast, *CITED2* expression has been reported to be suppressed by the M1 polarizing stimuli, IFNγ, and LPS, at 6 h post-treatment (197). Consistent with this, we also saw a drop in the levels of *CITED2* transcripts, but this was only temporary and was not statistically significant, with *CITED2* levels returning to baseline by 24 h post-stimulus (Fig. 5.1D).

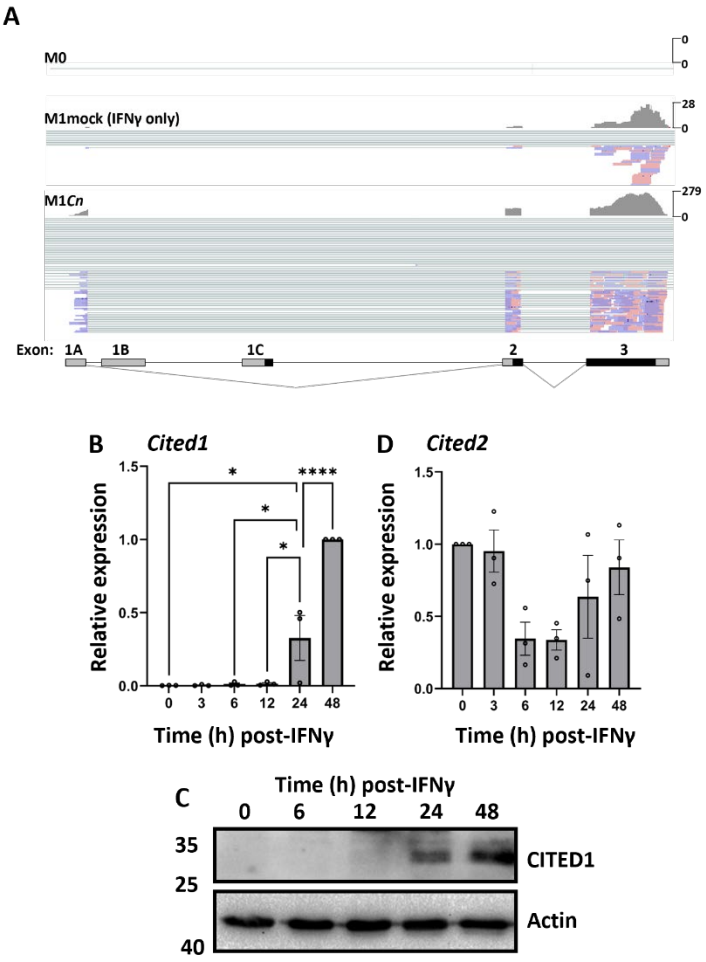

Figure 5.1. CITED1 expression is induced by IFNγ. (A) Alignment of RNAseq reads of the *CITED1* gene using Integrated Genome Viewer. Protein coding regions of exons are marked in black. (B+D) *CITED1* and *CITED2* mRNA levels were measured at different times post-IFNγ using qPCR. (C) Western blot analysis of IFNγ-treated RAW 264.7 cells for CITED1. Error is represented as S.E. Statistical differences between samples were appraised using one-way ANOVA followed by a Tukey's multiple comparison test. Statistical significance is indicated as follows *, $p < 0.05$; **, $p < 0.01$; ***, $p < 0.001$; ****, $p <$ 0. 0001.

To evaluate the impact of additional M1-polarizing stimuli on the expression of *CITED1* and *2*, macrophages were stimulated with LPS alone or in combination with IFNγ. Here, LPS alone did not influence *CITED1* expression, nor did it enhance the IFNγ-stimulated expression of the gene (Fig. 5.2A). However, treatment with LPS or IFNγ alone showed no influence on *CITED2* expression 24 h post-stimulation (Fig. 5.2B), and co-treatment with IFNγ and LPS stimulated a > 4-fold increase in *CITED2* levels. These contrasting expression patterns show that *CITED1* and *2* are controlled differently and presumably serve distinct roles in the modulation of the response to proinflammatory stimuli.

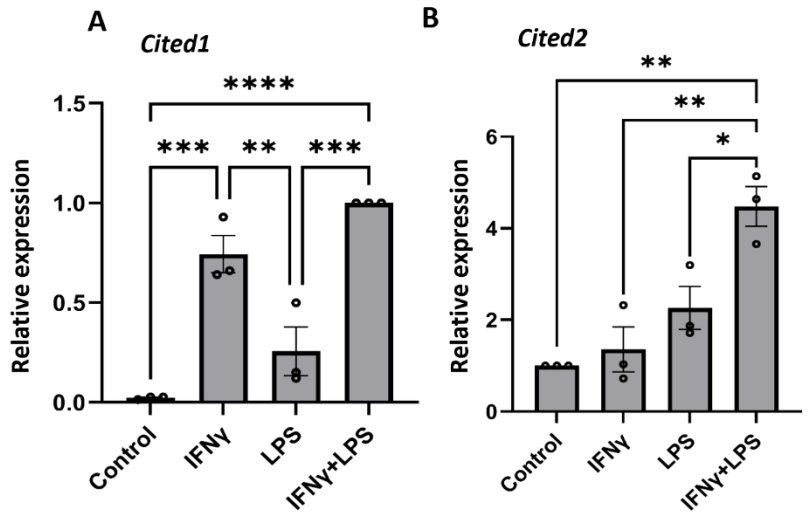

Figure 5.2. CITED1 and CITED2 respond differently to lipopolysaccharide (LPS). (A+B) RAW264.7 cells were incubated with IFNγ and/or LPS for 24 h for the indicated times, and expression of *CITED1+2* transcripts was measured using qRT-PCR. Error is represented as S.E. Statistical differences between samples were appraised using one-way ANOVA followed by a Tukey's multiple comparison test. Statistical significance is indicated as follows: *, $p < 0.05$; **, $p < 0.01$; ***, $p < 0.001$; ****, $p < 0.0001$.

The open-access Genotype-Tissue Expression (GTEx) database, which provides searchable gene expression data based on the molecular investigation of 54 non-diseased human tissue locations from approximately 1000 people, was used to investigate the hypothesis that the regulation of *CITED1* and *CITED2* are distinct from one another (293). Using this method, the expression of *CITED1* and *CITED2* was noticeably different. In contrast to *CITED2*, which was almost ubiquitously expressed, expression of *CITED1* was mostly restricted to the testis and pituitary (Fig. 5.3).

Experimental evidence supports these distinctions, demonstrating that only *CITED2* expression persists in mature renal tissues despite both *CITED1* and *2* being produced in the developing kidney (294). Overall, our findings show that the regulation of *CITED1* and *CITED2* differs in macrophages with respect to proinflammatory stimuli. Furthermore, the contrasting patterns of expression between these two CITED family genes in other tissues is indicative of more expansive differences in how they are controlled and are suggestive of distinct biological roles for CITED1 and 2.

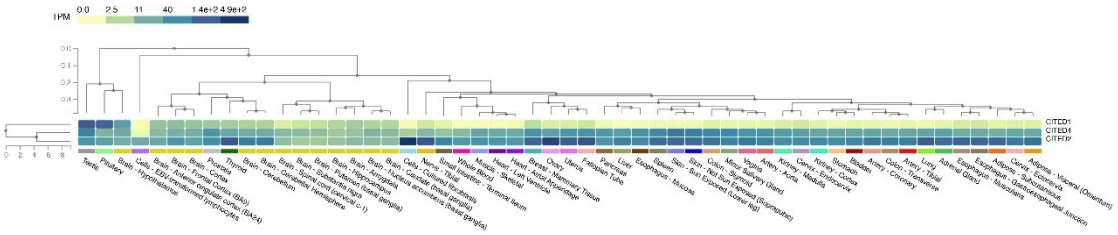

Figure 5.3. Tissue expression of CITED1-4. Genotype-Tissue Expression (GTEx) analysis of CITED family member expression across 54 different non-diseased tissues. Figure provided by Dr. Seipelt-Thiemann (MTSU).

5.3. *STAT1* regulates the expression of *CITED1*

The data in Chapter 5.2 suggest that *CITED1* and *2* are regulated differently in macrophages. However, the specifics of how the *CITED1* gene is expressed remain poorly understood. While several signaling pathways are activated when IFNγ-receptors are engaged (110), the JAK:STAT pathway is thought to be the primary coordinator of the transcriptional response with STAT1 transactivating ISGs activated either directly or through IRF1 (111,295), which is itself regulated by STAT1 (108,125) (Fig. 5.4A). To determine whether the STAT1-IRF1 axis also controls *CITED1*, we used the Eukaryotic Promoter Database (Swiss Institute of Bioinformatics) to identify transcription factor binding sites in a region from -2000 to 100 bp from the transcriptional start site of the murine *CITED1* gene (296,297). We identified a total of three STAT1 (-18, -724, and -1038) and two IRF1 (-1237, and -1297) potential cis-regulatory sites from this analysis (cut-off $p < 0.001$; Fig. 5.4B). Based on these findings and the relationship between STAT1 and IRF1, we postulated that STAT1 was necessary for IFNγ-stimulated *CITED1* expression.

To test this hypothesis, RAW264.7 cells were transduced with a lentiviral construct encoding the Cas9 endonuclease and either a non-targeting "scramble" gRNA or a gRNA targeting exon 9 of the *STAT1* gene. Clonal lines were produced and loss of STAT1 protein expression was assessed using western blotting (Fig. 5.4C). As predicted, in both STAT1 deficient clonal lines, IFNγ-stimulated *CITED1* RNA production was suppressed, but was unaffected in the scramble controls (80-fold increase; Fig. 5.4D). Consistent

with this result, western blotting revealed that CITED1 was detectable in IFNγ-stimulated scramble control cells, but not in STAT1 deficient cells (Fig. 5.4E). These findings suggested that STAT1 is required for IFNγ-stimulated *CITED1* expression. However, it is not clear from these data whether *CITED1* is regulated by STAT1 in a direct or indirect manner.

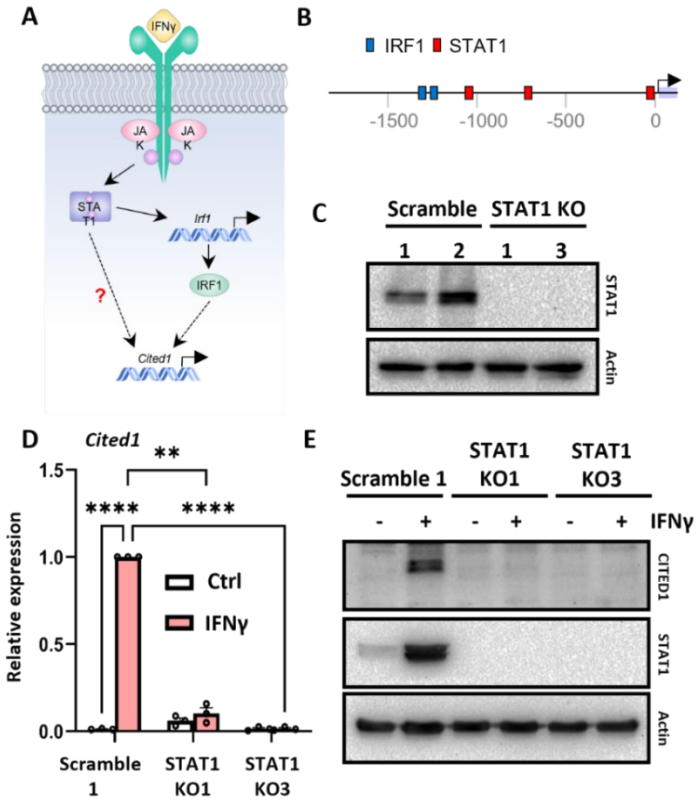

Figure 5.4. Expression of CITED1 is STAT1-dependent. (A) Schematic representation of the IFNγ-STAT1 signaling pathway. (B) Identification of potential STAT1 and IRF1 cis-regulatory sites using the Eukaryotic Promoter Database (EPD) and a *p*-value cutoff of ≤ 0.001. (C) Western blot analysis of RAW264.7 cell lines stably transduced with lentiviral constructs to express Cas9 and either non-targeting (scramble) or *STAT1*-targeting gRNA. RAW264.7 STAT1 KO cells and scramble controls were stimulated with IFNγ for 48 h. CITED1 expression was then appraised by (D) qRT-PCR and (E) western blotting. Error is represented as S.E. Statistical differences between samples were appraised using one-way ANOVA followed by a Tukey's multiple comparison test. Statistical significance is indicated as follows: **, $p < 0.01$; ****, $p < 0.0001$.

5.4. Production and validation of a Dox-inducible CITED1 overexpressed (OE) cell line

As a first step towards understanding the role of CITED1 in macrophages and their plasticity, CITED1 levels were manipulated using the lentiviral pINDUCER20 Tet-On system (298). The CITED1 coding sequence (CDS) was amplified using a plasmid construct expressing the full-length murine CITED1 (a gift from Dr. Mark P. de Caestecker's group at Vanderbilt University Medical Center). With the use of the In-Fusion recombination technique, the CDS was recombined into the pENTRAddgene Gateway donor vector. The CITED1 CDS was subsequently subcloned into pINDUCER20 using a Gateway cloning reaction. Following verification by Sanger sequencing, the completed pINDUCER20-CITED1 construct was packaged as infective lentiviral particles in Lenti-X 293T cells and then used to stably transduce RAW264.7 cells. Following the establishment of the cell line, western blotting studies were performed to identify the doxycycline (dox) dosage and incubation period necessary to obtain optimum CITED1 levels. First, we tested three concentrations of dox (30, 100, and 300 ng/mL) and found higher CITED1 expression when the cells were incubated with 100 ng/mL (Fig. 5.5A). Second, we harvested cells at different time points to determine when CITED1 levels peaked. CITED1 peaked at roughly 12 h post-treatment and stayed consistent for the remaining time (Fig. 5.5B).

It was next necessary to generate clonal cells expressing a high amount of CITED1 proteins after dox treatment. To achieve this, we utilized the dilution plating technique

to select clones from the polyclonal population of RAW264.7pINDUCER20-CITED1 cells that were originally generated. To identify the clones with the highest fold-change in exogenous CITED1 protein levels post-dox treatment, a western blotting analysis of these clonal lines was performed. Clone 1 had the greatest increase in CITED1 levels compared to the other clones and was used for all subsequent studies (Fig. 5.5C).

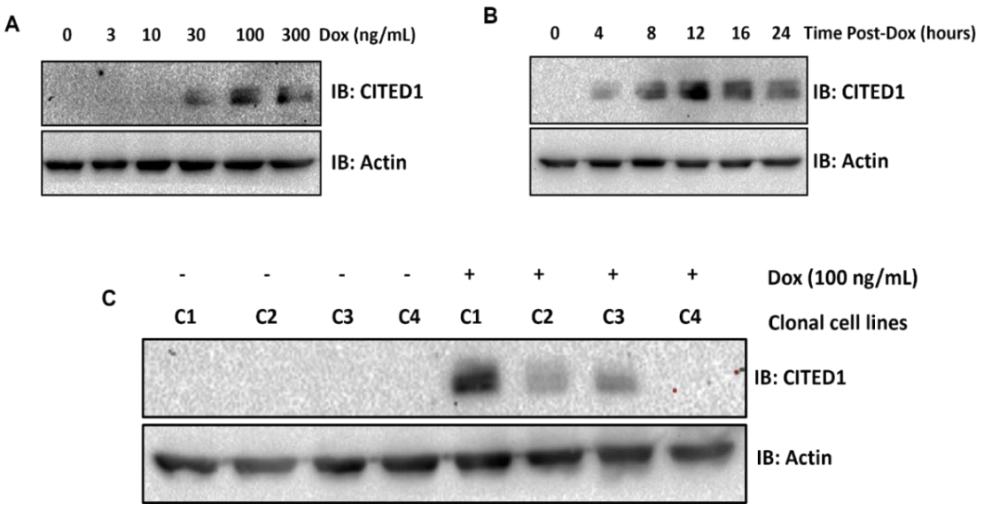

Figure 5.5: Optimization of ectopic CITED1 expression from a dox-inducible promoter. Western blot analysis for CITED1 in RAW264.7pINDUCER20-CITED1 cells (A) with increasing concentrations of dox for a period of 24 h, or (B) with 100 ng/mL dox at the indicated time points. (C) Clonal RAW264.7pINDUCER20-CITED1 cell populations were treated with 100 ng/mL dox for 24 h. β-actin was used as a loading control in all experiments.

5.5. CITED1 enhanced IFNγ-stimulated gene expression

CITED2 is a nuclear protein constitutively expressed in myeloid cells, including macrophages. Here, it prevents the interaction of NF-κB and HIF-1 with the CH1 domain of CBP/p300, thereby suppressing proinflammatory genes regulated by these transcription factors (196,202). Overexpression of CITED2 also decreases the expression of genes controlled by the STAT1-IRF1 axis. These include *Irf1, Irg1, F3, Tmem140*, and *Dnase13* (203). While CITED1 also interacts with the CH1 domain of CBP/p300, this association is comparatively weak, with CITED1 exhibiting a preference for binding to the CH2 domain with higher affinity (192,299). This led us to postulate that CITED1 could have distinct effects on STAT1- and IRF1-dependent gene expression and the M1 transcriptome as a whole. To investigate this, the RAW264.7 Dox-inducible CITED1 (DI-CITED1) cell line was utilized and pretreated with dox or vehicle for 24 h, followed by co-incubation with dox and IFNγ for a further 24 h, and gene expression was analyzed using RNAseq (Fig. 5.6A). To determine critical processes altered in each state, we performed pairwise comparisons for DEGs between no dox and dox-treated IFNγ-stimulated cells (IFNγ vs. dox+IFNγ; Table 5). Using a CuffDiff-based analysis pipeline, we identified 724 DEGs across both samples, and the findings from these analyses showed that the expression of many members of gene families strongly linked with the response to IFNγ was elevated in CITED1 overexpressing cells. This comprised members of the Ifit (*Ifit1*, *Ifit3*, and I*fit3b*), C-C motif chemokine ligand (*Ccl2*, *Ccl3*, *Ccl4*, and *Ccl7*), costimulatory molecules (*Cd40*, *Cd52*), and Isg (*Isg15* and *Isg20*) gene

families. A subset of these was validated by qRT-PCR (Fig. 5.6B). Many of the upregulated genes identified in this study were also expressed more strongly in earlier studies that looked at the IFNγ response in CITED2 deficient BMDMs (203). These contrasting expression patterns indicate that CITED1 and CITED2 play distinct and opposing roles in IFNγ-stimulated gene expression.

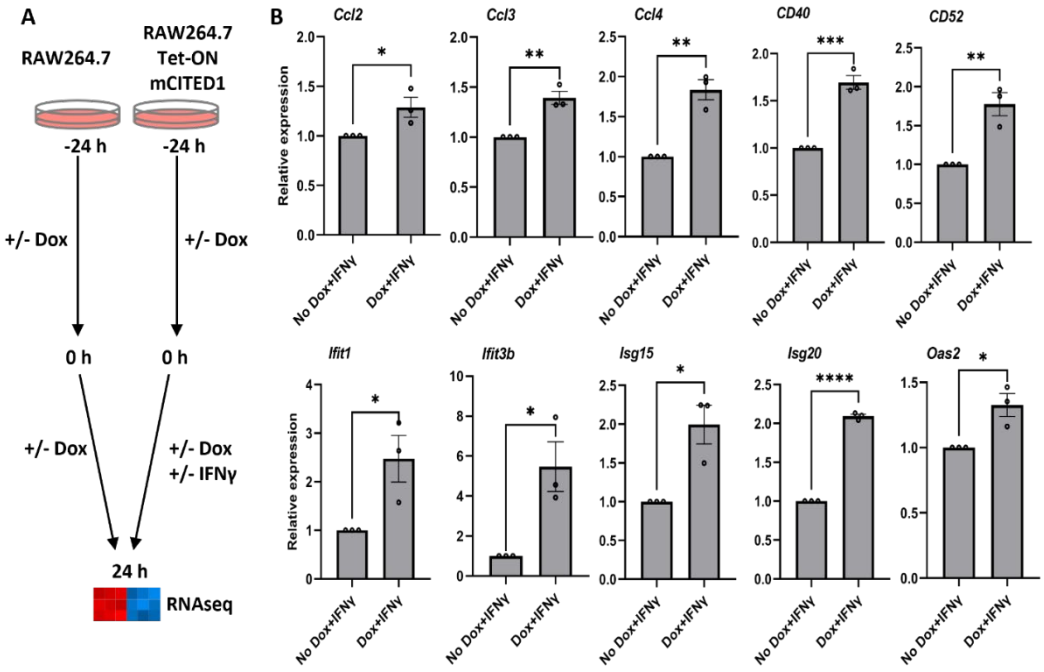

Figure 5.6. Up-regulation of interferon-simulated genes (ISGs) in CITED1 overexpressing (OE) cells. (A) Graphical representation of the design of CITED1 overexpression transcriptome profiling experiment. RAW264.7 CITED1 OE cells were incubated +/- dox for 24 h to overexpress CITED1 prior to co-treatment with IFNγ or vehicle for a further 24 h. Following treatments, total RNA was harvested for RNAseq. (B) A subset of DEGs was validated using qRT-PCR.

Table 5: Selected interferon-stimulated genes (ISGs) affected by CITED1 expression.

FC = Fold-change. CITED1 OE – CITED overexpression and CITED1 KO – CITED1 knockout

	Cited1 OE			Cited1 KO		
Gene	**FC**	**Direction**	***q*-value**	**FC**	**Direction**	***q*-value**
Cited1	7.55	UP	0.00039	6.71	DOWN	0.00036
Ccl2	2.32	UP	0.00039	39.3	DOWN	0.00036
Ccl3	2.4	UP	0.00039	40.96	DOWN	0.00036
Ccl4	2.5	UP	0.00039	22.97	DOWN	0.00036
Ccl7	2.18	UP	0.0118	70.93	DOWN	0.00285
Cd40	2.78	UP	0.00039	2.65	DOWN	0.00036
Cd52	2.12	UP	0.00039	2.91	DOWN	0.00036
Ifit1	5.11	UP	0.00039	15.57	DOWN	0.00036
Ifit3	5.43	UP	0.00039	18.77	DOWN	0.00036
Ifit3b	15.97	UP	0.00039	49.77	DOWN	0.00036
Isg15	3.99	UP	0.00039	7.51	DOWN	0.00036
Isg20	2.75	UP	0.00039	3.02	DOWN	0.00036
Mx1	4.95	UP	0.00039	8.77	DOWN	0.00036
Mx2	2.49	UP	0.00039	4.73	DOWN	0.00036
Oas2	3.28	UP	0.00039	9.14	DOWN	0.00036
Tlr9	2.45	UP	0.00039	2.24	DOWN	0.00036
Tmem14C	2.16	UP	0.00039	10.72	DOWN	0.00036

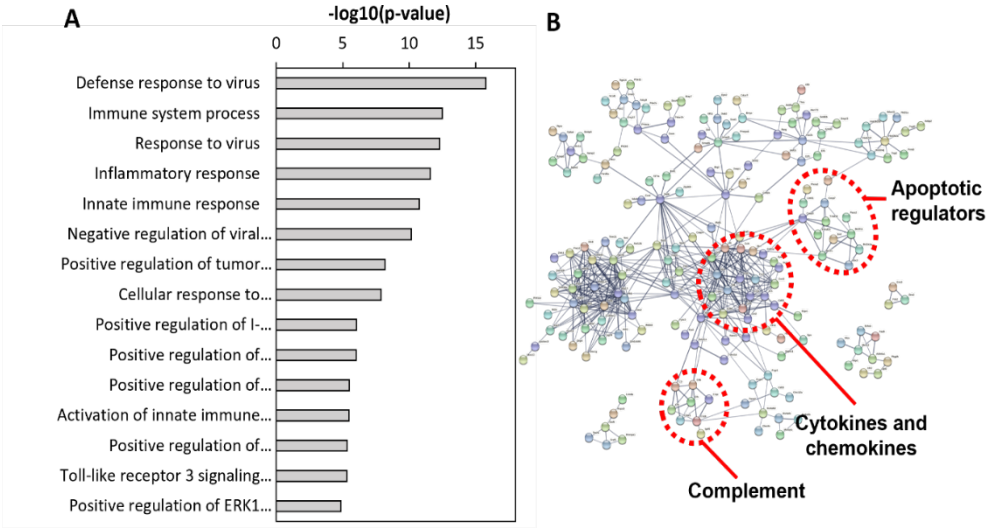

Figure 5.7. Gene ontology (GO) analysis of differentially expressed genes (DEGs) from IFNγ vs. dox+IFNγ. (A) Analysis of DEGs between -dox +IFNγ or +dox +IFNγ performed using the Database for Annotation Visualization and Integrated Discovery (DAVID). (B) Search Tool for the Retrieval of Interacting Genes/Proteins (STRING) analysis was performed on the same set of DEGs. GO terms are ranked by -log (p-value).

KEGG was utilized to conduct a GO analysis of DEGs from IFNγ vs. dox+IFNγ pairwise comparison. Significant GO terms included 'Defense response to the virus,' 'Innate immune response,' and 'Inflammatory response,' suggesting that these fundamental processes are impacted by CITED1 overexpression (Fig. 5.7A). An investigation of the protein interaction network was performed using STRING, enabling us to observe alterations in the IFNγ response induced by CITED1. As expected,

apoptosis (GO term 'Regulation of apoptotic process'; false discovery rate (FDR) 3.9×10^{-4}), cytokines and chemokines (GO term 'Regulation of cytokine production'; FDR 2.57×10^{-9}), and a much smaller cluster of complement system processes were observed (Fig. 5.7B).

To investigate the critical processes altered in each state, a pairwise comparison was performed between the IFNγ vs. dox+IFNγ DEG set and untreated control vs. IFNγ-treated cells (Ctrl vs. IFNγ). Of the 2776 DEGs associated with IFNγ-induced M1 polarization, 300 (10.8%) were affected by CITED1 overexpression (Fig. 5.8A). This is equivalent to 41.5% of all DEGs from the IFNγ vs. dox+IFNγ pairwise comparison. The majority of the genes common across the two sets of comparisons (255, or 85%) were concordant, suggesting that CITED1 increased the expression of a subset of IFNγ-responsive genes (Fig. 5.8B). This included genes like *Isg15*, *Isg20*, *Ifit* family, *CD40*, *CD52,* and the chemokines *Ccl2, Ccl3,* and *Ccl4* (Table 6). The analysis of this common pool of DEGs revealed GO terms 'Defense response to the virus' ($p = 6.84 \times 10^{-17}$; FDR $= 1.24 \times 10^{-13}$) and 'Negative regulation of viral genome replication ($p = 7.49 \times 10^{-10}$; FDR $= 2.72 \times 10^{-7}$) (Fig. 5.8C). These results altogether demonstrate that CITED1 increases the expression of a subset of IFNγ-stimulated genes.

Table 6. Top 50 genes (by FPKM) from IFNγ:dox+IFNγ common to Ctrl:IFNγ. FC = Fold change

Gene	FC	Direction	Total FPKM	*q*- value
Cd52	2.12	UP	2329.27	0.000387
Isg15	3.99	UP	1787.57	0.000387
Bst2	2.04	UP	1446.82	0.000387
Ccl4	2.5	UP	674.82	0.000387
Fcgr4	2.33	UP	552.6	0.000387
Ifi44l	2.15	UP	438.93	0.000387
Themis2	2.19	UP	389.28	0.000387
Cfb	2.5	UP	366.03	0.000387
Fcgr1	3.13	UP	361.47	0.000387
Csrp1	2.35	UP	355.71	0.000387
Ifit3	5.43	UP	350.19	0.000387
Trim30a	2.01	UP	348.06	0.000387
Parp12	2.02	UP	307.04	0.000387
Cd40	2.59	UP	291.73	0.000387
Scimp	2.6	UP	275.17	0.000387
Oas1a	2.19	UP	271.17	0.000387
H2-Q2	2.56	UP	267.82	0.040091
Tor3a	2.19	UP	240.19	0.000387
Phf11a	2.33	UP	232.95	0.000387
Gm12250	2.15	UP	201.73	0.000387
Rasgef1b	2.01	UP	200.94	0.001762
BC028528	2	UP	200.72	0.000387
Mxd1	3.08	UP	198.66	0.000387
Isg20	2.75	UP	189.72	0.000387
Cd47	2.2	UP	186	0.007728
Carhsp1	2.06	UP	163.53	0.000387
Fabp5	2.53	DOWN	159.99	0.000387
Tlr9	2.45	UP	158.5	0.000387
Parp14	2.14	UP	157.14	0.000387
Dusp2	3.52	UP	149.93	0.000387
Mov10	2.01	UP	147.62	0.000387
Oasl2	2.35	UP	141.88	0.000387
Ifit3b	15.97	UP	139.39	0.000387
Ccl2	2.32	UP	136.64	0.000387
Bcl2a1a	2.01	UP	135.35	0.000387
Ogfr	2.01	UP	134.24	0.000387
Peli1	2.11	UP	134.17	0.000387
Phf11d	2.03	UP	132.37	0.005147
Casp4	2.64	UP	129.57	0.000387
St3gal5	3.22	UP	128.3	0.010479
Gm18445	3.51	UP	126.26	0.000387
Sertad1	2.24	UP	125.42	0.000387
Il1rn	2.34	UP	119.59	0.00143
Rtp4	3.84	UP	119.05	0.000387
Havcr2	2.73	UP	113.57	0.000387
Stk40	2.07	UP	108.04	0.000387
Trafd1	2.05	UP	102.27	0.000387
Clcn7	2.97	UP	101.64	0.000747
Znfx1	3.24	UP	98.48	0.000387
Cited1	7.55	UP	98.23	0.000387

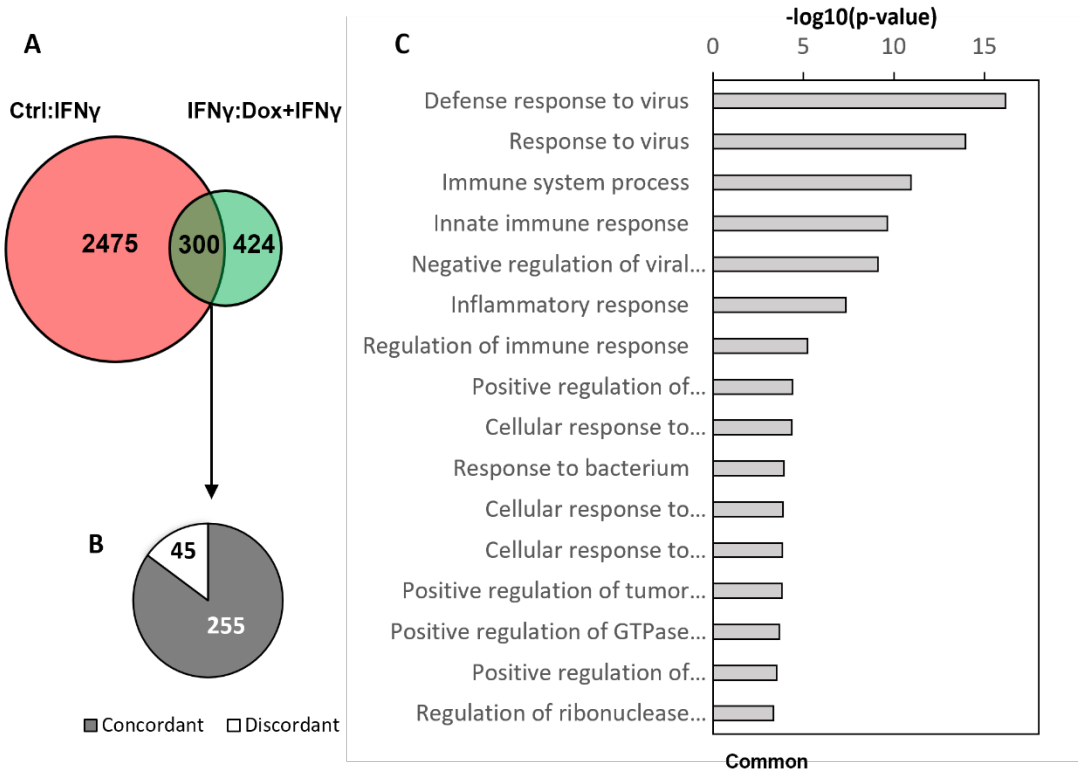

Figure 5.8. Effect of CITED1 expression on the M1 transcriptome. (A) Venn diagrams showing a subset of IFNγ-responsive genes affected by CITED1. (B) A total of 255 (85%) of the 300 differentially expressed genes (DEGs) common to Ctrl:IFNγ and IFNγ:dox+IFNγ were concordant, while 45 (15%) were discordant. (C) Gene ontology (GO) analysis was performed in the Database for Annotation Visualization and Integrated Discovery (DAVID) on common DEGs shown in (A). GO terms are ranked by -log(p-value).

5.6. CITED1 OE modulated the expression of STAT1 and IRF1 target genes

To further explore the effect of CITED1 on ISG expression, the IFNγ vs. dox+IFNγ dataset was reexamined using gene set enrichment analysis (GSEA). GSEA is a statistical approach that is used to identify phenotypic variations across datasets of transcriptomes for particular gene sets that have functional roles (300). Initial analysis was done to identify the top upregulated and downregulated genes (Fig. 5.9A). GSEA revealed that CITED1 increased the expression of a subset of IFNγ-stimulated genes that are shown to be inhibited by CITED2 (Fig. 5.9B and C), including *CD86, Ddx58, ifit* family genes*,* and *Oas3*, indicating that CITED1 and 2 have opposing effects on at least part of the M1 transcriptome (203). Enhanced expression of CITED1 was associated with a negative normalized enrichment score (NES; -1.56). It was conceivable that CITED1 influenced STAT1 and IRF1-dependent signaling since the CuffDiff and GSEA analyses revealed genes with ISRE cis-regulatory sites (301–303) and genes with both or composite ISRE and GAS sites (284,304,305). This hypothesis was tested via GSEA using STAT1- and IRF1-regulated gene lists (provided by the Mahabeleshwar lab, Case Western University) (127,203,306). According to the findings of this analysis, increased levels of CITED1 led to a substantial rise in the expression of genes regulated by STAT1 (Fig. 5.9D and E) and IRF1 (Fig. 5.9F and G). Overall, our findings show that CITED1 influences the two major transcription factor pathways that regulate macrophage activation.

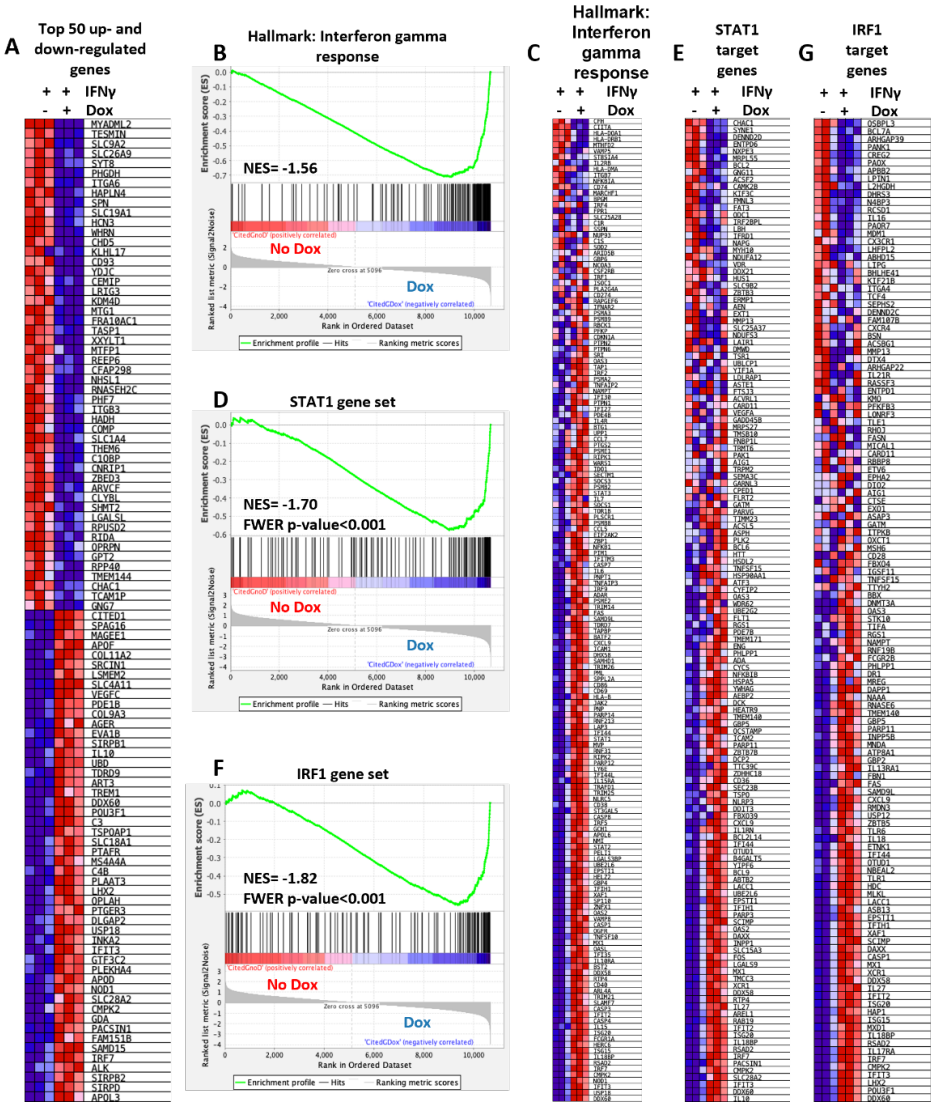

Figure 5.9. CITED1 modulates the expression of STAT1 and IRF1 target genes. (A) Heat map of the top 50 upregulated and downregulated genes in IFNγ-stimulated cells +/- dox pre-treatment. Gene Set Enrichment Analysis (GSEA) of (B+C) 'Interferon-gamma response.' (D+E) STAT1 and (F+G) IRF1 regulated genes. These were presented as heat maps and enrichment score plots. For all heatmaps, red and blue indicate increased and decreased expression, respectively.

5.7. Production and validation of CRISPR-Cas9 CITED1 Knockout cell line

To determine the role of loss of CITED1 expression in shaping the transcriptome of *Cn*-infected macrophages, we transduced RAW264.7 macrophages with a lentiviral construct that expressed the Cas9 enzyme and a sgRNA targeting exon 3 of the *Cited1* gene (Fig. 5.10A). Given that RAW264.7 cells are generated from male BALB/c mice, they only have one copy of the *Cited1* gene, which is encoded on the X chromosome. INDELs created by CRISPR gene editing were thus hemizygous. A total of 17 clonal cell lines were produced by dilution plating and selection with G418. To characterize the INDELS, genomic DNA was purified from each clone and used as a PCR template to amplify a 1.5 kb area around the sgRNA binding site. This was subcloned into the multiple cloning site of pCDNA3, and Sanger sequencing was performed using primers binding to sites flanking the MCS (Fig. 5.10B). Of the 17 clones screened, 9 contained frameshifts resulting in premature stop codons. Clones 6 and 9 were chosen for further research, with both showing a loss of *CITED1* mRNA and protein expression. as validated by multiplex RT-PCR and western blotting (Fig. 5.10C and D).

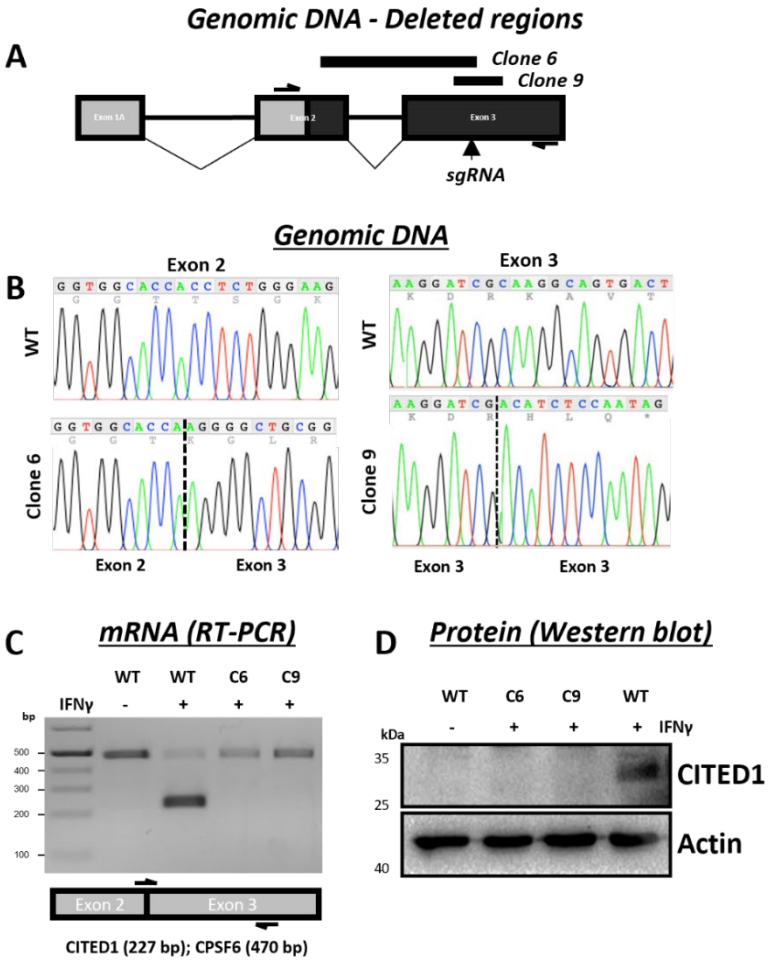

Figure 5.10. Characterization of *CITED1* knockout (KO) macrophages. A) Production of *Cited1* gene knockout by lentiviral transduction with a construct containing Cas9 and sgRNA targeting *Cited1* exon 3 (B) Chromatogram showing deletions and frameshifts in clones 6 and 9. (C+D) RAW264.7 WT and CITED1 KO clones were treated with IFNγ for 24 h. (C) Loss of *Cited1* mRNA levels, measured using RT-PCR. Upper band represents *Cpsf6*, used as an internal control. (D) Western blotting analysis shows a complete loss of CITED1 protein expression in clones 6 and 9.

5.8. CITED1 Knockout decreased the transcriptional response to IFNγ

To examine how the lack of CITED1 affected ISG expression, the CITED1 KO cell line was utilized and incubated with IFNγ for 48 h, and gene expression was analyzed using RNAseq. This was compared to RAW264.7 cells that were stably expressing Cas9 and a non-targeting scramble gRNA (Fig. 5.11A). The time course qRT-PCR and western blotting analyses showed high CITED1 expression in unaltered RAW264.7 cells 48 h post-IFNγ treatment, which led us to choose this time as the optimal sampling point (Fig. 5.1B and C). Many of the upregulated genes observed in the CITED1 OE study were observed to be downregulated when CITED1 expression was lost (Table 5). A subset of these genes was validated by qRT-PCR. All genes in this case, with the exception of *Cd52*, showed a statistically significant drop in expression in the CITED1 KO cells (Fig. 5.11B). GO terms associated with DEGs from the scramble IFNγ vs. CITED1 KO IFNγ pairwise comparison included 'response to the virus,' 'inflammatory response,' and 'positive regulation of tumor necrosis factor production,' indicating that *CITED1* loss impacted the response of macrophages to IFNγ (Fig. 5.11C).

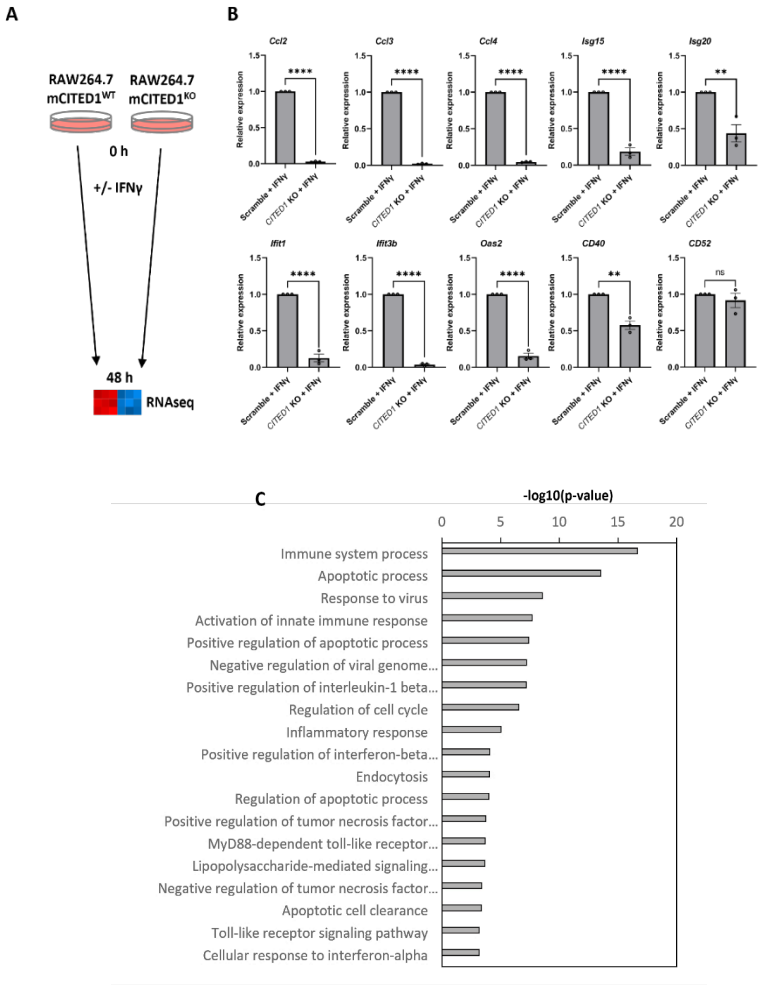

Figure 5.11. Downregulation of interferon-stimulated genes (ISGs) in CITED1 knockout (KO) cells. (A) Graphical representation of the design of the CITED1 KO transcriptome profiling experiment. RAW264.7 scramble control and CITED1 KO cells were incubated +/-IFNγ for 48 h. Following treatments, total RNA was harvested for RNAseq. (B) A subset of differentially expressed genes (DEGs) was validated using qRT-PCR. (C) Gene ontology (GO) analysis of DEGs of data set (A) in the Database for Annotation Visualization and Integrated Discovery (DAVID). GO terms are ranked by -log(p-value).

The same transcriptome dataset was examined using GSEA to determine whether the reduction of CITED1 expression had detrimental effects on the overall transcriptional response to IFNγ. GSEA revealed that loss of CITED1 attenuated the expression of a subset of ISGs. This produced a positive NES score for the 'Interferon gamma response' gene set, suggesting that this phenotype was more strongly associated with the wild-type rather than the CITED1 KO cells (Fig. 5.12A and B). In addition, using custom STAT1- and IRF1-regulated gene lists, CITED1 loss reversed the increased expression of numerous ISGs observed in CITED1 OE cells (Fig. 5.12C – F). Taken together, this gain- and loss-of-function approach revealed that CITED1 regulates an overlapping set of genes, indicating that it is indeed involved in the modulation of the transcriptional response to IFNγ and, unlike CITED2, largely acts as a positive regulator of STAT1 and IRF1-regulated genes (Fig. 5.13).

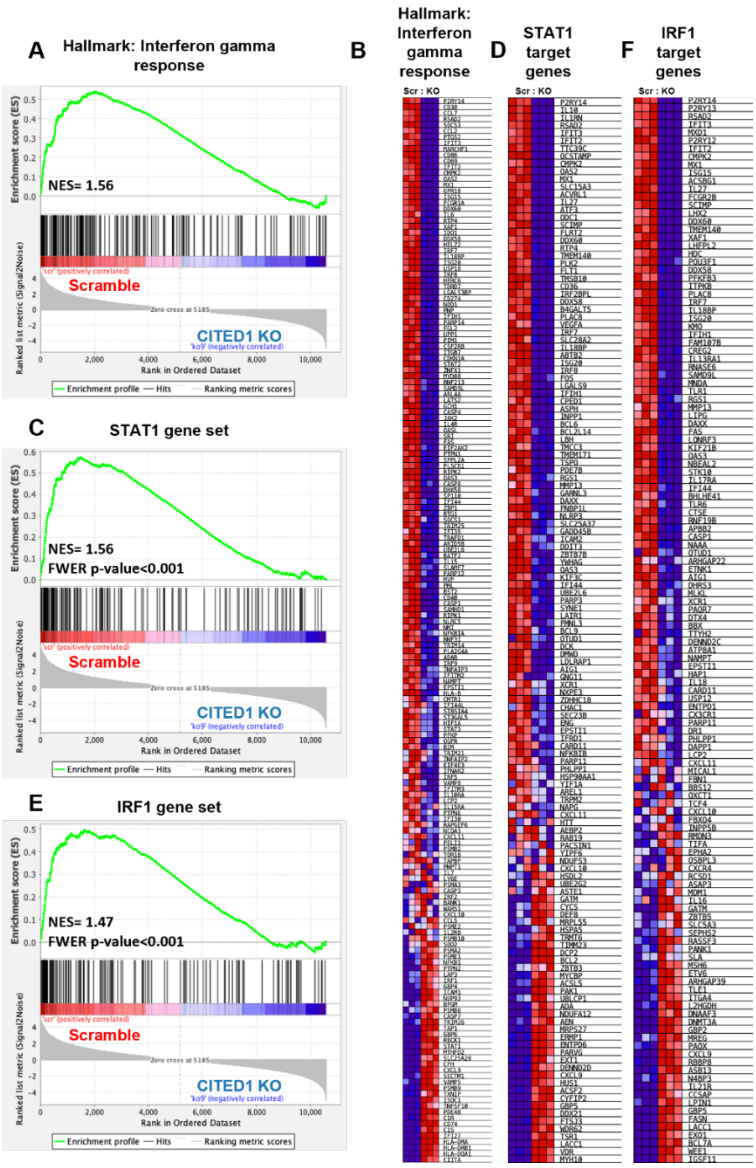

Figure 5.12. Loss of CITED1 negatively affects STAT1 and IRF1 target gene expression. Gene set enrichment analysis (GSEA) was performed using the transcriptome profiling dataset described in Figure 5.13A. (A+B) GSEA hallmark analysis of the 'Interferon gamma response,' (C+D) STAT1-, and (E+F) IRF1-regulated genes. These are presented as heat maps and enrichment score plots. For all heatmaps, red and blue indicate increased and decreased expression, respectively.

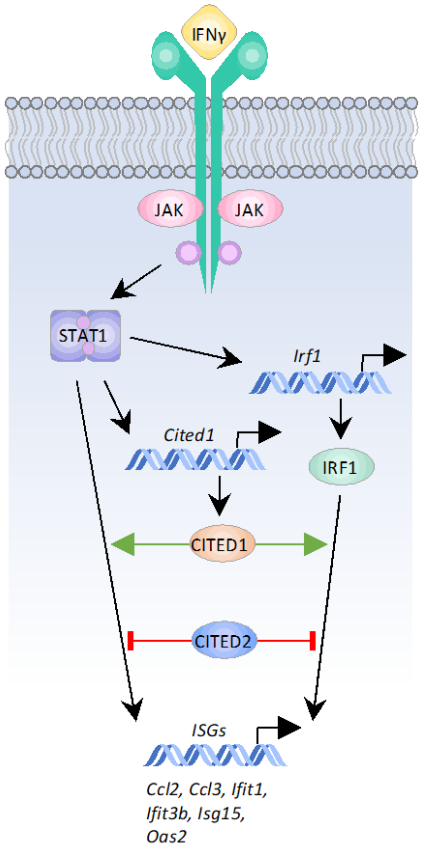

Figure 5.13. CITED1 as a positive regulator of interferon-stimulated gene (ISG) expression. The activation of STAT1 by IFNγ leads to an increase in the expression of IRF1. Together, STAT1 and IRF1 are responsible for the increased expression of a wide variety of ISGs. The findings of this study demonstrate that STAT1 is required for IFNγ-stimulation to induce CITED1 expression. While CITED1 proteins promote the expression of select ISGs, CITED2 has been shown to repress them.

5.9. IFNγ stimulated nuclear translocation and phosphorylation of CITED1

The data presented in Chapter 5.9 were collected by Maria Hite, an undergraduate student, with assistance from the author of this dissertation. CITED1 must be present in the nucleus to function as a transcriptional co-regulator. However, the subcellular localization of this protein varies depending on the kind of cell it is expressed in, and, in most cases, it is predominantly cytoplasmic. This is most likely because the CR2 domain contains a nuclear export sequence (NES) (217,307). Surprisingly, this same NES sequence is conserved between CITED1 and 2 (207), and yet CITED2 proteins are constitutively nuclear, which indicates that the effect of this motif on the subcellular localization of the CITED1 could potentially be overridden under the correct circumstances.

To determine the localization of the protein in macrophages and if IFNγ has any effect on the localization, RAW264.7 cells were stably transduced with pINDUCER20-EYFP-CITED1 to express full-length murine CITED1 with an N-terminal enhanced yellow fluorescent protein (EYFP) tag under the control of a doxycycline (dox)-dependent promoter. These cells were then treated with doxycycline for 24 h prior to IFNγ stimulation. EYFP-CITED1 was localized primarily in the cytoplasm prior to stimulation with IFNγ. However, post-IFNγ, the ratio of nuclear to cytoplasmic EYFP-CITED1 increased at 24 and 48 h, indicating that IFNγ stimulation promoted nuclear accumulation of EYFP-CITED1 (Fig. 5.14A and B).

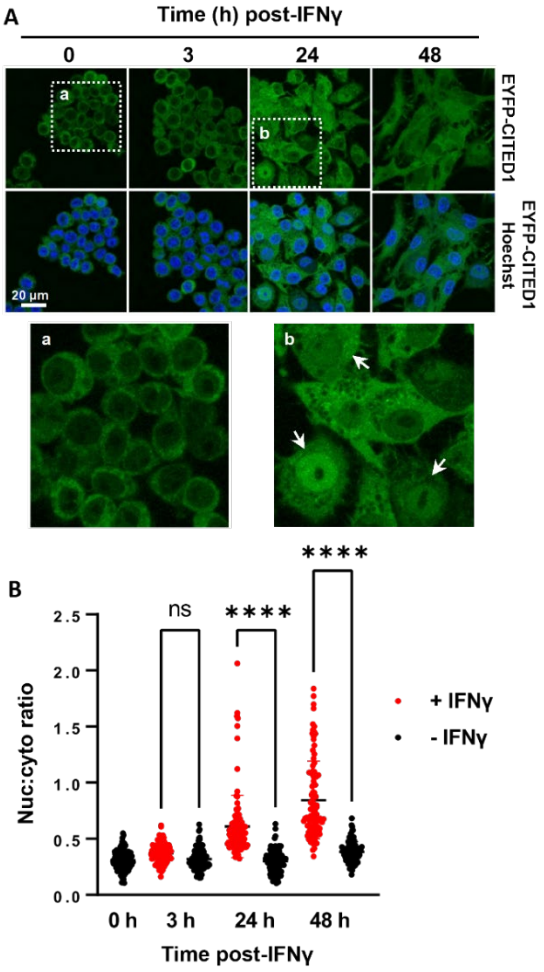

Figure 5.14. IFNγ increases nuclear localization of EYFP-CITED1. (A) EYFP-CITED1 cells from a dox-inducible promoter incubated with dox for 24 h prior to co-treatment with IFNγ for the indicated times and imaged by live cell confocal microscopy. Arrow heads mark cells where nuc:cyto EYFP-CITED1 ≥ 1. (B) Quantification of nuc:cyto EYFP-CITED1 in individual cells from the experiment described in (A). Data are plotted for ≥ 100 cells/condition. Statistical differences between samples were appraised using one-way ANOVA followed by Tukey's multiple comparison test. Statistical significance is indicated as follows: ****, $p < 0.0001$. Credit:Maria E. L. Hite.

Nuclear translocation of CITED1 in MC3T3-E1 mouse osteoblasts is stimulated by parathyroid (PTH) hormone. Here, PTH induces protein kinase C-dependent phosphorylation of CITED1 Ser-79, and this post-translational modification was necessary but not sufficient for the nuclear accumulation of the protein (308,309). Given that IFNγ also stimulates protein kinase C (PKC) activity, we investigated whether IFNγ-induced translocation of CITED1 was associated with the phosphorylation of the protein. To achieve this, RAW264.7 cells expressing untagged CITED1 from a dox-dependent promoter were used to create a pre-existing pool of ectopic CITED1 in cells prior to IFNγ stimulation. Due to the relatively small size of the protein (~27 kDa), phosphorylation of CITED1 retards its migration through SDS-PAGE gels so that phosphorylated species appear as higher molecular weight bands (~2 kDa size difference), facilitating the detection of CITED1 phosphorylation without the use of phospho-specific antibodies (217). In cells treated with only doxycycline, CITED1 was depicted as two major bands: a band with high mobility exhibiting the greatest intensity and a band with lower mobility that was much fainter (Fig. 5.15A). However, in cells treated with IFNγ for 24 h, CITED1 migrated as a single lower mobility band. This suggests that upon exposure to IFNγ, the existing pool of CITED1 proteins switches from a dephosphorylated state to a predominantly phosphorylated one. To confirm this, lambda protein phosphatase (λ PP) was used to dephosphorylate protein samples prior to SDS-PAGE. In samples treated with λ PP, CITED1 ran as just the high mobility band, indicating the lower mobility band of CITED1 was phosphorylated, whereas the higher mobility band represented a dephosphorylated state (Fig. 5.15B). These findings, taken

as a whole, suggest that nuclear translocation of CITED1 is accompanied by its phosphorylation post-IFNγ stimulation. However, while these data show a correlation between these two events, this is not evidence of causality.

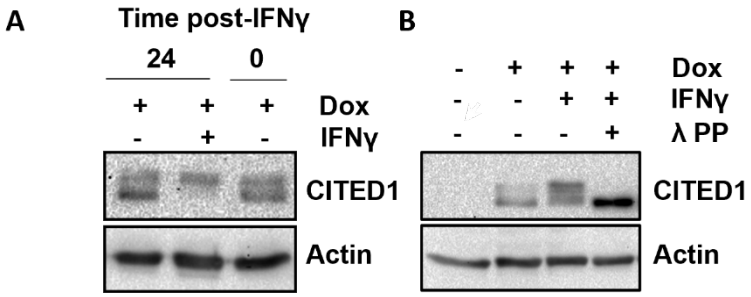

Figure 5.15. IFNγ stimulates CITED1 phosphorylation. (A) RAW264.7 Tet-On CITED1 cells were treated +/- doxycycline (dox) for 24 h to stimulate exogenous CITED1 expression prior to incubation with IFNγ for a further 24 h. Protein samples were separated on SDS-PAGE and analyzed by western blotting. (B) Cells were treated as described in (A) but were lysed at 6 h post-IFNγ treatment in 1% Triton-X buffer, and lambda protein phosphatase (λ PP) was used to dephosphorylate protein samples. Credit:Maria E. L. Hite.

5.10 Discussion

Until recently, it was believed that CITED2 was the sole member of the CITED family to be expressed in macrophages (197). The data presented in this chapter demonstrate for the first time that the CITED1 protein acts as a positive regulator of a subset of ISGs, as it is an IFNγ-responsive gene (Fig. 5.1B and C). We further showed that the responses of *CITED1* and *2* to proinflammatory stimuli differ. *CITED1* is essentially transcriptionally silent in the absence of stimuli and is only expressed in cells that have been treated with IFNγ for ≥ 24 h (Fig. 5.1A and B). Due to its delayed expression, *CITED1* is unable to influence the first stages of an IFNγ response and does not participate in the control of basal STAT1-regulated gene expression. Instead, it may enhance IFNγ-responsive gene expression at later times. Consistent with prior reports, we also demonstrate that *CITED2* is constitutively expressed in macrophages and transiently downregulated at 6 h post-IFNγ (Fig. 5.1D) (197). This pattern of expression is consistent with a model where CITED2 operates to suppress ISG expression in response to transient proinflammatory signals but can temporarily be downregulated if these signals persist to allow for the unhindered expression of STAT1- and IRF1-directed gene expression.

Although the exact mechanism behind the divergent effects of these two CITED proteins has yet to be elucidated, it might be related to how they interact with CBP/p300. CITED2 inhibits the ability of proinflammatory transcriptional regulators, including STATs, p65, and HIF1α, to recruit CBP/p300 to cis-regulatory sites

(197,198,202,203). This is achieved by interacting with the N-terminal CH1 domain of CBP/p300, the same area employed for docking with the above transcription factors (182,196,200,201). While CITED1 interacts with CH1, it has a higher affinity for the CH2 domain, which is found inside a core region of CBP/p300 that contains HAT activity (192). Thus, it is plausible that CITED1 binding through CH2 may still make it possible for CBP/p300 complexes to be formed with proinflammatory transcription factors via CH1. In this situation, CITED1 may interact with both proteins and stabilize these complexes. An additional explanation for these findings is a feedback link between *CITED1* and *2*, similar to that seen for other gene families (310,311). For instance, CITED1 may indirectly increase ISG expression by inhibiting *Cited2* gene expression or CITED2 CBP/p300 binding. These hypotheses were contradicted by the results, which showed no change in *Cited2* expression in our transcriptome profiling investigations and no rise in CITED2 protein expression in the CITED1 deficient cells.

Our findings unequivocally demonstrate that *CITED1* is downstream of STAT1. The Eukaryotic Promoter Database analysis revealed that the *CITED1* promoter contains putative cis-regulatory sites for both STAT1 and IRF1 (Fig. 5.4B). It might be controlled by each transcription factor independently, or it could be a member of a substantial number of ISGs, including *Gbp2*, *Lmp2*, and *Socs1*, that are co-regulated by both transcription factors (128,133,283). A further thorough investigation of these ISG promoters has shown that only a small number are controlled by STAT1 on their own. Instead, STAT1 binding predominantly occurs in conjunction with IRF1 binding, or IRF1 binding occurs on its own (128). In light of the fact that STAT1 is responsible for inducing

Irf1 expression as a component of the first wave of ISG transcription, the coordinated regulation of *CITED1* by both of these transcription factors would represent a coherent feed-forward loop (104). This form of regulation filters transitory stimuli, enabling target gene expression only if the activating signal persists long enough to accumulate both transcriptional regulators. IRF1, produced rapidly as part of the initial wave of ISG expression, plateaus around 6 h post-IFNγ in RAW264.7 cells, indicating that the kinetics of this feed-forward loop does not adequately explain the much-delayed expression of *CITED1*, which occurs 24–48 h post-IFNγ (312,313). These data suggest that *CITED1* gene regulation is more complicated and requires further investigation.

This work also demonstrates that the activity of the CITED1 protein is controlled by changing subcellular localization. Ectopic EYFP-CITED1 proteins are mostly cytosolic in unstimulated macrophages but accumulate in the nucleus post-treatment (Fig. 5.14A and B). This indicates that CITED1 may be inactive in the cytoplasm in the absence of stimulus, like many other transcriptional regulators (e.g., STAT1, NF-κB, and NF-AT). When cells receive an appropriate signal, such as IFNγ in this case, this signal promotes nuclear localization of the protein (314–319). Although the mechanism by which IFNγ stimulation enhances the nuclear accumulation of CITED1 is currently unknown, mechanistic findings from other systems may be useful. Parathyroid hormone (PTH) promotes the nuclear translocation of CITED1 in the osteoblastic cell line MC3T3-E1 (308). Here, the PKC-dependent phosphorylation of the protein at Ser79 was necessary for CITED1 to localize in the nucleus. This was required, but not sufficient, for PTH-induced CITED1 nuclear localization in osteoblasts. Interestingly, IFNγ activates a

specific isoform of PKC (297,298), suggesting that a similar mechanism could exist in our system to promote phosphorylation and nuclear localization.

Our combined gain- and loss-of-function strategy enabled us to confidently identify putative CITED1-regulated genes. These include members of the Isg (*Isg15* and *Isg20*), Ifit (*Ifit1* and *Ifit3b*) gene families, and the C-C motif chemokine family genes, *Ccl2* and *Ccl3*. The chemokine system is a well-established regulator of immune cell migration and inflammatory diseases, including cancer, obesity, atherosclerosis, and metabolic disorders (320,321). ISG proteins promote macrophage polarization and increase the generation of NO in response to viral infection (322,323), whereas the Ifit proteins serve as ubiquitin-like regulators that prevent viral replication in host cells (324). This study's most noteworthy outcome was the heightened expression of the hallmark IFNγ response, STAT1, and IRF1- regulated gene set in CITED1 OE cells, indicating CITED1 expression potentiates the effects of IFNγ stimulation and the associated transcription factor pathways. Loss of CITED1 expression completely reversed the increased expression of IFNγ-stimulated gene expression. Based on these observations, we present CITED1 proteins as positive regulators of select ISGs (Fig. 5.13). Altogether, our results provide new insights into the biological role that CITED1 plays in the regulation of macrophage innate immune function and the M1 transcriptome. However, a more precise and comprehensive understanding is required for the regulation of CITED1, which our lab will follow up on in the future.

CHAPTER SIX: FINAL DISCUSSION

6.1 Introduction

Fungi are often underappreciated as major pathogens by public health officials. However, they are responsible for 1.5 million fatalities yearly, placing a tremendous economic burden on society (325). With appropriate diagnosis and therapies, these infections may be prevented. However, serious side effects associated with existing treatments and the rise of novel drug-resistant strains present a clear and escalating challenge for the management of fungal diseases, including cryptococcosis (326). A deeper understanding of how *Cn* interacts with the immune system is needed to address this challenge and develop new, efficient therapies.

It is becoming more and more evident that the development of the illness is determined by the interactions between *Cn* and the immune responses of the host (327,328). The macrophage is perhaps the most significant player in the interaction that occurs between *Cn* and the host immune system (329,330). They are perhaps most responsible for the control of nascent *Cn* infections and are capable of efficiently ingesting and killing yeast cells, and yet these same cells can act as a growth niche for *Cn* and aid in its dissemination from the lungs (73,82,107). One potential explanation for this duality is the plastic nature of the macrophage phenotype. Multiple studies have shown that anticryptococcal activity of these cells requires an intact IFNγ-JAK/STAT1 signaling pathway and the expression of the STAT1-regulated gene, *Nos2* (67). Disruption of this pathway in mouse models renders macrophages unable to control *Cn* infection, leading to unfavorable outcomes.

Many infections relevant to human illness hijack endogenous signaling systems to alter host phagocytes into an advantageous growth niche, including the IFNγ-JAK/STAT1 signaling pathway (68,161,253,254). While there is strong evidence that *Cn* also disrupts macrophage polarization and proinflammatory activity, it is still unclear how this is accomplished at the molecular level, which is a crucial and ongoing subject in the area.

The JAK/STAT and NF-κB signaling pathways are the two primary controllers of the transcriptional programs underlying macrophage polarization (108,141,167,285). Earlier studies have indicated that there are 757 genes that are differently expressed between M0 and M1 and 436 genes between M0 and M2, although our own and more recent studies have indicated far broader transcriptional changes accompany the polarization of macrophages. Regardless, these changes are largely controlled by the above pathways (101). It has remained an open question as to whether intracellular *Cn* affects the activity of these pathways or others that regulate microbicidal activity and the survival of host macrophages. The first suggestion that intracellular *Cn* might influence macrophage stress response pathways, along with altering protein translation rate in host cells, was reported by the Casadevall lab (233). Although this and several earlier studies have used transcriptome profiling to measure gene expression changes induced by intracellular *Cn* on macrophages (233,258,259,331), the data presented in this dissertation was the first to use these techniques to comprehensively and specifically investigate the effect of intracellular *Cn* on macrophage polarization.

Our research demonstrates that intracellular *Cn* disrupts the M1 macrophage transcriptome profile. When analyzed in conjunction with parallel experiments measuring the effect of *Cn* infection on the M2 transcriptome, we were also able to decern a common 'transcriptional signature' of macrophage-*Cn* infection, a set of gene expression changes occurring regardless of the polarization environment of the host cells. Determining a mechanism for this identified a transcriptional co-regulator, CITED1, that was found to be a regulator of macrophage polarization and proinflammatory gene expression patterns. In this chapter, these findings will be discussed within the context of the recent literature, as well as potential caveats associated with the techniques used.

6.2 Outcomes and conclusions arising from this work

The experiments and data presented here were designed to address the overarching goal of the study, i.e., to better understand the macrophage:*Cn* host:pathogen interaction. More specifically, we wanted to determine how the macrophage transcriptome is affected by intracellular *Cn* growth and the mechanisms regulating altered macrophage gene expression. This was accomplished by infecting macrophages with opsonized *Cn* and assessing the changes in gene expression using an unbiased RNAseq-based gene expression profiling. These data showed that the M1 and M2 transcriptomes were severely disrupted in *Cn*-infected macrophages, either actively driving cells toward or actively maintaining them at a more M0-like state (Fig. 4.2 and

4.4). We saw a 40% increase in iNOS levels in *Cn*-infected M1 macrophages. This is not consistent with the RNAseq data suggesting a reversal of M1 gene expression (Fig. 4.1). Clearly, these effects are mixed, and some aspects of the M1 phenotype are preserved or even enhanced during *Cn* infection. When GO analysis was performed using KEGG, we discovered an enrichment of genes linked to essential M1 macrophage processes, such as "endocytosis," "phagosome," and "chemokines," only in the M0:M1mk DEG pool (Fig. 4.2). This finding suggests that these processes were hampered in *Cn*-infected M1 cells. Additionally, the M0:M1*Cn* pool alone showed enrichment of DEGs connected to JAK-STAT and NF-κB signaling (Fig. 4.2), supporting the idea that *Cn* infection influenced pathways involved in the formation of the M1 transcriptional profile.

The identification of a transcriptome signature of *Cn*-infection—a collection of genes that are often and uniformly affected in both polarization states—may be the study's most important finding. We uncovered the upregulation of a relatively small pool of eight functionally diverse genes (Tables 3 and 4) among DEGs from mock vs. *Cn*-infected cells to investigate a potential mechanism of the altered gene expression (Tables 3 and 4). This group included the transcriptional regulators *Cited1*, *Hsf3*, and *Jarid2*, the cytokine *Ccl2*, and the anti-apoptotic factor *Bcl2a1a*. The top three genes all encoded transcriptional regulators, but *Cited1* showed the greatest fold increase in expression.

Further investigation revealed that in the absence of stimuli, *Cited1* is transcriptionally silent and is only expressed in cells that have been treated with IFNγ for ≥ 24 h (Fig. 5.1). Our data demonstrate that *Cited1* is downstream of the JAK:STAT

portion of the pathway, suggesting it is regulated by JAK:STAT (Fig. 5.4). Additionally, the phosphorylation of exogenous CITED1 increased within 24 h post-IFNγ treatment (Fig. 5.15). Previous research conducted in HEK cells demonstrates that CITED1 phosphorylation is dependent upon the cell cycle (217). However, rapid phosphorylation shifts of CITED1 observed in this study point to the possibility of alternative regulation beyond that provided by the cell cycle alone. Moreover, EYFP-CITED1 proteins are mostly cytosolic in unstimulated macrophages but accumulate in the nucleus after IFNγ treatment (Fig. 5.14). The mechanisms that regulate the subcellular localization of CITED1 in macrophages have not been investigated; however, it is likely that the leucine-rich NES in the CR2 domain of CITED1 is responsible for the net cytosolic distribution of the protein in cells that have not been stimulated with IFNγ (217). This, however, cannot be the only reason as this NES is also conserved between CITED1 and 2, present within the same location in the CR2 domain, and yet CITED2 is constitutively nuclear in cells (196).

Examining the role of CITED1 expression in the macrophage response to IFNγ using a dual gain- and loss-of-function approach revealed potential CITED1-regulated genes, such as *Ccl2*, *Ifit3b*, *Isg15*, and *Oas2* (Table 5). Ectopic expression of CITED1 enhanced the expression of these ISGs, and as expected, loss of CITED1 expression reversed the increased expression of these and numerous other ISGs observed in CITED1 overexpressing cells (Fig. 5.6 and 5.11). Taken together, these findings demonstrate that CITED1 contributes to the maintenance of proinflammatory gene expression during periods of prolonged IFNγ exposure.

6.3 General issues associated with techniques used in this research

The nature of this work and approaches utilized here were reliant on lentiviral transduced RAW 264.7 cells, and thus the overexpression of exogenous proteins. A doxycycline-inducible overexpression system is a tool that may be used to examine the function of a large number of genes in mammalian cells (332). This tool is very adaptable and has a broad range of applications. Nevertheless, during the course of the last decade, a few publications have urged users of this method to exercise extreme caution. The levels of CITED1 in our system were present at much greater concentrations than the endogenous protein. This may have caused non-physiological interactions with other proteins and possibly impacted their behavior and phenotype.

Recently, a study provided some recommendations on how to reduce the likelihood of incorrect interpretations of the data obtained via the use of doxycycline-inducible overexpression systems (333). One of these was using a minimal concentration of doxycycline, and we explored this idea by testing different concentrations of dox (30, 100, and 300 ng/ mL), finding that 100 ng/mL of doxycycline served as an ideal minimal concentration to elicit ectopic CITED1 expression. It has been established that doxycycline may itself stimulate changes in gene expression; however, the majority of these were found at doses at least 10 times greater than the ones utilized here (334–336). Second, producing appropriate controls would further reduce spurious or artifactual changes associated with this approach. For this study, we produced parallel dox-treated control samples using unmodified RAW264.7 cells to

identify any dox-induced gene expression changes in our cells. These were minimal and were subtracted from our DEG lists as part of our bioinformatics pipeline.

A similar level of care was employed in our experiments using gene-edited cells. Here, we produced control cells by transduction with lentiviral constructs to express the Cas9 endonuclease and a non-targeting 'scramble' guide RNA. This allowed for accurate comparisons with edited cells as they were transduced and manipulated in the same way.

Finally, we assert that our approach using both overexpression and genetic knockout helps to circumvent concerns associated with either strategy. As anticipated, the opposite phenotype was observed between overexpression and knockout comparison, providing confidence that the detected changes were genuine. There is still a level of uncertainty about whether the measured responses accurately represent the activities of endogenous protein and indeed whether these changes are a direct consequence of the co-activator functions of the protein. This could be addressed in future transcriptional profiling studies using CITED1 mutants lacking the CR2 domain required for CBP/p300 interaction, which is essential for CITED1 co-regulatory functions. However, this was not feasible during the time constraints of this study.

6.4 Recently published work in the field

6.4.1 Macrophage:*Cn* transcriptome profiling

During the studies carried out in this dissertation, the innate immunity and *Cn* fields have begun to expand and show a deeper interest in the transcriptome

reprogramming of the host (337). A wide variety of pathogens manipulate host cell molecular processes as a part of intracellular survival mechanisms, often by altering the activity of the main regulators of macrophage polarization (338). In a couple of *in vitro* studies, it has been shown that *Cn* may decrease NO production, most likely by limiting the expression of *Nos2* in cell lines, which results in macrophages adopting an M2-like phenotype (79,80). These prior studies measured NO production using macrophage cell lines that are different from those in our research. Although attempts were made in this study to opsonize *Cn* to promote macrophage infection, it is not entirely clear how successful this was and what proportion of the macrophages were actually infected. Several earlier studies have looked at the impact of *Cn* exposure on the transcriptome of monocytes and macrophages (233,258,339–342). The Coehlo group found alterations in the activity of the HIF-1 signaling pathway, which has also been shown in pulmonary fungal infections (343). The Chen et al. study revealed that the NF-κB, JAK-STAT, TNF, and TLR signaling pathways were also impacted (258). Transcription factors associated with these pathways, including HIF1(175,177), NF-κB p65 (146,167), STAT1(67,107,108,113,115), STAT2 (178) and p53 (179–181), enhance or inhibit macrophage proinflammatory and microbicidal activities. These transcription factors govern inflammatory and metabolic gene programs that determine macrophage activation. Uncontrolled inflammation may cause excessive cytokine production, tissue dysfunction, and chronic illnesses (344). To minimize tissue damage from uncontrolled inflammation, macrophage IFNγ signaling is limited by the production of anti-

inflammatory cytokines, IL-4, and IL-13, stimulating M2 polarization and reducing the expression of many ISGs (218,285,286).

6.4.2 CITED1, a putative positive regulator of inflammatory gene expression

Numerous cell-intrinsic negative regulatory systems exist in macrophages, which may limit and prevent excessive proinflammatory gene expression (345). Recently published data in this field has begun to show the importance of CITED2 in restraining broad inflammatory gene expression in macrophages and neutrophils (197,198,203,346,347). CITED2 serves as a negative regulator by attenuating NF-κB and HIF1α transcriptional activity in macrophages (197,198). In this case, it limits the ability of HIF1 and p65-containing NF-κB transcription factors to bind the CH1 domain of CBP/p300, hence suppressing the production of proinflammatory genes. Furthermore, CITED2 deficient cells heighten IFNγ-induced STAT1 and IRF1 target gene expression in macrophages (203). Because of the structural similarities between the two CITED proteins (208), these timely papers about CITED2 led us to devise experiments, compare them and draw conclusions about the role of CITED1 in enhancing IFNγ-regulated gene expression. However, the mechanisms by which this is achieved have yet to be elucidated.

According to recent research, CBP promotes STAT1 acetylation and reverses the modifications of the protein associated with IFN-dependent activation (348). In brief, CBP acetylates two amino acid side chains in STAT1 that stimulate the recruitment of a nuclear tyrosine-protein phosphatase that removes the Y701 activating

phosphorylation required for STAT1 dimerization and nuclear translocation. This leads to STAT1 inactivation and nuclear export. Given that CITED1 binds to the CH2 domain of CBP/p300, which is associated with the HAT activity of the protein, we speculate that CITED1 may antagonize STAT1 acetylation, which could result in the continued activation and nuclear occupancy of STAT1, thereby enhancing the STAT1-mediated ISG expression we observe in CITED1-expressing cells. When taken together with the known antagonistic effects of CITED2 on STAT1 activity, this suggests a mechanism by which CITED 1 and 2 operate together to tune the timing and magnitude of the IFNγ response.

When considering how the findings of this study could be leveraged in the development of new anticryptococcal therapeutic strategies, we could invoke a recent study that has used structural elements of CITED2 as a potential anticancer drug. Based on the CR2 domain of CITED2, the authors developed a cell-permeable peptide capable of inhibiting HIF1 signaling in cancer cells and demonstrated that CITED2-mediated inactivation of HIF-1 is a potential action in providing a potential therapeutic for the treatment of cancer (349). If our model of how CITED1 enhances STAT1 signaling is correct, we suggest that a similar peptide based on the CITED1 CR2 domain could be developed that would enhance the IFNγ response and fungicidal activity of macrophages.

6.4 Future Research

The data presented here provide the foundation for examining the transcriptome of host macrophages as a route for understanding the mechanisms by which intracellular *Cn* impacts the activity of signaling pathways and other transcriptional regulators that control macrophage polarization and innate immune function. These experiments were all performed using RAW 264.7 cells, murine-leukemia macrophage-like cell lines that have been demonstrated to recapitulate the behaviors of bone marrow-derived macrophages to microbial ligands (82,350). They are, however, phenotypically different from primary macrophages and may not always behave in the same way during intracellular *Cn* infection. This could be addressed by performing a limited number of experiments in a murine alveolar macrophage cell line (MH-S) and human monocyte and macrophage cell lines (THP-1, U937) to recapitulate key results. These studies will enable us to more accurately assess the biological significance and role of CITED1 expression in macrophages of different species.

One of the study's intriguing findings is *Cited1*, a gene that responds to IFNγ and is regulated by STAT-1. However, it is unclear if STAT1 directly controls *Cited1* expression or whether IRF1 expression downstream of STAT1 is necessary for *Cited1* expression. This is an ongoing investigation in our lab using the CRISPR-Cas9 KO approach, enabling us to determine if IRF1 is required for *Cited1* expression.

In this dissertation, I examined how CITED1 expression affects the transcriptional changes accompanying IFNγ-stimulated M1 polarization at 24 h in

CITED1 OE lines and 48 h in *Cited1* KO lines. To provide a comprehensive and comparative picture of CITED1 function and effect, transcriptional profiling could be repeated in both cell lines at additional time points. Based on prior reports and the apparent contrasting behavior of CITED1 and CITED2, it is possible that these proteins may have an antagonist role in STAT1- and IRF1-dependent gene expression. This hypothesis could be tested in the future by measuring the transcriptional changes in IFNγ-stimulated RAW264.7 CITED2 OE and KO macrophages. The resulting CITED2-regulated genes could be compared to our existing CITED gene list to measure the overlap of CITED family members.

Although CITED1 and CITED2 both have CR2 domains, their interactions with CBP/p300 are unique. We postulate that these differences may be responsible for their differing effects on ISG expression. The effects of CITED1 and CITED2 on p65:CBP/p300 and STAT1:CBP/p300 chromatin complexes could be assessed by by co-immunoprecipitations (co-IP) using Flag-STAT1 and Flag-p65 constructs. A follow-up experiment might be conducted utilizing mutants of deltaCR2 that are unable to bind CBP/p300, Flag-DeltaN-CITED1, and assessing the levels of STAT1 and CBP by co-IP. Additionally, these truncated versions may also be used to assess their impact on STAT1-regulated genes, which will help us to clarify the role of CITED1 domains in enhancing STAT1-regulated gene expression. In this study, it was observed that CITED1 elevates STAT1-regulated gene expression and is itself STAT1-regulated; however, the underlying mechanism is unclear. To examine whether CITED1 increases STAT1-regulated gene expression by inhibiting CBP-dependent acetylation of STAT1,

pINDUCER20-CITED1 cells might be used to evaluate STAT1 acetylation and phosphorylation by western blotting and live cell microscopy.

This work demonstrates that CITED1 activity is also controlled by its subcellular localization, which is driven by the phosphorylation status of the protein. We identified six putative serine phosphorylation sites (Ser17, 67, 69, 73, 79, and 147; NetPhos-3.1 analysis, phosphorylation site scores >0.90), most of which are conserved between human and murine CITED1 sequences. However, actual phosphorylation sites are unknown. This could be verified experimentally by isolating Flag-tagged CITED1 before and after IFNγ treatment and evaluating the protein via tandem mass spectrometry. Information from these studies could be used in the future to create mutants by substituting alanine and glutamate for phosphorylated residues. These mutant variants of CITED1 might aid in identifying the regions that may be crucial for the IFNγ-stimulated phosphorylation of the protein and nuclear translocation.

While our findings show that CITED1 is upregulated in *Cn*-infected cells, the role of this protein in suppressing the M1 transcriptome and impairing *Cn* killing has yet to be investigated. To ascertain the role played by CITED1 induction in influencing the transcriptome of macrophages infected with *Cn*, IFNγ-stimulated WT and *Cited1* KO cells will be infected with H99S, and the transcriptional response will be evaluated by RNASeq. Data from these experiments will allow us to establish genes regulated during *Cn*-infection in a CITED1-dependent and CITED1-independent manner. To assess how CITED1 expression affects macrophage phenotype, subsequent tests could be conducted to evaluate changes in macrophage fungicidal activity by antifungal activity

assays, host macrophage viability by FACS analysis of annexin-V and PI-stained cells, and western blotting of cytosolic and mitochondrial fractionated cells to measure caspase c release. As *Cn*-infection caused M1 macrophages to upregulate the expression of *Ccl22*, *Ccl2,* and *Ccl5*, investigating the expression of these genes in *Cited1* KO cells using ELISA will enable us to examine the impact of altered CITED1 levels on the expression of these genes and a broader panel of cytokines crucial to the innate immune response to *Cn*. These proposed experiments would solidify the results here by demonstrating the role of CITED1 expression in impacting the transcriptome and anti-fungal activity of M1 polarized macrophages.

6.5 Final comments

In recent years, it has become increasingly common for biologists to take a more extensive, holistic approach in studying the dynamic nature of macrophage polarization in *Cn* infections and signaling networks rather than focusing on the activities of individual proteins. Given the relevance of macrophage polarization in the efficacy of an immune response to *Cn* and in preventing tissue damage that accompanies uncontrolled or prolonged inflammation, improving our knowledge of the global transcriptome and pathways that are affected may help in the identification of novel molecular targets for therapeutic intervention in cryptococcosis or other diseases.

I hope I have been able to contribute to a greater understanding of the specific impacts of intracellular *Cn* on known regulators of macrophage polarization while also

reporting the broader effects of the pathogen on host cells. Additionally, through my work, I have taken the first step towards characterizing a previously unknown role for CITED1 as a regulator of macrophage function and proinflammatory gene expression. Through a combination of focused and unbiased experimental approaches, I am certain that the results presented here have led to an improved understanding of the altered molecular signaling and gene expression patterns in host macrophages during intracellular *Cn* infection. There is still much to understand about CITED1, and these findings provide only a first glimpse of its regulation and how it fits within the mechanisms that control macrophage phenotype. Future research might reveal the significance of certain CITED1 regions or domains in boosting the expression of IFNγ-regulated genes. The aforementioned information might be used to create a cell-permeable peptide in the future that is derived from the chosen areas of CITED1 to increase the antibacterial activity of macrophages. In this regard, I feel that our work has a high possibility of adding new insights to the *Cn* and broader microbial pathogens and innate immunity fields.

I believe these approaches and findings offer significance beyond macrophage:*Cn* interactions and may provide insights into how changes in gene expression driving macrophage polarization are regulated in inflammatory illnesses like rheumatoid arthritis or Crohn's disease, autoimmune diseases, and infections.

REFERENCES

1. McClelland EE, Casadevall A, Eisenman HC. Pathogenesis of Cryptococcus neoformans. In: Kavanagh K, editor. New Insights in Medical Mycology: *Springer Netherlands*; 2007:131–57.

2. Mitchell TG, Perfect JR. Cryptococcosis in the era of AIDS - 100 years after the discovery of Crypotcoccus neoformans., *Clinical Microbiology Reviews*. 1995. 8. 515–48.

3. Casadevall A, Perfect JR. Cryptococcus neoformans, American Society of Microbiology; 1998.

4. Rajasingham R, Smith RM, Park BJ, Jarvis JN, Govender NP, Chiller TM, et al. Global burden of disease of HIV-associated cryptococcal meningitis: an updated analysis. *The Lancet Infectious Diseases*. 2017 Aug 1;17(8):873–81.

5. Garcia-Hermoso D, Janbon G, Dromer F. Epidemiological evidence for dormant Cryptococcus neoformans infection *Journal of Clinical Microbiology*. 1999;37(10):3204–9.

6. Goldman DL, Lee SC, Mednick AJ, Montella L, Casadevall A. Persistent Cryptococcus neoformans pulmonary infection in the rat is associated with intracellular parasitism, decreased inducible nitric oxide synthase expression, and altered antibody responsiveness to cryptococcal polysaccharide. *Infection and Immunology*. 2000 Feb;68(2):832–8.

7. Hull CM, Heitman J. Genetics of *Cryptococcus neoformans*. *Annual Review of Genetics*. 2002 Dec 28;36(1):557–615.

8. Smith KD, Achan B, Hullsiek KH, McDonald TR, Okagaki LH, Alhadab AA, et al. Increased antifungal drug resistance in clinical isolates of Cryptococcus neoformans in Uganda. *Antimicrobial Agents and Chemotherapy*. 2015 Dec;59(12):7197–204.

9. Coelho C, Bocca AL, Casadevall A. The Intracellular life of *Cryptococcus neoformans*. *Annual Review of Pathology: Mechanisms of Disease*. 2014 Jan 24;9(1):219–38.

10. Li SS, Kyei SK, Timm-Mccann M, Ogbomo H, Jones GJ, Shi M, et al. The NK receptor NKp30 mediates direct fungal recognition and killing and is diminished in NK cells from HIV-infected patients. *Cell Host & Microbe*. 2013;14(4):387–97.

11. Price MS, Perfect JR. Host defenses against cryptococcosis. *Immunological Investigations*. 2011; 40(7–8):786–808.

12. LeibundGut-Landmann S, Wüthrich M, Hohl TM. Immunity to fungi. *Current Opinion in Immunology*, 2012; 24(4):449–58.

13. Baumgarth N. B-1 cell heterogeneity and the regulation of natural and antigen-induced IgM production. *Frontiers in Immunology*. 2016 Sep 9;7(SEP):324.

14. Panda S, Ding JL. Natural antibodies bridge innate and adaptive immunity. *Journal of Immunology*. 2015; 194(1):13–20.

15. Levitz SM, Tabuni A. Binding of Cryptococcus neoformans by human cultured macrophages. Requirements for multiple complement receptors and actin. *Journal of Clinical Investigation*. 1991;87(2):528.

16. Lipscomb MF, Alvarellos T, Toews GB, Tompkins R, Evans Z, Koo G, et al. Role of natural killer cells in resistance to Cryptococcus neoformans infections in mice. *The American Journal of pathology*. 1987;128(2):354.

17. Chun FZ, Ling LM, Jones GJ, Gill MJ, Krensky AM, Kubes P, et al. Cytotoxic CD4+ T cells use granulysin to kill Cryptococcus neoformans, and activation of this pathway is defective in HIV patients. *Blood*. 2007;109(5):2049–57.

18. Hill JO, Harmsen AG. Intrapulmonary growth and dissemination of an avirulent strain of Cryptococcus neoformans in mice depleted of CD4+ or CD8+ T cells. *The Journal of Experimental Medicine*. 1991; 173(3):755–8.

19. Ma LL, Spurrell JCL, Wang JF, Neely GG, Epelman S, Krensky AM, et al. CD8 T cell-mediated killing of Cryptococcus neoformans requires granulysin and is dependent on CD4 T cells and IL-15. *The Journal of Immunology*. 2002;169(10):5787–95.

20. Diamond RD, May JE, Kane MA, Frank MM, Bennett JE. The role of the classical and alternate complement pathways in host defenses against Cryptococcus neoformans infection. *The Journal of Immunology*. 1974;112(6).

21. Zaragoza O, Taborda CP, Casadevall A. The efficacy of complement-mediated phagocytosis of Cryptococcus neoformans is dependent on the location of C3 in the polysaccharide capsule and involves both direct and indirect C3-mediated interactions. *European Journal of Immunolgy*. 2003;33(7):1957–67.

22. Taborda CP, Casadevall A. CR3 (CD11b/CD18) and CR4 (CD11c/CD18) are involved in complement-independent antibody-mediated phagocytosis of Cryptococcus neoformans. *Immunity*. 2002; 16(6):791–802.

23. Vecchiarelli A, Pietrella D, Lupo P, Bistoni F, McFadden DC, Casadevall A. The polysaccharide capsule of Cryptococcus neoformans interferes with human dendritic cell maturation and activation. *Journal of leukocyte biology*. 2003;74(3):370–8.

24. Gjomarkaj M, Pace E, Melis M, Spatafora M, Profita M, Vignola AM, et al. Phenotypic and functional characterization of normal rat pleural macrophages in comparison with autologous peritoneal and alveolar macrophages. *American Journal of Respiratory Cell and Molecular Biology.* 1999;20(1):135–42.

25. Zaragoza O, Rodrigues ML, de Jesus M, Frases S, Dadachova E, Casadevall A. The capsule of the fungal pathogen Cryptococcus neoformans. *Advances in Applied Microbiology*,. 2009;68:133–216.

26. Reese AJ, Doering TL. Cell wall alpha-1,3-glucan is required to anchor the Cryptococcus neoformans capsule. *Molecular Microbiology*. 2003;50(4):1401–9.

27. Yauch LE, Mansour MK, Levitz SM. Receptor-mediated clearance of Cryptococcus neoformans capsular polysaccharide in vivo. *Infection and Immunity*. 2005;73(12):8429–32.

28. Shoham S, Huang C, Chen JM, Golenbock DT, Levitz SM. Toll-like receptor 4 mediates intracellular signaling without TNF-alpha release in response to Cryptococcus neoformans polysaccharide capsule. *Journal of Immunology*. 2001;166(7):4620–6.

29. Nakamura K, Miyagi K, Koguchi Y, Kinjo Y, Uezu K, Kinjo T, et al. Limited contribution of Toll-like receptor 2 and 4 to the host response to a fungal infectious pathogen, Cryptococcus neoformans. *FEMS Immunology and Medical Microbiology*. 2006;47(1):148–54.

30. Zhang Y, Wang F, Bhan U, Huffnagle GB, Toews GB, Standiford TJ, et al. TLR9 signaling is required for generation of the adaptive immune protection in Cryptococcus neoformans-infected lungs. *The American Journal of Pathology*. 2010;177(2):754.

31. Nakamura K, Miyazato A, Xiao G, Hatta M, Inden K, Aoyagi T, et al. Deoxynucleic acids from Cryptococcus neoformans activate myeloid dendritic cells via a TLR9-dependent pathway. *The Journal of Immunology*. 2008;180(6):4067–74.

32. Taylor PR, Tsoni SV, Willment JA, Dennehy KM, Rosas M, Findon H, et al. Dectin-1 is required for beta-glucan recognition and control of fungal infection. *Nature Immunology*. 2007;8(1):31–8.

33. Steele C, Rapaka RR, Metz A, Pop SM, Williams DL, Gordon S, et al. The beta-glucan receptor dectin-1 recognizes specific morphologies of Aspergillus fumigatus. *PLoS Pathogens*. 2005;1(4):0323–34.

34. Nakamura K, Kinjo T, Saijo S, Miyazato A, Adachi Y, Ohno N, et al. Dectin-1 is not required for the host defense to Cryptococcus neoformans. *Microbiology and Immunology*. 2007;51(11):1115–9.

35. Kozel TR, Pfrommer GST. Activation of the complement system by Cryptococcus neoformans leads to binding of iC3b to the yeast. *Infection and Immunity*. 1986;52(1):1–5.

36. Kozel TR, Wilson MA, Pfrommer GST, Schlageter AM. Activation and binding of opsonic fragments of C3 on encapsulated Cryptococcus neoformans by using an alternative

complement pathway reconstituted from six isolated proteins. *Infection and Immunity*. 1989;57(7):1922.

37. Levitz SM, Tabuni A. Binding of Cryptococcus neoformans by human cultured macrophages. Requirements for multiple complement receptors and actin. *Journal of Clinical Investigation*. 1991;87(2):528.

38. Luo Y, Cook E, Fries BC, Casadevall A. Phagocytic efficacy of macrophage-like cells as a function of cell cycle and Fcγ receptors (FcγR) and complement receptor (CR)3 expression. *Clinical and Experimental Immunology*. 2006;145(2):380.

39. Syme RM, Spurrell JCL, Amankwah EK, Green FHY, Mody CH. Primary Dendritic Cells Phagocytose Cryptococcus neoformans via Mannose Receptors and Fcγ Receptor II for Presentation to T Lymphocytes. *Infection and Immunity*. 2002;70(11):5972.

40. Kozel TR. Opsonization and phagocytosis of Cryptococcus neoformans. *Archives of medical research*. 1993; 24(3), 211–218.

41. Feldmesser M, Kress Y, Novikoff P, Casadevall A. Cryptococcus neoformans is a facultative intracellular pathogen in murine pulmonary infection. *Infection and Immunity*. 2000;68(7):4225–37. 58526

42. Larsen RA, Pappas PG, Perfect J, Aberg JA, Casadevall A, Cloud GA, et al. Phase I evaluation of the safety and pharmacokinetics of murine-derived anticryptococcal antibody 18B7 in subjects with treated cryptococcal meningitis. *Antimicrobial Agents and Chemotherapy*. 2005;49(3):952.

43. Ginhoux F, Jung S. Monocytes and macrophages: developmental pathways and tissue homeostasis. *Nature Review Immunology*. 2014;14(6):392–404.

44. Gal AA, Koss MN, Hawkins J, Evans S, Einstein H. The pathology of pulmonary cryptococcal infections in the acquired immunodeficiency syndrome. *Archives of Pathology & Laboratory Medicine*. 1986;110(6):502–7.

45. Calverley M, Harmsen A. The facultative intracellular pathogen Cryptococcus neoformans is susceptible to in vivo clearance by alveolar macrophages (P4211). The *Journal of Immunology*. 2013;190.

46. Grinsell M, Weinhold LC, Cutler JE, Han Y, Kozel TR. In Vivo Clearance of glucuronoxylomannan, the major capsular polysaccharide of *Cryptococcus neoformans:* a critical role for tissue macrophages. *The Journal of Infectious Diseases*. 2001;184(4):479–87.

47. Bolaños B, Mitchell TG. Killing of Cryptococcus neoformans by rat alveolar macrophages. *Journal of Medical and Veterinary Mycology*. 1989;27(4):219–28.

48. Levitz SM, DiBenedetto DJ. Paradoxical role of capsule in murine bronchoalveolar macrophage-mediated killing of Cryptococcus neoformans. *The Journal of Immunology*. 1989;142(2).

49. Tucker SC, Casadevall A. Replication of Cryptococcus neoformans in macrophages is accompanied by phagosomal permeabilization and accumulation of vesicles containing polysaccharide in the cytoplasm. *Proceedings of the National Academy of Sciences*. 2002;99(5):3165–70.

50. Voelz K, Lammas DA, May RC. Cytokine signaling regulates the outcome of intracellular macrophage parasitism by Cryptococcus neoformans. *Infection and Immunity*. 2009;77(8):3450–7.

51. Alvarez M, Casadevall A. Phagosome Extrusion and Host-Cell Survival after Cryptococcus neoformans Phagocytosis by Macrophages. *Current Biology*. 2006;16(21):2161–5.

52. Charlier C, Nielsen K, Daou S, Brigitte M, Chretien F, Dromer F. Evidence of a role for monocytes in dissemination and brain invasion by Cryptococcus neoformans. *Infection and Immunity*. 2009;77(1):120–7.

53. McQuiston TJ, Williamson PR. Paradoxical roles of alveolar macrophages in the host response to Cryptococcus neoformans. *Journal of Infection and Chemotherapy : Official Journal of the Japan Society of Chemotherapy*. 2012;18(1):1–9.

54. Charlier C, Nielsen K, Daou S, Brigitte M, Chretien F, Dromer F. Evidence of a role for monocytes in dissemination and brain invasion by Cryptococcus neoformans. *Infection and Immunity*. 2009;77(1):120–7.

55. Tseng HK, Huang TY, Wu AYJ, Chen HH, Liu CP, Jong A. How Cryptococcus interacts with the blood-brain barrier. *Future Microbiology*. 2015;10(10):1669–82.

56. Ma H, Croudace JE, Lammas DA, May RC. Expulsion of live pathogenic yeast by macrophages. *Current Biology*. 2006;16(21):2156–60.

57. Charlier C, Nielsen K, Daou S, Brigitte M, Chretien F, Dromer F. Evidence of a Role for Monocytes in Dissemination and Brain Invasion by Cryptococcus neoformans. *Infection and Immunity*. 2009;77(1):120.

58. Uicker WC, Doyle HA, Mccracken JP, Langlois M, Buchanan KL. Cytokine and chemokine expression in the central nervous system associated with protective cell-mediated immunity against Cryptococcus neoformans. *Medical Mycology*. 2005;43(1), 27–38

59. Koguchi Y, Kawakami K. Cryptococcal infection and Th1-Th2 cytokine balance. *International Review of Immunology*. 2002;21(4–5):423–8.

60. Martinez FO, Sica A, Mantovani A, Locati M. Macrophage activation and polarization. *Frontier Bioscieces*. 2008;13:453–61.

61. MacMicking J, Xie Q wen, Nathan C. Nitric oxide and macrophage function. *Annual Review Immunology*. 2002;15(1):323–50.

62. Ding AH, Nathan CF, Stuehr DJ. Release of reactive nitrogen intermediates and reactive oxygen intermediates from mouse peritoneal macrophages. Comparison of activating cytokines and evidence for independent production. *The Journal of Immunology*. 1988;141(7).

63. Gruenheid S, Gros P. Genetic susceptibility to intracellular infections: Nramp1, macrophage function and divalent cations transport. *Current Opinion in Microbiology*. 2000;3(1):43–8.

64. Carlin JM, Borden EC, Byrne GI. Interferon-induced indoleamine 2,3-dioxygenase activity inhibits Chlamydia psittaci replication in human macrophages. *Journal of interferon research*. 1989;9(3):329–37.

65. Granger DL, Hibbs JB, Perfect JR, Durack DT. Specific amino acid (L-arginine) requirement for the microbiostatic activity of murine macrophages. *The Journal of Clinical Investigation*. 1988;81(4):1129–36.

66. Arora S, Hernandez Y, Erb-Downward JR, McDonald RA, Toews GB, Huffnagle GB. Role of IFN-gamma in regulating T2 immunity and the development of alternatively activated macrophages during allergic bronchopulmonary mycosis. *The Journal of Immunology*. 2005;174(10):6346–56.

67. Wager CML, Hole CR, Wozniak KL, Olszewski MA, Mueller M, Wormley FL. STAT1 signaling within macrophages is required for antifungal activity against Cryptococcus neoformans. *Infection and Immunity*. 2015;83(12):4513–27.

68. Ashida H, Mimuro H, Ogawa M, Kobayashi T, Sanada T, Kim M, et al. Cell death and infection: A double-edged sword for host and pathogen survival. Vol. 195, *Journal of Cell Biology.* 2011.931–42.

69. Lykens JE, Terrell CE, Zoller EE, Divanovic S, Trompette A, Karp CL, et al. Mice with a selective impairment of IFN-γ signaling in macrophage lineage cells demonstrate the critical role of IFN-γ–activated macrophages for the control of protozoan parasitic infections in vivo. *The Journal of Immunology*. 2010;184(2):877–85.

70. Dalton DK, Pitts-Meek S, Keshav S, Figari IS, Bradley A, Stewart TA. Multiple Defects of Immune Cell Function in Mice with Disrupted Interferon-γ Genes. *Science*. 1993;259(5102):1739–42.

71. Kak G, Raza M, Tiwari BK. Interferon-gamma (IFN-γ): Exploring its implications in infectious diseases. *Biomolecule Concepts*. 2018;9(1):64–79.

72. Filipe-Santos O, Bustamante J, Chapgier A, Vogt G, de Beaucoudrey L, Feinberg J, et al. Inborn errors of IL-12/23- and IFN-gamma-mediated immunity: molecular, cellular, and clinical features. *Seminars in Immunology*. 2006;18(6):347–61.

73. Hardison SE, Ravi S, Wozniak KL, Young ML, Olszewski MA, Wormley FL. Pulmonary infection with an interferon-γ-producing cryptococcus neoformans strain results in classical macrophage activation and protection. *American Journal of Pathology*. 2010;176(2):774–85.

74. He W, Casadevall A, Lee SC, Goldman DL. Phagocytic activity and monocyte chemotactic protein expression by pulmonary macrophages in persistent pulmonary cryptococcosis. *Infection and Immunity*. 2003;71(2):930–6.

75. Gordon S, Martinez FO. Alternative activation of macrophages: mechanism and functions. *Immunity*. 2010;32(5):593–604.

76. Arora S, Olszewski MA, Tsang TM, McDonald RA, Toews GB, Huffnagle GB. Effect of Cytokine Interplay on Macrophage Polarization during Chronic Pulmonary Infection with Cryptococcus neoformans. *Infection and Immunity*. 2011;79(5):1915–26.

77. Rath M, Müller I, Kropf P, Closs EI, Munder M. Metabolism via arginase or nitric oxide synthase: Two competing arginine pathways in macrophages. *Frontiers in Immunology*. 2014;5:532.

78. Hesse M, Modolell M, la Flamme AC, Schito M, Fuentes JM, Cheever AW, et al. Differential regulation of nitric oxide synthase-2 and arginase-1 by type 1/type 2 cytokines in vivo: granulomatous pathology is shaped by the pattern of L-arginine metabolism. *The Journal of Immunology*. 2001;167(11):6533–44.

79. Naslund PK, Miller WC, Granger DL. Cryptococcus neoformans fails to induce nitric oxide synthase in primed murine macrophage-like cells. *Infection and Immunity*. 1995;63(4):1298–304.

80. Xiao G, Miyazato A, Inden K, Nakamura K, Shiratori K, Nakagawa K, et al. Cryptococcus neoformans inhibits nitric oxide synthesis caused by CpG-oligodeoxynucleotide-stimulated macrophages in a fashion independent of capsular polysaccharides. *Microbiology and Immunology*. 2008;52(3):171–9.

81. Johnston SA, May RC. Cryptococcus interactions with macrophages: evasion and manipulation of the phagosome by a fungal pathogen. *Cellular Microbiology*. 2013;15(3):403–11.

82. Davis MJ, Tsang TM, Qiu Y, Dayrit JK, Freij JB, Huffnagle GB, et al. Macrophage M1/M2 polarization dynamically adapts to changes in cytokine microenvironments in cryptococcus neoformans infection. *mBio*. 2013 Jun 18;4(3).

83. Zhang Y, Wang F, Tompkins KC, McNamara A, Jain A v, Moore BB, et al. Robust Th1 and Th17 immunity supports pulmonary clearance but cannot prevent systemic dissemination of highly virulent Cryptococcus neoformans H99. *The American Journal of Pathology*. 2009;175(6):2489–500.

84. Chen GH, McNamara DA, Hernandez Y, Huffnagle GB, Toews GB, Olszewski MA. Inheritance of Immune Polarization Patterns Is Linked to Resistance versus Susceptibility to Cryptococcus neoformans in a Mouse Model. *Infection and Immunity*. 2008;76(6):2379.

85. Smith LM, Dixon EF, May RC. The fungal pathogen Cryptococcus neoformans manipulates macrophage phagosome maturation. *Cellular Microbiology*. 2015;17(5):702–13.

86. Diamond RD, Bennett JE. Growth of Cryptococcus neoformans within human macrophages in vitro. *Infection and Immunity*. 1973;7(2):231.

87. Feldmesser M, Kress Y, Casadevall A. Intracellular crystal formation as a mechanism of cytotoxicity in murine pulmonary Cryptococcus neoformans infection. *Infection and Immunity*. 2001;69(4):2723–7.

88. Ma H, Croudace JE, Lammas DA, May RC. Expulsion of Live Pathogenic Yeast by Macrophages. *Current Biology*. 2006;16(21):2156–60.

89. Alvarez M, Casadevall A. Cell-to-cell spread and massive vacuole formation after Cryptococcus neoformans infection of murine macrophages. *BMC Immunology*. 2007;8:16.

90. Alvarez M, Saylor C, Casadevall A. Antibody action after phagocytosis promotes Cryptococcus neoformans and Cryptococcus gattii macrophage exocytosis with biofilm-like microcolony formation. *Cellular Microbiology*. 2008;10(8):1622.

91. Ma H, Croudace JE, Lammas DA, May RC. Direct cell-to-cell spread of a pathogenic yeast. *BMC Immunology*. 2007;8(1):1–5.

92. Charlier C, Nielsen K, Daou S, Brigitte M, Chretien F, Dromer F. Evidence of a role for monocytes in dissemination and brain invasion by Cryptococcus neoformans. *Infection and Immunity*. 2009;77(1):120–7.

93. Perfect JR. Cryptococcosis. *Infectious Disease Clinics of North America*. 1989;3(1):77–102.

94. Shao X, Mednick A, Alvarez M, van Rooijen N, Casadevall A, Goldman DL. An Innate Immune System Cell Is a Major Determinant of Species-Related Susceptibility Differences to Fungal Pneumonia. *The Journal of Immunology*. 2005;175(5):3244–51.

95. Kwon-Chung KJ, Edman JC, Wickes BL. Genetic association of mating types and virulence in Cryptococcus neoformans. *Infection and Immunity*. 1992;60(2):602–5.

96. Zaragoza O, Alvarez M, Telzak A, Rivera J, Casadevall A. The Relative Susceptibility of Mouse Strains to Pulmonary Cryptococcus neoformans Infection Is Associated with Pleiotropic Differences in the Immune Response. *Infection and Immunity*. 2007;75(6):2729.

97. Olszewski MA, Noverr MC, Chen GH, Toews GB, Cox GM, Perfect JR, et al. Urease expression by Cryptococcus neoformans promotes microvascular sequestration, thereby enhancing central nervous system invasion. *The American Journal of Pathology*. 2004;164(5):1761–71.

98. Huffnagle GB, Lipscomb MF. Pulmonary cryptococcosis. *The American Journal of Pathology*. 1992;141(6):1517.

99. Chen GH, McNamara DA, Hernandez Y, Huffnagle GB, Toews GB, Olszewski MA. Inheritance of Immune Polarization Patterns Is Linked to Resistance versus Susceptibility to Cryptococcus neoformans in a Mouse Model. *Infection and Immunity*. 2008;76(6):2379.

100. Osterholzer JJ, Surana R, Milam JE, Montano GT, Chen GH, Sonstein J, et al. Cryptococcal Urease Promotes the Accumulation of Immature Dendritic Cells and a Non-Protective T2 Immune Response within the Lung. *The American Journal of Pathology*. 2009;174(3):932–43.

101. Beyer M, Mallmann MR, Xue J, Staratschek-Jox A, Vorholt D, Krebs W, et al. High-Resolution Transcriptome of Human Macrophages. *PLoS One*. 2012;7(9).

102. Jablonski KA, Amici SA, Webb LM, Ruiz-Rosado JDD, Popovich PG, Partida-Sanchez S, et al. Novel markers to delineate murine M1 and M2 macrophages. *PLoS One*. 2015;10(12).

103. Boehm U, Klamp T, Groot M, Howard JC. Cellular responses to interferon-gamma. The *Annual Review of Immunology*. 1997;15:749–95.

104. Schroder K, Hertzog PJ, Ravasi T, Hume DA. Interferon-γ: an overview of signals, mechanisms and functions. *Journal of Leukocyte Biology*. 2004;75(2):163–89.

105. Platanias LC. Mechanisms of type-I- and type-II-interferon-mediated signalling. *Nature Review of Immunology*. 2005;5(5):375–86

106. Meraz MA, White JM, Sheehan KCF, Bach EA, Rodig SJ, Dighe AS, et al. Targeted disruption of the Stat1 gene in mice reveals unexpected physiologic specificity in the JAK-STAT signaling pathway. *Cell*. 1996;84(3):431–42.

107. Hardison SE, Herrera G, Young ML, Hole CR, Wozniak KL, Wormley FL. Protective Immunity against Pulmonary Cryptococcosis Is Associated with STAT1-Mediated Classical Macrophage Activation. *The Journal of Immunology*. 2012;189(8):4060–8.

108. Sikorski K, Chmielewski S, Olejnik A, Wesoly JZ, Heemann U, Baumann M, et al. STAT1 as a central mediator of IFNγ and TLR4 signal integration in vascular dysfunction. *JAK-STAT*. 2012;1(4):241.

109. Levy DE, Darnell JE. Stats: transcriptional control and biological impact. *Nature Reviews. Molecular Cell Biology*. 2002;3(9):651–62.

110. Ramana C v., Gil MP, Schreiber RD, Stark GR. Stat1-dependent and -independent pathways in IFN-gamma-dependent signaling. *Trends in Immunology*. 2002;23(2):96–101.

111. Durbin JE, Hackenmiller R, Simon MC, Levy DE. Targeted disruption of the mouse Stat1 gene results in compromised innate immunity to viral disease. *Cell*. 1996;84(3):443–50.

112. Gavrilescu LC, Butcher BA, del Rio L, Taylor GA, Denkers EY. STAT1 is essential for antimicrobial effector function but dispensable for gamma interferon production during Toxoplasma gondii infection. *Infection and Immunity*. 2004;72(3):1257–64.

113. Lang C, Hildebrandt A, Brand F, Opitz L, Dihazi H, Lüder CGK. Impaired chromatin remodelling at STAT1-regulated promoters leads to global unresponsiveness of Toxoplasma gondii-infected macrophages to IFN-γ. *PLoS Pathogens*. 2012;8(1).

114. Kernbauer E, Maier V, Stoiber D, Strobl B, Schneckenleithner C, Sexl V, et al. Conditional stat1 ablation reveals the importance of interferon signaling for immunity to Listeria monocytogenes infection. *PLoS Pathogens.* 2012;8(6).

115. Wager CML, Hole CR, Wozniak KL, Olszewski MA, Floyd L. Wormley Jr. STAT1 Signaling is Essential for Protection against Cryptococcus neoformans Infection in Mice. *Journal of Immunology.* 2014;193(8):4060.

116. Takaki H, Minoda Y, Koga K, Takaesu G, Yoshimura A, Kobayashi T. TGF-beta1 suppresses IFN-gamma-induced NO production in macrophages by suppressing STAT1 activation and accelerating iNOS protein degradation. *Genes to Cells : Devoted to Molecular & Cellular Mechanisms*. 2006;11(8):871–82.

117. Kincaid EZ, Ernst JD. Mycobacterium tuberculosis exerts gene-selective inhibition of transcriptional responses to IFN-gamma without inhibiting STAT1 function. *The Journal of Immunology*. 2003;171(4):2042–9.

118. Olias P, Etheridge RD, Zhang Y, Holtzman MJ, Sibley LD. Toxoplasma effector recruits the Mi-2/NuRD complex to repress stat1 transcription and block IFN-γ-dependent gene expression. *Cell and Host Microbe*. 2016;20(1):72.

119. Miyamoto M, Fujita T, Kimura Y, Maruyama M, Harada H, Sudo Y, et al. Regulated expression of a gene encoding a nuclear factor, IRF-1, that specifically binds to IFN-beta gene regulatory elements. *Cell*. 1988;54(6):903–13.

120. Pine R, Decker T, Kessler DS, Levy DE, Darnell JE. Purification and cloning of interferon-stimulated gene factor 2 (ISGF2): ISGF2 (IRF-1) can bind to the promoters of both beta interferon- and interferon-stimulated genes but is not a primary transcriptional activator of either. *Molecular and Cellular Biology*. 1990;10(6):2448–57.

121. Escalante CR, Yie J, Thanos D, Aggarwal AK. Structure of IRF-1 with bound DNA reveals determinants of interferon regulation. *Nature*. 1998;391(6662):103–6.

122. Goodbourn S, Maniatis T. Overlapping positive and negative regulatory domains of the human beta-interferon gene. *Proceedings of the National Academy of Sciences of the United States of America*. 1988;85(5):1447–51.

123. Lohoff M, Mak TW. Roles of interferon-regulatory factors in T-helper-cell differentiation. *Nature Reviews Immunology*. 2005;5(2):125–35.

124. Günthner R, Anders HJ. Interferon-regulatory factors determine macrophage phenotype polarization. *Mediators of Inflammation*. 2013; 731023.

125. Decker T, Kovarik P, Meinke A. GAS elements: a few nucleotides with a major impact on cytokine-induced gene expression. *Journal of Interferon & Cytokine Research : The Official Journal of the International Society for Interferon and Cytokine Research*. 1997;17(3):121–34.

126. Kamijo R, Harada H, Matsuyama T, Bosland M, Gerecitano J, Shapiro D, et al. Requirement for transcription factor IRF-1 in NO synthase induction in macrophages. *Science*. 1994;263(5153):1612–5.

127. Langlais D, Barreiro LB, Gros P. The macrophage IRF8/IRF1 regulome is required for protection against infections and is associated with chronic inflammation. *The Journal of Experimental Medicine*. 2016;213(4):585.

128. Abou El Hassan M, Huang K, Eswara MBK, Xu Z, Yu T, Aubry A, et al. Properties of STAT1 and IRF1 enhancers and the influence of SNPs. *BMC Molecular Biology*. 2017;18(1):6.

129. Cooper AM, Pearl JE, Brooks J v., Ehlers S, Orme IM. Expression of the nitric oxide synthase 2 gene is not essential for early control of Mycobacterium tuberculosis in the murine lung. *Infection and Immunity*. 2000;68(12):6879–82.

130. Fehr T, Schoedon G, Odermatt B, Holtschke T, Schneemann M, Bachmann MF, et al. Crucial role of interferon consensus sequence binding protein, but neither of interferon regulatory factor 1 nor of nitric oxide synthesis for protection against murine listeriosis. *The Journal of Experimental Medicine*. 1997;185(5):921–31.

131. Dror N, Alter-Koltunoff M, Azriel A, Amariglio N, Jacob-Hirsch J, Zeligson S, et al. Identification of IRF-8 and IRF-1 target genes in activated macrophages. *Molecular Immunology*. 2007;44(4):338–46.

132. Kumatori A, Yang D, Suzuki S, Nakamura M. Cooperation of STAT-1 and IRF-1 in interferon-γ-induced transcription of the gp91phox gene. *Journal of Biological Chemistry*. 2002;277(11):9103–11.

133. Ramsauer K, Farlik M, Zupkovitz G, Seiser C, Kröger A, Hauser H, et al. Distinct modes of action applied by transcription factors STAT1 and IRF1 to initiate transcription of the IFN-γ-inducible gbp2 gene. *Proceedings of the National Academy of Sciences of the United States of America*. 2007;104(8):2849.

134. Platanitis E, Decker T. Regulatory networks involving STATs, IRFs, and NFκB in inflammation. *Frontiers in Immunology*. 2018;9:2542.

135. Michalska A, Blaszczyk K, Wesoly J & Bluyssen HAR. A Positive feedback amplifier circuit that regulates interferon (IFN)-stimulated gene expression and controls type I and type II IFN responses. *Frontiers in Immunology.* 2018;9:28.

136. Okada Y, Wu D, Trynka G, Raj T, Terao C, Ikari K, et al. Genetics of rheumatoid arthritis contributes to biology and drug discovery. *Nature.* 2014;506(7488):376–81.

137. Beecham AH, Patsopoulos NA, Xifara DK, Davis MF, Kemppinen A, Cotsapas C, et al. Analysis of immune-related loci identifies 48 new susceptibility variants for multiple sclerosis. *Nature Genetics*. 2013;45(11):1353–62.

138. Jostins L, Ripke S, Weersma RK, Duerr RH, McGovern DP, Hui KY, et al. Host-microbe interactions have shaped the genetic architecture of inflammatory bowel disease. *Nature*. 2012;491(7422):119–24.

139. Graham DS, Morris DL, Bhangale TR, Criswell LA, Syvänen AC, Rönnblom L, et al. Association of NCF2, IKZF1, IRF8, IFIH1, and TYK2 with systemic lupus erythematosus. *PLoS Genetics*. 2011;7(10)

140. Hayden MS, Ghosh S. NF-κB, the first quarter-century: remarkable progress and outstanding questions. *Genes & Development*. 2012;26(3):203.

141. Gilmore TD. Introduction to NF-kappaB: players, pathways, perspectives. *Oncogene*. 2006;25(51):6680–4.

142. Liu T, Zhang L, Joo D, Sun SC. NF-κB signaling in inflammation. *Signal Transduction and Targeted Therapy 2017 2:1*. 2017;2(1):1–9.

143. Karin M, Delhase M. The I kappa B kinase (IKK) and NF-kappa B: key elements of proinflammatory signalling. *Seminars in Immunology*. 2000;12(1):85–98.

144. Oeckinghaus A, Ghosh S. The NF-kappaB family of transcription factors and its regulation. *Cold Spring Harbor perspectives in biology*. 2009;1(4).

145. Silverman N, Maniatis T. NF-kappaB signaling pathways in mammalian and insect innate immunity. *Genes & Development*. 2001;15(18):2321–42.

146. Ben-Abdallah M, Sturny-Leclère A, Avé P, Louise A, Moyrand F, Weih F, et al. Fungal-induced cell cycle impairment, chromosome instability and apoptosis via differential activation of NF-κB. *PLoS Pathogens*. 2012;8(3).

147. Lowenstein CJ, Alley EW, Raval P, Snowman AM, Snyder SH, Russell SW, et al. Macrophage nitric oxide synthase gene: two upstream regions mediate induction by interferon gamma and lipopolysaccharide. *Proceedings of the National Academy of Sciences of the United States of America*. 1993;90(20):9730.

148. Sharif O, Bolshakov VN, Raines S, Newham P, Perkins ND. Transcriptional profiling of the LPS induced NF-κB response in macrophages. *BMC Immunology*. 2007;8(1):1–17.

149. Xies QW, Kashiwabara Y, Nathan C. Role of transcription factor NF-kappa B/Rel in induction of nitric oxide synthase. *Journal of Biological Chemistry*. 1994;269(7):4705–8.

150. Catz SD, Johnson JL. Transcriptional regulation of bcl-2 by nuclear factor kappa B and its significance in prostate cancer. *Oncogene*. 2001;20(50):7342–51.

151. Tsujimoto Y. Role of Bcl-2 family proteins in apoptosis: Apoptosomes or mitochondria? *Genes to cells : devoted to molecular & cellular mechanisms*. 1998;3(11):697–707.

152. Ye Z, Petrof EO, Boone D, Claud EC, Sun J. Salmonella effector AvrA regulation of colonic epithelial cell inflammation by deubiquitination. *The American Journal of Pathology*. 2007;171(3):882–92.

153. Negrate GL, Faustin B, Welsh K, Loeffler M, Krajewska M, Hasegawa P, et al. Salmonella secreted factor L deubiquitinase of Salmonella typhimurium inhibits NF-kappaB, suppresses IkappaBalpha ubiquitination and modulates innate immune responses. *The Journal of Immunology*. 2008;180(7):5045–56.

154. Ramos-Marques E, Zambrano S, Tierrez A, Bianchi ME, Agresti A, Garcıa-del Portillo F. Single-cell analyses reveal an attenuated NF-κB response in the Salmonella-infected fibroblast. *Virulence*. 2017;8(6):719.

155. Khweek AA, Kanneganti A, Guttridge DCD, Amer AO. The Sphingosine-1-Phosphate Lyase (LegS2) contributes to the restriction of Legionella pneumophila in murine macrophages. *PLoS One*. 2016;11(1):e0146410.

156. Ge J, Xu H, Li T, Zhou Y, Zhang Z, Li S, et al. A Legionella type IV effector activates the NF-kappaB pathway by phosphorylating the IkappaB family of inhibitors. *Proceedings of the National Academy of Sciences of the United States of America*. 2009;106(33):13725–30.

157. Bartfeld S, Engels C, Bauer B, Aurass P, Flieger A, Brüggemann H, et al. Temporal resolution of two-tracked NF-κB activation by Legionella pneumophila. *Cellular Microbiology*. 2009;11(11):1638–51.

158. Molestina RE, Sinai AP. Host and parasite-derived IKK activities direct distinct temporal phases of NF-κB activation and target gene expression following Toxoplasma gondii infection. *Journal of Cell Science*. 2005;118(24):5785–96.

159. Molestina RE, Sinai AP. Detection of a novel parasite kinase activity at the Toxoplasma gondii parasitophorous vacuole membrane capable of phosphorylating host IkappaBalpha. *Cellular Microbiology*. 2005;7(3):351–62.

160. Zhai W, Wu F, Zhang Y, Fu Y, Liu Z. The immune escape mechanisms of mycobacterium tuberculosis. *International Journal of Molecular Sciences,* 2019;20(2).

161. Awuh JA, Haug M, Mildenberger J, Marstad A, Ngoc Do CP, Louet C, et al. Keap1 regulates inflammatory signaling in Mycobacterium avium-infected human macrophages. *Proceedings of the National Academy of Sciences of the United States of America*. 2015;112(31):E4272–80.

162. Carneiro LAM, Travassos LH, Soares F, Tattoli I, Magalhaes JG, Bozza MT, et al. Shigella induces mitochondrial dysfunction and cell death in nonmyleoid cells. *Cell Host and Microbe*. 2009;5(2):123–36.

163. Shoham S, Huang C, Chen JM, Golenbock DT, Levitz SM. Toll-like receptor 4 mediates intracellular signaling without TNF-alpha release in response to Cryptococcus neoformans polysaccharide capsule. *The Journal of Immunology*. 2001;166(7):4620–6.

164. Piccioni M, Monari C, Kenno S, Pericolini E, Gabrielli E, Pietrella D, et al. A purified capsular polysaccharide markedly inhibits inflammatory response during endotoxic shock. *Infection and Immunity*. 2013;81(1):90.

165. Monari C, Kozel TR, Paganelli F, Pericolini E, Perito S, Bistoni F, et al. Microbial immune suppression mediated by direct engagement of inhibitory Fc receptor. *The Journal of Immunology*. 2006;177(10):6842–51.

166. Monari C, Bistoni F, Casadevall A, Pericolini E, Pietrella D, Kozel TR, et al. Glucuronoxylomannan, a microbial compound, regulates expression of costimulatory molecules and production of cytokines in macrophages. *Journal of Infectious Diseases*. 2005;191(1):127–37.

167. Hayes JB, Sircy LM, Heusinkveld LE, Ding W, Leander RN, McClelland EE, et al. Modulation of macrophage inflammatory nuclear factor κB (NF-κB) signaling by intracellular Cryptococcus neoformans. *Journal of Biological Chemistry*. 2016;291(30):15614–27.

168. Jahnke A, P. Johnson J. Synergistic activation of intercellular adhesion molecule 1 (ICAM-1) by TNF-α and IFN-γ is mediated by p65/p50 and p65/c-Rel and interferon-responsive factor Statlα (p91) that can be activated by both IFN-γ and IFN-α. *FEBS Letters*. 1994;354(2):220–6.

169. Ohmori Y, Hamilton TA. The interferon-stimulated response element and a kappa B site mediate synergistic induction of murine IP-10 gene transcription by IFN-gamma and TNF-alpha. *The Journal of Immunology*. 1995;154(10).

170. Pine R. Convergence of TNFα and IFNγ signalling pathways through synergistic induction of IRF-1/ISGF-2 is mediated by a composite GAS/κB promoter element. *Nucleic Acids Research*. 1997;25(21):4346–54.

171. Ohmori Y, Schreiber RD, Hamilton TA. Synergy between interferon-γ and tumor necrosis factor-α in transcriptional activation is mediated by cooperation between signal transducer and activator of transcription 1 and nuclear factor κB. *Journal of Biological Chemistry*. 1997 Jun 6;272(23):14899–907.

172. Farlik M, Reutterer B, Schindler C, Greten F, Vogl C, Müller M, et al. Nonconventional initiation complex assembly by STAT and NF-kappaB transcription factors regulates nitric oxide synthase expression. *Immunity*. 2010;33(1):25–34.

173. Hiroi M, Ohmori Y. Transcriptional synergism between NF-κB and STAT1. *Journal of Oral Biosciences*. 2005 Jan 1;47(3):230–42.

174. Hiroi M, Ohmori Y. The transcriptional coactivator CREB-binding protein cooperates with STAT1 and NF-kappa B for synergistic transcriptional activation of the CXC ligand 9/monokine induced by interferon-gamma gene. *The Journal of Biological Chemistry*. 2003;278(1):651–60.

175. Wang T, Liu H, Lian G, Zhang SY, Wang X, Jiang C. HIF1 α-induced glycolysis metabolism is essential to the activation of inflammatory macrophages. *Mediators in Inflammation*. 2017.

176. Nizet V, Johnson RS. Interdependence of hypoxic and innate immune responses. *Nature Reviews Immunology*. 2009;9(9):609–17.

177. Peyssonnaux C, Datta V, Cramer T, Doedens A, Theodorakis EA, Gallo RL, et al. HIF-1alpha expression regulates the bactericidal capacity of phagocytes. *The Journal of Clinical Investigation*. 2005;115(7):1806–15.

178. Gopal R, Lee B, McHugh KJ, Rich HE, Ramanan K, Mandalapu S, et al. STAT2 signaling regulates macrophage phenotype during influenza and bacterial super-infection. *Frontiers in Immunology*. 2018;9:2151.

179. Liu G, Park YJ, Tsuruta Y, Lorne E, Abraham E. p53 attenuates lipopolysaccharide-induced NF-kappaB activation and acute lung injury. *The Journal of Immunology*. 2009;182(8):5063–71.

180. Komarova EA, Krivokrysenko V, Wang K, Neznanov N, Chernov M v., Komarov PG, et al. p53 is a suppressor of inflammatory response in mice. *FASEB Journal : Official Publication of the Federation of American Societies for Experimental Biology*. 2005;19(8):1030–2.

181. Li L, Ng DSW, Mah WC, Almeida FF, Rahmat SA, Rao VK, et al. A unique role for p53 in the regulation of M2 macrophage polarization. *Cell Death and Differentiation*. 2014;22(7):1081–93.

182. Freedman SJ, Sun ZYJ, Kung AL, France DS, Wagner G, Eck MJ. Structural basis for negative regulation of hypoxia-inducible factor-1alpha by CITED2. *Nature Structural Biology*. 2003;10(7):504–12.

183. Lambert PF, Kashanchi F, Radonovich MF, Shiekhattar R, Brady JN. Phosphorylation of p53 serine 15 increases interaction with CBP. *The Journal of Biological Chemistry*. 1998;273(49):33048–53.

184. Gerritsen ME, Williams AJ, Neish AS, Moore S, Shi Y, Collins T. CREB-binding protein/p300 are transcriptional coactivators of p65. *Proceedings of the National Academy of Sciences of the United States of America*. 1997;94(7):2927–32.

185. Gu W, Roeder RG. Activation of p53 sequence-specific DNA binding by acetylation of the p53 C-terminal domain. *Cell*. 1997;90(4):595–606.

186. Bragança J, Swingler T, Marques FIR, Jones T, Eloranta JJ, Hurst HC, et al. Human CREB-binding protein/p300-interacting transactivator with ED-rich Tail (CITED) 4, a new member of the CITED Family, functions as a co-activator for transcription factor AP-2 *. *Journal of Biological Chemistry*. 2002;277(10):8559–65.

187. Andrews JE, O'Neill MJ, Binder M, Shioda T, Sinclair AH. Isolation and expression of a novel member of the CITED family. *Mechanisms of Development* 2000;95(1–2):305–8.

188. Yahata T, Takedatsu H, Dunwoodie SL, Bragança J, Swingler T, Withington SL, et al. Cloning of mouse cited4, a member of the CITED family p300/CBP-binding transcriptional coactivators: Induced expression in mammary epithelial cells. *Genomics*. 2002;80(6):601–13.

189. Shioda T, Fenner MH, Isselbacher KJ. msg1, a novel melanocyte-specific gene, encodes a nuclear protein and is associated with pigmentation. *Proceedings of the National Academy of Sciences of the United States of America*. 1996;93(22):12298.

190. Gnanapackiam S, Devakanmalai HE, Zumrut E˘, Rul M. Cited3 activates Mef2c to control muscle cell differentiation and survival. *Biology Open*. 2:505–14.

191. Boyle S, Misfeldt A, Chandler KJ, Deal KK, Southard-Smith EM, Mortlock DP, et al. Fate mapping using Cited1-CreERT2 mice demonstrates that the cap mesenchyme contains self-renewing progenitor cells and gives rise exclusively to nephronic epithelia. *Developmental Biology*. 2008;313(1):234–45.

192. Yahata T, de Caestecker MP, Lechleider RJ, Andriole S, Roberts AB, Isselbacher KJ, et al. The MSG1 Non-DNA-binding Transactivator Binds to the p300/CBP Coactivators, Enhancing Their Functional Link to the Smad Transcription Factors *. *Journal of Biological Chemistry*. 2000;275(12):8825–34.

193. Qu X, Lam E, Doughman YQ, Chen Y, Chou YT, Lam M, et al. Cited2, a coactivator of HNF4alpha, is essential for liver development. *The EMBO Journal*. 2007;26(21):4445–56.

194. Chou YT, Yang YC. Post-transcriptional control of Cited2 by transforming growth factor beta. Regulation via Smads and Cited2 coding region. *The Journal of Biological Chemistry*. 2006;281(27):18451–62.

195. Glenn DJ, Maurer RA. MRG1 binds to the LIM domain of Lhx2 and may function as a coactivator to stimulate glycoprotein hormone α-subunit gene expression. *Journal of Biological Chemistry*. 1999 Dec 17;274(51):36159–67.

196. Bhattacharya S, Michels CL, Leung MK, Arany ZP, Kung AL, Livingston DM. Functional role of p35srj, a novel p300/CBP binding protein, during transactivation by HIF-1. *Genes & Development*. 1999;13(1):64.

197. Kim GD, Das R, Rao X, Zhong J, Deiuliis JA, Ramirez-Bergeron DL, et al. CITED2 restrains proinflammatory macrophage activation and response. *Molecular and Cellular Biology*. 2018;38(5).

198. Pong Ng H, Kim GD, Ricky Chan E, Dunwoodie SL, Mahabeleshwar GH. CITED2 limits pathogenic inflammatory gene programs in myeloid cells. *The FASEB Journal*. 2020;34(9):12100–13.

199. Tien ES, Davis JW, vanden Heuvel JP. Identification of the CREB-binding protein/p300-interacting protein CITED2 as a peroxisome proliferator-activated receptor alpha coregulator. *The Journal of Biological Chemistry*. 2004;279(23):24053–63.

200. Berlow RB, Dyson HJ, Wright PE. Hypersensitive termination of the hypoxic response by a disordered protein switch. *Nature*. 2017;543(7645):447–51.

201. Wojciak JM, Martinez-Yamout MA, Dyson HJ, Wright PE. Structural basis for recruitment of CBP/p300 coactivators by STAT1 and STAT2 transactivation domains. *The EMBO Journal*. 2009;28(7):948.

202. Lou X, Sun S, Chen W, Zhou Y, Huang Y, Liu X, et al. Negative feedback regulation of NF-κB action by CITED2 in the nucleus. *The Journal of Immunology*. 2011;186(1):539–48.

203. Zafar A, Pong Ng H, Diamond-Zaluski R, Kim GD, Ricky Chan E, Dunwoodie SL, et al. CITED2 inhibits STAT1-IRF1 signaling and atherogenesis. *FASEB Journal: Official Publication of the Federation of American Societies for Experimental Biology*. 2021;35(9).

204. Dunwoodie SL, Rodriguez TA, Beddington RSP. Msg1 and Mrg1, founding members of a gene family, show distinct patterns of gene expression during mouse embryogenesis. *Mechanisms of Development*. 1998;72(1–2):27–40.

205. Novitskaya T, Baserga M, de Caestecker MP. Organ-specific defects in insulin-like growth factor and insulin receptor signaling in late gestational asymmetric intrauterine growth restriction in Cited1 mutant mice. *Endocrinology*. 2011;152(6):2503.

206. Plisov S, Tsang M, Shi G, Boyle S, Yoshino K, Dunwoodie SL, et al. Cited1 is a bifunctional transcriptional cofactor that regulates early nephronic patterning. *Journal of the American Society of Nephrology*. 2005;16(6):1632–44.

207. Shi G, Boyle SC, Sparrow DB, Dunwoodie SL, Shioda T, de Caestecker MP. The Transcriptional Activity of CITED1 Is Regulated by Phosphorylation in a Cell Cycle-dependent Manner *. *Journal of Biological Chemistry*. 2006;281(37):27426–35.

208. Yahata T, Shao W, Endoh H, Hur J, Coser KR, Sun H, et al. Selective coactivation of estrogen-dependent transcription by CITED1 CBP/p300-binding protein. *Genes & Development*. 2001;15(19):2598–612.

209. Prasad ML, Pellegata NS, Kloos RT, Barbacioru C, Huang Y, de La Chapelle A. CITED1 protein expression suggests Papillary Thyroid Carcinoma in high throughput tissue microarray-based study. *Thyroid: Official Journal of the American Thyroid Association*. 2004;14(3):169–75.

210. Prasad ML, Pellegata NS, Huang Y, Nagaraja HN, de La Chapelle A, Kloos RT. Galectin-3, fibronectin-1, CITED-1, HBME1 and cytokeratin-19 immunohistochemistry is useful for the differential diagnosis of thyroid tumors. *Modern Pathology : An Official Journal of the United States and Canadian Academy of Pathology, Inc*. 2005;18(1):48–57.

211. Li H, Ahmed NU, Fenner MH, Ueda M, Isselbacher KJ, Shioda T. Regulation of expression of MSG1 melanocyte-specific nuclear protein in human melanocytes and melanoma cells. *Experimental Cell Research*. 1998;242(2):478–86.

212. Sedghizadeh PP, WJD, ACM, & PML. MSG-1 expression in benign and malignant melanocytic lesions of cutaneous and mucosal epithelium. *Medical Science Monitor: International Medical Journal of Experimental and Clinical Research*. 2005;11(7):189–94.

213. Lovvorn HN, Westrup J, Opperman S, Boyle S, Shi G, Anderson J, et al. CITED1 expression in wilms' tumor and embryonic kidney. *Neoplasia*. 2007;9(7):589.

214. Wang Y, Huang H, Hu F, Li J, Zhang L, Pang H. CITED1 contributes to the progression of papillary thyroid carcinoma via the Wnt/β-catenin signaling pathway. *Oncotargets and Therapy*. 2019;12:6769.

215. Pai SG, Carneiro BA, Mota JM, Costa R, Leite CA, Barroso-Sousa R, et al. Wnt/beta-catenin pathway: modulating anticancer immune response. *Journal of Hematology & Oncology*. 2017;10(1).

216. Shioda T, Lechleider RJ, Dunwoodie SL, Li H, Yahata T, de Caestecker MP, et al. Transcriptional activating activity of Smad4: roles of SMAD hetero-oligomerization and enhancement by an associating transactivator. *Proceedings of the National Academy of Sciences of the United States of America*. 1998;95(17):9785–90.

217. Shi G, Boyle SC, Sparrow DB, Dunwoodie SL, Shioda T, de Caestecker MP. The transcriptional activity of CITED1 is regulated by phosphorylation in a cell cycle-dependent manner. *The Journal of Biological Chemistry*. 2006;281(37):27426–35.

218. Wang N, Liang H, Zen K. Molecular mechanisms that influence the macrophage M1-M2 polarization balance. *Frontiers in Immunology*. 2014;5:614.

219. Merchant N, Lyons E, Goff S, Vaughn M, Ware D, Micklos D, et al. The iPlant collaborative: cyber infrastructure for enabling data to discovery for the life sciences. PLoS Biology. 2016;14(1):e1002342.

220. Babraham Bioinformatics - FastQC A quality control tool for high throughput sequence Data. https://www.bioinformatics.babraham.ac.uk/projects/fastqc/

221. Dobin A, Davis CA, Schlesinger F, Drenkow J, Zaleski C, Jha S, et al. STAR: Ultrafast universal RNA-seq aligner. Bioinformatics. 2013 Jan;29(1):15–21.

222. Gruening BA. galaxytools: July 2016 release (Version 07.2016). Zenodo. 2016;

223. Liao Y, Smyth GK, Shi W. featureCounts: an efficient general purpose program for assigning sequence reads to genomic features. *Bioinformatics*. 2014;30(7):923–30.

224. Afgan E, Baker D, van den Beek M, Blankenberg D, Bouvier D, Čech M, et al. The Galaxy platform for accessible, reproducible and collaborative biomedical analyses: 2016 update. *Nucleic Acids Research*. 2016;44(W1):W3–10.

225. Robinson MD, McCarthy DJ, Smyth GK. edgeR: a Bioconductor package for differential expression analysis of digital gene expression data. *Bioinformatics*. 2010;26(1):139–40.

226. Pertea M, Pertea GM, Antonescu CM, Chang TC, Mendell JT, Salzberg SL. StringTie enables improved reconstruction of a transcriptome from RNA-seq reads. *Nature Biotechnology*. 2015;33(3):290–5.

227. Trapnell C, Hendrickson DG, Sauvageau M, Goff L, Rinn JL, Pachter L. Differential analysis of gene regulation at transcript resolution with RNA-seq. *Nature Biotechnology* 2012;31(1):46–53.

228. Huang DW, Sherman BT, Lempicki RA. Systematic and integrative analysis of large gene lists using DAVID bioinformatics resources. *Nature Protocols*. 2009;4(1):44–57.

229. Szklarczyk D, Gable AL, Lyon D, Junge A, Wyder S, Huerta-Cepas J, et al. STRING v11: protein–protein association networks with increased coverage, supporting functional discovery in genome-wide experimental datasets. *Nucleic Acids Research*. 2019;47(D1):D607–13.

230. Mitterstiller AM, Haschka D, Dichtl S, Nairz M, Demetz E, Talasz H, et al. Heme oxygenase 1 controls early innate immune response of macrophages to Salmonella Typhimurium infection. *Cellular Microbiology*. 2016;18(10):1374–89.

231. Gobert AP, Verriere T, Asim M, Barry DP, Piazuelo MB, Sablet T de, et al. Heme oxygenase-1 dysregulates macrophage polarization and the immune response to Helicobacter pylori. *The Journal of Immunology*. 2014;193(6):3013–22.

232. Srikumar S, Kröger C, Hébrard M, Colgan A, Owen S v., Sivasankaran SK, et al. RNA-seq brings new insights to the intra-macrophage transcriptome of Salmonella Typhimurium. *PLoS Pathogens*. 2015;11(11):e1005262.

233. Coelho C, Oliveira Souza AC, da Silveira Derengowski L, de Leon-Rodriguez C, Wang B, Leon-Rivera R, et al. Macrophage mitochondrial and stress response to ingestion of Cryptococcus neoformans. *The Journal of Immunology*. 2015;199(5):1944–1944.

234. Mitterstiller AM, Haschka D, Dichtl S, Nairz M, Demetz E, Talasz H, et al. Heme oxygenase 1 controls early innate immune response of macrophages to Salmonella Typhimurium infection. *Cellular Microbiology*. 2016;18(10):1374–89.

235. Rosenberger CM, Scott MG, Gold MR, Hancock REW, Finlay BB. Salmonella typhimurium infection and lipopolysaccharide stimulation induce similar changes in macrophage gene expression. *The Journal of Immunology*. 2000;164(11):5894–904.

236. Nagabhushanam V, Solache A, Ting LM, Escaron CJ, Zhang JY, Ernst JD. Innate inhibition of adaptive immunity: mycobacterium tuberculosis-induced IL-6 inhibits macrophage responses to IFN-γ. *The Journal of Immunology*. 2003;171(9):4750–7.

237. Bolanos B, Mitchell TG. Phagocytosis and killing of Cryptococcus neoformans by rat alveolar macrophages in the absence of serum. *Journal of Leukocyte Biology*. 1989;46(6):521–8.

238. Levitz SM, DiBenedetto DJ. Paradoxical role of capsule in murine bronchoalveolar macrophage-mediated killing of Cryptococcus neoformans. *The Journal of Immunology*. 1989;142(2):659–65.

239. Kozel TR, Gotschlich EC. The capsule of cryptococcus neoformans passively inhibits phagocytosis of the yeast by macrophages. *The Journal of Immunology*. 1982;129(4).

240. Mukherjee, S., Feldmesser, M., & Casadevall A. J774 murine macrophage-like cell interactions with Cryptococcus neoformans in the presence and absence of opsonins. *Journal of Infectious Diseases*. 1996;173(5):1222–31.

241. S M, S L, J M, MD S, A C. Monoclonal antibodies to Cryptococcus neoformans capsular polysaccharide modify the course of intravenous infection in mice. *Infection and Immunity*. 1994;62(3):1079–88.

242. Mukherjee S, Lee SC, Casadevall A. Antibodies to Cryptococcus neoformans glucuronoxylomannan enhance antifungal activity of murine macrophages. *Infection and Immunity*. 1995;63(2):573.

243. Dromer F., Charreire J., Contrepois A., Carbon C. YP. Protection of mice against experimental cryptococcosis by anti-Cryptococcus neoformans monoclonal antibody. *Infection and Immunity*. 1987;55(3):749–52.

244. Casadevall A, Cleare W, Feldmesser M, Glatman-Freedman A, Goldman DL, Kozel TR, et al. Characterization of a murine monoclonal antibody to Cryptococcus neoformans polysaccharide that is a candidate for human therapeutic studies. *Antimicrobial Agents and Chemotherapy*. 1998 Jun;42(6):1437–46.

245. Nicola AM, Robertson EJ, Albuquerque P, Derengowski L da S, Casadevall A. nonlytic exocytosis of cryptococcus neoformans from macrophages occurs in vivo and is influenced by phagosomal pH. *mBio*. 2011;2(4).

246. Ma H, Croudace JE, Lammas DA, May RC. Expulsion of live pathogenic yeast by macrophages. *Current Biology*. 2006 Nov 7;16(21):2156–60.

247. Suh HW, Yun S, Song H, Jung H, Park YJ, Kim TD, et al. TXNIP interacts with hEcd to increase p53 stability and activity. *Biochemical and Biophysical Research Communications*. 2013;438(2):264–9.

248. Sheldon KE, Shandilya H, Kepka-Lenhart D, Poljakovic M, Ghosh A, Morris SM. Shaping the murine macrophage phenotype: IL-4 and cyclic AMP synergistically activate the arginase I promoter. *The Journal of Immunology*. 2013;191(5):2290–8.

249. Waldhart AN, Dykstra H, Peck AS, Boguslawski EA, Madaj ZB, Wen J, et al. Phosphorylation of TXNIP by AKT mediates acute influx of glucose in response to insulin. *Cell Reports*. 2017;19(10):2005.

250. Erdely A, Kepka-Lenhart D, Clark M, Zeidler-Erdely P, Poljakovic M, Calhoun WJ, et al. Inhibition of phosphodiesterase 4 amplifies cytokine-dependent induction of arginase in macrophages. *American Journal of Physiology Lung Cellular and Molecular Physiology*. 2006;290(3):L534-9

251. Park YJ, Yoon SJ, Suh HW, Kim DO, Park JR, Jung H, et al. TXNIP deficiency exacerbates endotoxic shock via the induction of excessive nitric oxide synthesis. *PLoS Pathogens*. 2013 Oct;9(10):e1003646.

252. Jung H, Kim MJ, Kim DO, Kim WS, Yoon SJ, Park YJ, et al. TXNIP maintains the hematopoietic cell pool by switching the function of p53 under oxidative stress. *Cell Metabolism*. 2013;18(1):75–85.

253. Calegari-Silva TC, Vivarini AC, Miqueline M, dos Santos GRRM, Teixeira KL, Saliba AM, et al. The human parasite Leishmania amazonensis downregulates iNOS expression via NF-κB p50/p50 homodimer: role of the PI3K/Akt pathway. *Open Biology*. 2015;5(9).

254. Nelson RH, Nelson DE. Signal Distortion: How intracellular pathogens alter host cell fate by modulating NF-κB dynamics. *Frontiers in Immunology*. 2018;9:2962.

255. Müller U, Stenzel W, Köhler G, Werner C, Polte T, Hansen G, et al. IL-13 induces disease-promoting type 2 cytokines, alternatively activated macrophages and allergic inflammation

during pulmonary infection of mice with Cryptococcus neoformans. *The Journal of Immunology*. 2007;179(8):5367–77.

256. Jain A v., Zhang Y, Fields WB, McNamara DA, Choe MY, Chen GH, et al. Th2 but not Th1 immune bias results in altered lung functions in a murine model of pulmonary Cryptococcus neoformans infection. *Infection and Immunity*. 2009;77(12):5389–99.

257. Milam JE, Herring-Palmer AC, Pandrangi R, McDonald RA, Huffnagle GB, Toews GB. Modulation of the pulmonary type 2 T-cell response to Cryptococcus neoformans by intratracheal delivery of a tumor necrosis factor alpha-expressing adenoviral vector. *Infection and Immunity*. 2007;75(10):4951–8.

258. Chen S, Yan H, Zhang L, Kong W, Sun Y, Zhang W, et al. Cryptococcus Neoformans Infection and Immune Cell Regulation in Human Monocytes. *Cellular Physiology and Biochemistry*. 2015 Aug 28;37(2):537–47.

259. Chen Y, Toffaletti DL, Tenor JL, Litvintseva AP, Fang C, Mitchell TG, et al. The Cryptococcus neoformans transcriptome at the site of human meningitis. *mBio*. 2014 Feb 4;5(1).

260. Monari C, Pericolini E, Bistoni G, Casadevall A, Kozel TR, Vecchiarelli A. Cryptococcus neoformans capsular glucuronoxylomannan induces expression of Fas ligand in macrophages. *The Journal of Immunology*. 2005;174(6):3461–8.

261. Fonseca FL, Nohara LL, Cordero RJB, Frases S, Casadevall A, Almeida IC, et al. Immunomodulatory effects of serotype B glucuronoxylomannan from Cryptococcus gattii correlate with polysaccharide diameter. *Infection and Immunity*. 2010;78(9):3861–70.

262. Zheng SJ, Lamhamedi-Cherradi SE, Wang P, Xu L, Chen YH. Tumor suppressor p53 inhibits autoimmune inflammation and macrophage function. *Diabetes*. 2005;54(5):1423–8.

263. Vazquez A, Bond EE, Levine AJ, Bond GL. The genetics of the p53 pathway, apoptosis and cancer therapy. *Nature Reviews Drug Discovery*. 2008;7(12):979–87.

264. Liu G, Park YJ, Tsuruta Y, Lorne E, Abraham E. p53 attenuates lipopolysaccharide-induced NF-κB activation and acute lung injury. *The Journal of Immunology*. 2009;182(8):5063–71.

265. Siegl C, Rudel T. Modulation of p53 during bacterial infections. *Nature Reviews Microbiology*. 2015;13(12):741–8.

266. Zong WX, Edelstein LC, Chen C, Bash J, Gélinas C. The prosurvival Bcl-2 homolog Bfl-1/A1 is a direct transcriptional target of NF-kappaB that blocks TNFalpha-induced apoptosis. *Genes and Development*. 1999;13(4):382–7.

267. Li L, Ng DSW, Mah WC, Almeida FF, Rahmat SA, Rao VK, et al. A unique role for p53 in the regulation of M2 macrophage polarization. *Cell Death and Differentiation*. 2015;22(7):1081–93.

268. Xia Y, Liu N, Xie X, Bi G, Ba H, Li L, et al. The macrophage-specific V-ATPase subunit ATP6V0D2 restricts inflammasome activation and bacterial infection by facilitating autophagosome-lysosome fusion. *Autophagy*. 2019;15(6):960–75.

269. De Leon-Rodriguez CM, Rossi DCP, Fu MS, Dragotakes Q, Coelho C, Guerrero Ros I, et al. The outcome of the Cryptococcus neoformans– macrophage interaction depends on phagolysosomal membrane integrity. *The Journal of Immunology*. 2018;201(2):583–603.

270. Zong WX, Edelstein LC, Chen C, Bash J, Gélinas C. The prosurvival Bcl-2 homolog Bfl-1/A1 is a direct transcriptional target of NF-kappaB that blocks TNFalpha-induced apoptosis. *Genes and Development*. 1999 Feb 15;13(4):382-7.

271. Kathania M, Raje CI, Raje M, Dutta RK, Majumdar S. Bfl-1/A1 acts as a negative regulator of autophagy in mycobacteria infected macrophages. *The International Journal of Biochemistry & Cell Biology*. 2011;43(4):573–85.

272. Zhang L, Zhang K, Li H, Coelho C, de Souza Gonçalves D, Fu MS, et al. Cryptococcus neoformans-infected macrophages release proinflammatory extracellular vesicles: Insight into their components by multi-omics. *mBio*. 2021;12(2).

273. Lumbroso D, Soboh S, Maimon A, Schif-Zuck S, Ariel A, Burstyn-Cohen T. Macrophage-derived protein S facilitates apoptotic polymorphonuclear cell clearance by resolution phase macrophages and supports their reprogramming. *Frontiers in Immunology*. 2018:358.

274. McBryan J, Howlin J, Kenny PA, Shioda T, Martin F. ERα–CITED1 co-regulated genes expressed during pubertal mammary gland development: implications for breast cancer prognosis. *Oncogene*. 2007;26(44):6406–19.

275. Gordon S, Plüddemann A. Tissue macrophages: heterogeneity and functions. *BMC Biology*. 2017;15(1):1–18.

276. Takeuchi O, Akira S. Pattern recognition receptors and inflammation. *Cell*. 2010;140(6):805–20.

277. Murray PJ, Allen JE, Biswas SK, Fisher EA, Gilroy DW, Goerdt S, et al. Macrophage activation and polarization: nomenclature and experimental guidelines. *Immunity*. 2014;41(1):14–20.

278. Lawrence T, Natoli G. Transcriptional regulation of macrophage polarization: enabling diversity with identity. *Nature Reviews Immunology*. 2011;11(11):750–61.

279. Dorrington MG, Fraser IDC. NF-κB signaling in macrophages: Dynamics, crosstalk, and signal integration. *Frontiers in Immunology*. 2019;10:705.

280. Fitzgerald KA, Kagan JC. Toll-like receptors and the control of immunity. *Cell*. 2020;180(6):1044–66.

281. Michalska A, Blaszczyk K, Wesoly J, Bluyssen HAR. A positive feedback amplifier circuit that regulates interferon (IFN)-stimulated gene expression and controls type I and type II IFN responses. *Frontiers in Immunology*. 2018;9:28.

282. Kröger A, Köster M, Schroeder K, Hauser H, Mueller PP. Activities of IRF-1. *The Official Journal of the International Society for Interferon and Cytokine Research*. 2002;22(1):5–14.

283. Chatterjee-Kishore M, Kishore R, Hicklin DJ, Marincola FM, Ferrone S. Different requirements for signal transducer and activator of transcription 1alpha and interferon regulatory factor 1 in the regulation of low molecular mass polypeptide 2 and transporter associated with antigen processing 1 gene expression. *The Journal of Biological Chemistry*. 1998;273(26):16177–83.

284. Wong LH, Sim H, Chatterjee-Kishore M, Hatzinisiriou I, Devenish RJ, Stark G, et al. Isolation and characterization of a human STAT1 gene regulatory element: inducibility by interferon (IFN)

types I and II and role of IFN regulatory factor-1. *Journal of Biological Chemistry*. 2002;277(22):19408–17.

285. Shuai K, Liu B. Regulation of JAK–STAT signalling in the immune system. *Nature Reviews Immunology*. 2003;3(11):900–11.

286. Murray PJ, Smale ST. Restraint of inflammatory signaling by interdependent strata of negative regulatory pathways. *Nature Immunology*. 2012;13(10):916–24.

287. Yoshimura A, Naka T, Kubo M. SOCS proteins, cytokine signalling and immune regulation. *Nature Reviews Immunology*. 2007;7(6):454–65.

288. Liau NPD, Laktyushin A, Lucet IS, Murphy JM, Yao S, Whitlock E, et al. The molecular basis of JAK/STAT inhibition by SOCS1. *Nature Communications*. 2018;9(1):1–14.

289. Wilson HM. SOCS proteins in macrophage polarization and function. *Frontiers in Immunology*. 2014;5:357.

290. Leung MK, Jones T, Michels CL, Livingston DM, Bhattacharya S. Molecular cloning and chromosomal localization of the human CITED2 gene encoding p35srj/Mrg1. *Genomics*. 1999;61(3):307–13.

291. Aguirre KM, Gibson GW. Differing requirement for inducible nitric oxide synthase activity in clearance of primary and secondary Cryptococcus neoformans infection. *Medical Mycology*. 2000;38(5):343–53.

292. Du J, Yang YC. Cited2 in hematopoietic stem cell function. *Current Opinion in Hematology*. 2013;20(4):301–7.

293. Lonsdale J, Thomas J, Salvatore M, Phillips R, Lo E, Shad S, et al. The Genotype-Tissue Expression (GTEx) project. *Nature Genetics*. 2013;45(6):580–5.

294. Boyle S, Shioda T, Perantoni AO, de Caestecker M. Cited1 and Cited2 are differentially expressed in the developing kidney but are not required for nephrogenesis. *Developmental Dynamics*. 2007;236(8):2321–30.

295. Meraz MA, White JM, Sheehan KCF, Bach EA, Rodig SJ, Dighe AS, et al. Targeted Disruption of the Stat1 Gene in Mice Reveals Unexpected Physiologic Specificity in the JAK–STAT Signaling Pathway. *Cell*. 1996;84(3):431–42.

296. Dreos R, Ambrosini G, Périer RC, Bucher P. The Eukaryotic Promoter Database: expansion of EPDnew and new promoter analysis tools. *Nucleic Acids Research*. 2015;43:D92–6.

297. Dreos R, Ambrosini G, Groux R, Perier RC, Bucher P. The eukaryotic promoter database in its 30th year: focus on non-vertebrate organisms. *Nucleic Acids Research*. 2017;45(D1):D51–5.

298. Meerbrey KL, Hu G, Kessler JD, Roarty K, Li MZ, Fang JE, et al. The pINDUCER lentiviral toolkit for inducible RNA interference in vitro and in vivo. *Proceedings of the National Academy of Sciences of the United States of America*. 2011;108(9):3665–70.

299. Zhang JJ, Vinkemeier U, Gu W, Chakravarti D, Horvath CM, Darnell JE. Two contact regions between Stat1 and CBP/p300 in interferon gamma signaling. *Proceedings of the National Academy of Sciences of the United States of America.* 1996;93(26):15092–6.

300. Subramanian A, Tamayo P, Mootha VK, Mukherjee S, Ebert BL, Gillette MA, et al. Gene set enrichment analysis: A knowledge-based approach for interpreting genome-wide expression profiles. *Proceedings of the National Academy of Sciences of the United States of America*. 2005;102(43):15545–50.

301. Testoni B, Völlenkle C, Guerrieri F, Gerbal-Chaloin S, Blandino G, Levrero M. Chromatin dynamics of gene activation and repression in response to interferon alpha (IFN(alpha)) reveal new roles for phosphorylated and unphosphorylated forms of the transcription factor STAT2. *The Journal of Biological Chemistry*. 2011;286(23):20217–27.

302. Bluyssen HAR, Vlietstra RJ, Faber PW, Smit EME, Hagemeijer A, Trapman J. Structure, chromosome localization, and regulation of expression of the interferon-regulated mouse Ifi54/Ifi56 gene family. *Genomics*. 1994;24(1):137–48.

303. Ronni T, Matikainen S, Lehtonen A, Palvimo J, Dellis J, van Eylen F, et al. The proximal interferon-stimulated response elements are essential for interferon responsiveness: a promoter analysis

of the antiviral MxA gene. *Journal of Interferon & Cytokine Research: The Official Journal of the International Society for Interferon and Cytokine Research*. 1998;18(9):773–81.

304. Ohtomo T, Sugamata Y, Ozaki Y, Ono K, Yoshimura Y, Kawai S, et al. Molecular cloning and characterization of a surface antigen preferentially overexpressed on multiple myeloma cells. *Biochemical and Biophysical Research Communications*. 1999;258(3):583–91.

305. Yan R, Qureshi S, Zhong Z, Wen Z, Darnell JE. The genomic structure of the STAT genes: multiple exons in coincident sites in Stat1 and Stat2. *Nucleic Acids Research*. 1995;23(3):459.

306. Semper C, Leitner NR, Lassnig C, Parrini M, Mahlakõiv T, Rammerstorfer M, et al. STAT1β is not dominant negative and is capable of contributing to gamma interferon-dependent innate immunity. *Molecular and Cellular Biology*. 2014;34(12):2235.

307. Howlin J, McBryan J, Napoletano S, Lambe T, McArdle E, Shioda T, et al. CITED1 homozygous null mice display aberrant pubertal mammary ductal morphogenesis. *Oncogene*. 2005;25(10):1532–42.

308. Lin Z, Feng R, Li J, Meng Y, Yuan L, Fu Z, et al. Nuclear translocation of CBP/p300-interacting protein CITED1 induced by parathyroid hormone requires serine phosphorylation at position 79 in its 63–84 domain. *Cellular Signaling*. 2014;26(11):2436–45.

309. Yang D, Guo J, Divieti P, Shioda T, Bringhurst FR. CBP/p300-interacting protein CITED1 modulates parathyroid hormone regulation of osteoblastic differentiation. *Endocrinology.* 2008;149(4):1728–35.

310. Waltermann A, Kartasheva NN, Dobbelstein M. Differential regulation of p63 and p73 expression. *Oncogene*. 2003;22(36):5686–93.

311. Grob TJ, Novak U, Maisse C, Barcaroli D, Lüthi AU, Pirnia F, et al. Human delta Np73 regulates a dominant negative feedback loop for TAp73 and p53. *Cell Death and Differentiation*. 2001;8(12):1213–23.

312. Mangan S, Alon U. Structure and function of the feed-forward loop network motif. *Proceedings of the National Academy of Sciences of the United States of America*. 2003;100(21):11980–5.

313. Guinn ZP, Petro TM. Interferon regulatory factor 3 plays a role in macrophage responses to interferon-γ. *Immunobiology*. 2019;224(4):565–74.

314. Zhu J, McKeon F. Nucleocytoplasmic shuttling and the control of NF-AT signaling. *Cellular and Molecular Life Sciences*. 2000;57(3):411–20.

315. Picard D, Kumar V, Chambon P, Yamamoto KR. Signal transduction by steroid hormones: nuclear localization is differentially regulated in estrogen and glucocorticoid receptors. *Cell Regulation*. 1990;1(3):291.

316. Decker T, Kovarik P. Serine phosphorylation of STATs. *Oncogene*. 2000;19(21):2628–37.

317. Karin M, Delhase M. The I kappa B kinase (IKK) and NF-kappa B: key elements of proinflammatory signalling. *Seminars in Immunology*. 2000;12(1):85–98.

318. Ruff VA, Leach KL. Direct demonstration of NFATp dephosphorylation and nuclear localization in activated HT-2 cells using a specific NFATp polyclonal antibody. *The Journal of Biological Chemistry*. 1995;270(38):22602–7.

319. Nelson DE, Ihekwaba AEC, Elliott M, Johnson JR, Gibney CA, Foreman BE, et al. Oscillations in NF-κB signaling control the dynamics of gene expression. *Science*. 2004;306(5696):704–8.

320. Ruytinx P, Proost P, van Damme J, Struyf S. Chemokine-induced macrophage polarization in inflammatory conditions. *Frontiers in Immunology*. 2018;9:1930.

321. Mantovani A, Sica A, Sozzani S, Allavena P, Vecchi A, Locati M. The chemokine system in diverse forms of macrophage activation and polarization. *Trends in Immunology*. 2004;25(12):677–86.

322. Baldanta S, Fernández-Escobar M, Acín-Perez R, Albert M, Camafeita E, Jorge I, et al. ISG15 governs mitochondrial function in macrophages following vaccinia virus infection. *PLoS Pathogens*. 2017;13(10):e1006651.

323. Schoggins JW, Rice CM. Interferon-stimulated genes and their antiviral effector functions. *Current Opinions in Virology*. 2011;1(6):519–25.

324. Fensterl V, Sen GC. Interferon-Induced Ifit Proteins: Their role in viral pathogenesis. The *Journal of Virology*. 2015;89(5):2462.

325. Brown GD, Denning DW, Gow NAR, Levitz SM, Netea MG, White TC. Hidden killers: human fungal infections. *Science Translational Medicine*. 2012;4(165).

326. Spadari C de C, Wirth F, Lopes LB, Ishida K. New approaches for cryptococcosis treatment. *Microorganisms*. 2020;8(4).

327. Perfect JR, Dismukes WE, Dromer F, Goldman DL, Graybill JR, Hamill RJ, et al. Clinical practice guidelines for the management of cryptococcal disease: 2010 update by the infectious diseases society of america. *Clinical Infectious Diseases : An Official Publication of the Infectious Diseases Society of America*. 2010;50(3):291–322.

328. Mansour MK, Reedy JL, Tam JM, Vyas JM. Macrophage-Cryptococcus interactions: An update. *Current Fungal Infection Reports*. 2014;8(1):109–15.

329. Osterholzer JJ, Milam JE, Chen GH, Toews GB, Huffnagle GB, Olszewski MA. Role of dendritic cells and alveolar macrophages in regulating early host defense against pulmonary infection with Cryptococcus neoformans. *Infection and Immunity*. 2009;77(9):3749–55.

330. Monga DP. Role of macrophages in resistance of mice to experimental cryptococcosis. *Infection and Immunity*. 1981;32(3):975–8.

331. Derengowski L da S, Paes HC, Albuquerque P, Tavares AHFP, Fernandes L, Silva-Pereira I, et al. The transcriptional response of Cryptococcus neoformans to ingestion by Acanthamoeba castellanii and macrophages provides insights into the evolutionary adaptation to the mammalian host. *Eukaryotic Cell.* 2013;12(5):761–74.

332. Meerbrey KL, Hu G, Kessler JD, Roarty K, Li MZ, Fang JE, et al. The pINDUCER lentiviral toolkit for inducible RNA interference in vitro and in vivo. *Proceedings of the National Academy of Sciences of the United States of America*. 2011;108(9):3665–70.

333. Boeck J de, Verfaillie C. Doxycycline inducible overexpression systems: How to induce your gene of interest without inducing misinterpretations. *Molecular Biology of the Cell*. 2021;32(17):1517–22.

334. Moullan N, Mouchiroud L, Wang X, Ryu D, Williams EG, Mottis A, et al. Tetracyclines Disturb Mitochondrial Function across Eukaryotic Models: A Call for Caution in Biomedical Research. *Cell Reports*. 2015;10(10):1681–91.

335. Sauer B, Luger A, Lorenz NI, Engel AL, Braun Y, Voss M, et al. P04.50 Doxycycline impairs mitochondrial function and protects human glioma cells from hypoxia-induced cell death: implications of using Tet-inducible systems. *Neuro-Oncology*. 2018;20(Suppl 3):iii290.

336. Ahler E, Sullivan WJ, Cass A, Braas D, York AG, Bensinger SJ, et al. Doxycycline Alters Metabolism and Proliferation of Human Cell Lines. *PLoS One*. 2013;8(5):e64561.

337. Greengo SD, 0000-0002-8912-7782. Host-microbe interactions between Cryptococcus neoformans and Phagocytes. 2022

338. Thiriot JD, Martinez-Martinez YB, Endsley JJ, Torres AG. Hacking the host: exploitation of macrophage polarization by intracellular bacterial pathogens. *Pathogens and Diseases*. 2020;78(1).

339. Hansakon A, Mutthakalin P, Ngamskulrungroj P, Chayakulkeeree M, Angkasekwinai P. Cryptococcus neoformans and Cryptococcus gattii clinical isolates from Thailand display diverse phenotypic interactions with macrophages. *Virulence*. 2019;10(1):26–36.

340. Heung LJ, Hohl TM. Inflammatory monocytes are detrimental to the host immune response during acute infection with Cryptococcus neoformans. *PLoS Pathogens*. 2019;15(3):e1007627.

341. Leopold Wager CM, Hole CR, Campuzano A, Castro-Lopez N, Cai H, Caballero Van Dyke MC, et al. IFN-γ immune priming of macrophages in vivo induces prolonged STAT1 binding and protection against Cryptococcus neoformans. *PLoS Pathogens*. 2018;14(10):e1007358.

342. Hawkins AN, Determann BF, Nelson BN, Wozniak KL. Transcriptional changes in pulmonary phagocyte subsets dictate the outcome following interaction with the fungal pathogen Cryptococcus neoformans. *Frontiers in Immunology*. 2021;12.

343. Grahl N, Dinamarco TM, Willger SD, Goldman GH, Cramer RA. Aspergillus fumigatus mitochondrial electron transport chain mediates oxidative stress homeostasis, hypoxia responses and fungal pathogenesis. *Molecular Microbiology*. 2012;84(2):383–99.

344. Murray PJ, Wynn TA. Protective and pathogenic functions of macrophage subsets. *Nature Reviews Immunology*. 2011.;11(11):723–37.

345. Pedraza-Alva G, Pérez-Martínez L, Valdez-Hernández L, Meza-Sosa KF, Ando-Kuri M. Negative regulation of the inflammasome: keeping inflammation under control. *Immunology Reviews*. 2015;265(1):231–57.

346. Kranc KR, Schepers H, Rodrigues NP, Bamforth S, Villadsen E, Ferry H, et al. Cited2 Is an essential regulator of adult hematopoietic stem cells. *Cell Stem Cell*. 2009;5(6):659–65.

347. Chen Y, Haviernik P, Bunting KD, Yang YC. Cited2 is required for normal hematopoiesis in the murine fetal liver. *Blood*. 2007;110(8):2889.

348. Krämer OH, Knauer SK, Greiner G, Jandt E, Reichardt S, Gührs KH, Stauber RH, Böhmer FD, Heinzel T. A phosphorylation-acetylation switch regulates STAT1 signaling. *Genes and Development*. 2009;23(2):223-35.

349. Qin X, Chen H, Tu L, Ma Y, Liu N, Zhang H, et al. Potent inhibition of HIF1α and p300 interaction by a constrained peptide derived from CITED2. *Journal of Medicinal Chemistry*. 2021;64(18):13693–703.

350. Berghaus LJ, Moore JN, Hurley DJ, Vandenplas ML, Fortes BP, Wolfert MA, et al. Innate immune responses of primary murine macrophage-lineage cells and RAW 264.7 cells to ligands of Toll-like receptors 2, 3, and 4. *Comparative Immunology, Microbiology and Infectious Diseases*. 2010;33(5):443–54.